SERIAL NO. SSC-66

FINAL REPORT

(Project SR-108)

on

CRITICAL STRESSES FOR SLIP, TWINNING, AND CLEAVAGE IN SINGLE CRYSTALS OF IRON

by

J. J. COX, JR.
Carnegie Institute of Technology

Transmitted through

NATIONAL RESEARCH COUNCIL'S

COMMITTEE ON SHIP STEEL

Advisory to

SHIP STRUCTURE COMMITTEE

Division of Engineering and Industrial Research
National Academy of Sciences - National Research Council
Washington, D. C.

February 1, 1954

SERIAL NO. SSC-66
BuShips Project NS-011-078

SHIP STRUCTURE COMMITTEE

MEMBER AGENCIES:
BUREAU OF SHIPS, DEPT. OF NAVY
MILITARY SEA TRANSPORTATION SERVICE, DEPT. OF NAVY
UNITED STATES COAST GUARD, TREASURY DEPT.
MARITIME ADMINISTRATION, DEPT. OF COMMERCE
AMERICAN BUREAU OF SHIPPING

ADDRESS CORRESPONDENCE TO:
SECRETARY
SHIP STRUCTURE COMMITTEE
U. S. COAST GUARD HEADQUARTERS
WASHINGTON 25, D. C.

February 1, 1953

Dear Sir:

As part of its research program related to the improvement of hull structures of ships, the Ship Structure Committee is sponsoring an investigation on critical stresses for slip, twinning, and cleavage in single crystals of iron at the Carnegie Institute of Technology. Herewith is a copy of the Final Report, SSC-66, of the investigation, entitled "Critical Stresses for Slip, Twinning, and Cleavage in Single Crystals of Iron" by J. J. Cox, Jr.

The project has been conducted with the advisory assistance of the Committee on Ship Steel of the National Academy of Sciences-National Research Council.

Any questions, comments, criticism or other matters pertaining to the Report should be addressed to the Secretary, Ship Structure Committee.

This Report is being distributed to those individuals and agencies associated with and interested in the work of the Ship Structure Committee.

Yours sincerely,

K. K. Cowart

K. K. COWART
Rear Admiral, U. S. Coast Guard
Chairman, Ship Structure
Committee

FINAL REPORT

(Project SR-108)

on

CRITICAL STRESSES FOR SLIP, TWINNING, AND CLEAVAGE IN SINGLE CRYSTALS OF IRON

by

J. J. Cox, Jr.

CARNEGIE INSTITUTE OF TECHNOLOGY
METALS RESEARCH LABORATORY

under

Department of the Navy
Bureau of Ships Contract NObs-50230
BuShips Project No. NS-011-078

for

SHIP STRUCTURE COMMITTEE

SYNOPSIS

An X-Ray, optical and metallographic study of the stresses for--and mechanisms of--slip, twinning and fracture in single crystals of iron prepared from decarburized mild steel has been made.

The selection of the glide ellipse has been found to be a function of the relative difficulty of atom motions at various positions along a ⟨111⟩ ; this function being affected by temperature and distribution of stress. A critical shear stress criterion applies.

Twinning has been found to occur on {112} type planes and in ⟨111⟩ directions below -170° C. as predicted by a critical shear stress law, mutatis mutandis. The twinning stress is greatly affected by slip.

Brittle fracture could be accounted for by a critical normal stress theory within wide limits of error. Ductile fractures predominated for specimens where a cleavage plane, {001}, was more than 65 degrees axis. Various effects of prestraining were observed.

TABLE OF CONTENTS

LIST OF FIGURES ii

LIST OF TABLES viii

LITERATURE REVIEW

Slip

Defining the process. 1
Taylor's & Elam's banal theory. 2
Taylor's mathematical analysis. 3
Fahrenhorst & Schmid's indirect observations. . 5
Deformation of silicon ferrite. 6
Di-planar cooperative slip. 7
Opinsky's & Smoluchowski's Theoretical treatment 9
New observations on Non-crystallographic slip . 11
Dislocations and slip 13
The modified Taylor analysis. 13
Summary of the various theories 21

Twinning

Introduction. 25
Types of twins. 26
Atom movements in b.c.c. twinning 26
Critical resolved shear stress as a twinning criterion 32
Energy criteria for twinning in metals. 33
Miscellaneous observations. 34

Cleavage:

General considerations. 35
Theories of cleavage strengths. 37
Experimental work on alpha iron 38

EXPERIMENTAL PROCEDURE AND TECHNIQUES

Attempts at growth by various methods. 40
Specimen preparation 43
Decarburization: Equipment & technique. 46
Furnace construction. 46
Gas purification, saturation, distribution. . . 49
Technique 53
Determination of the critical strain for exaggerated grain growth. 55
Electropolishing 61
X-Ray determination of crystal orientation 68
Determination of glide ellipse and fracture surface by optical trace methods. 71
Tensile testing of the crystals. 78
The tensile machine 78
Stress and strain measurements. 79
Temperature baths 85

EXPERIMENTAL RESULTS AND DISCUSSION 86

Introduction 86
Slip 87
Behavior of the glide ellipse at various temperatures 89
Change in the glide ellipse with temperature . . 91
Variation of the Critical resolved shear stress with temperature 98
Surface manifestations of slip 101
Asterism and lattice distortion. 104
Twinning 107
Fracture 115
Introduction 115
Large specimens. 115
Small specimens. 121
Brittle fractures. 122
Ductile fractures. 125
The nature of the fracture surface 128

CONCLUSIONS 135

ACKNOWLEDGMENT 138

BIBLIOGRAPHY. 139

LIST OF FIGURES

No.	Title	Page
1.	Relative values of critical resolved normal and shear stresses for slip twinning and cleavage in single crystals of low silicon ferrite.	8
2.	Critical resolved shear stress of the (110) plane for ingot iron single crystals.	12
3.	Plan view of atoms on a (111) plane	15
4a.	Side view of (110) slip	15
4b.	Side view of (123) slip	15
5a.	Side view of (112) slip to the left	17
5b.	Side view of (112) slip to the right.	17
6.	Hypothetical S_ψ/S_{110} versus ψ curve	22
7.	Qualitative S_ψ/S_{110} versus ψ curve for various alloys and test conditions.	23
8a.	Lattice slip (classical).	27
8b.	Lattice twinning (classical).	27
9.	Body centered cubic unit cell	29
10.	(110) projection of bcc. lattice.	29
11.	(110) projection of bcc. lattice with twinning shear applied to the first atom layer	29
12.	Bcc. twin two atom layers thick	30
13.	Plan view of (112) plane.	30
14.	Fracture stress for cleavage as affected by reduction in area at the fracture.	39
15.	S.A.E. 1008 stock "as received"	44
16.	Dimensions of single crystal test bars.	45

No.	Title	Page
17.	Layout of furnace windings.	47
18.	Cross section of furnace.	47
19.	Flow sheet of gas system.	50
20.	Water vapor-hydrogen-iron equilibrium diagram .	51
21.	Gas system.	52
22.	Vapor pressure of water versus temperature. . .	52
23.	Specimens in racks.	54
24.	S.A.E. 1008 "as decarburized"	56
25.	Tool for making gauge marks	58
26.	Grain size of strain anneal specimens as a function of strain.	60
27.	Photograph of electropolisher	64
28.	Wiring diagram of electropolisher	66
29.	Specimens electropolished--and etched	67
30.	Goniometer and camera on X-Ray machine.	70
31.	Goniometer and long specimen.	70
32.	Standard (001) projection with tensile axis . .	72
33.	Coordinates for calculation of resolved shear stress.	72
34.	Coordinates for calculation of resolved normal stress.	72
35.	Hypothetical specimen with slip traces.	75
36.	Goniometer and specimen on metallograph	76
37.	Standard (001) projection showing specimen axis, slip data and axis migration.	77

No.	Title	Page
38.	Tensile machine, accessories and recording equipment.	80
39.	Load--time curve for slip.	81
40a.	Orientation of slip specimens.	88
40b.	Slip orientations with respect to regions of highest resolved shear stress.	88
41.	Summary of slip planes, maximum shear planes, and various crystallographic planes for all specimens tested in slip	90
42.	ψ versus χ for room temperature slip	92
43--46.	Stereographic projections of specimens tested for slip behavior showing slip plane data, axis migrations, and maximum shear stress poles: Specimens A-7, BR-3, A-1 and A-3	95
47--50.	Stereographic projections of specimens tested for slip behavior showing slip plane data, axis migrations, and maximum shear stress poles: Specimens A-5, A-4, A-12 and A-6	96
51--54.	Stereographic projections of specimens tested for slip behavior showing slip plane data, axis migrations, and maximum shear stress poles: Specimens A-9, A-11, D-3 and BR-2.	97
55.	Variation of resolved shear stress with temperature for slip and twinning.	99
56.	Slip lines and twins at--196°C	102
57.	Wavy slip lines.	102
58.	Straight slip lines.	103
59.	Slip lines in scratch.	103
60.	Slip lines in scratch (dark field)	105
61.	Clustering of slip lines	105

No.	Title	Page
62.	Laue photogram of undistorted specimen.	106
63.	Laue photogram of strained specimen	106
64.	Orientation of twinning specimens	108
65.	Twinning near a fracture surface.	114
66.	Load--time curve for twinning	114
67.	Cross-hatched twins	116
68.	Notched twins	116
69.	Fracture orientations	117
70.	Fracture orientations (prestrained)	117
71.	Fracture orientations (large specimens)	117
72.	Resolved normal stress versus orientation for large specimens	120
73.	Resolved normal stress versus orientation for small specimens	123
74.	Fracture stress of ductile specimens versus reduction in area at the fracture	127
75.	Fracture specimens (side view).	129
76.	Fracture specimens (side view).	129
77.	Fracture specimens (side view).	130
78.	Fracture specimens, prestrained (side view) . . .	130
79.	Fracture specimens, prestrained (side view) . . .	130
80.	Fractograph of specimen BR-1.	131
81.	Fractograph of specimen BR-3.	131
82.	Fractograph of specimen of shear area	133
83.	Fractograph of specimen A-10.	133

LIST OF TABLES

I	Ratios of critical shearing strengths of (110), (112), and (123) planes of silicon ferrite at various temperatures.	10
II	Atom movements for slip on various planes of the [111] zone.	18
III	Force required for various atom movements in the [111] zone.	20
IV	Shearing strength of various planes in the [111] zone in relation to the strength of the (110) plane. . . .	20
V	Cooling media for the tensile tests at various temperatures.	85
VI	Stress at yielding resolved onto various planes of the [111] zone.	98
VII	Resolved shear stress for twinning in the experimentally observed twins.	109
VIII	Resolved shear and normal stresses for various twin systems. . . . . after page.	112
IX	Fracture data for large specimens	118
X	Fracture data for small specimens	124

I. LITERATURE REVIEW

Barrett[1] has reviewed the existing literature on the plastic deformation of single crystals and included the basic facts relating to the three processes: slip, twinning, and cleavage for most crystal systems. This dissertation is concerned only with the body-centered cubic lattice and, hence, the data concerning other space forms are reported only insofar as they apply to body-centered cubic deformation. The literature review that follows is by no means complete and was not so intended. However, most all the important data and qualitative observations are reported or described even though the bibliography does not contain a reference to the original work. In such cases, the references are cited from review papers and the original authors are credited. The survey is divided into three parts which correspond to the three parts of the experimental work.

A. Slip

Defining the Process

The process of slip is classically defined as the movement of one block of atoms or lattice over another for an integral number of atom distances. The crystallographic plane upon which the displacement occurs is called the slip or glide plane; and the direction in that plane, the slip or glide direction. Experimentally, we know that slip is

accompanied by work hardening, bending of the glide plane (flexural glide), cross slip and many other related processes. This textbook picture, however, can still be used when comparing slip with twinning or with cleavage although it is much too simple to be correct.

In face-centered cubic and hexagonal metals, the slip plane is normally the plane of highest atom density while the direction is the direction of closest atom spacing in that plane. Metallographic observation of the traces of the slip planes on polished surfaces of these metals have shown more or less straight lines which have been geometrically analyzed to confirm these results. The body-centered cubic metals have also been shown to exhibit slip on the close-packed direction, but the straight-line traces indicative of uni-planar slip have not been found. Instead, the slip lines were always wavy and in many instances widely branched and forked. It is for this reason that much contention is found in the literature concerning the nature of body-centered cubic slip and its origin.

Taylor's and Elam's Banal Theory

The work of Taylor and Elam[2] was the first systematic investigation into the slip mechanistics of α-iron. They used small crystals obtained from Edwards and Pfiel measuring two millimeters on an edge. The slip directions were determined

from distortions of a gridwork engraved on the polished surfaces of the specimens. Data obtained in this work indicated that slip took place along the close-packed [111] directions and on a plane which lay adjacent to or coincided with the plane of maximum shear stress containing the slip direction. In the tension tests, when the slip plane did not coincide with the maximum shear stress plane, it was always inclined toward the nearest (112) plane. On this basis, they concluded that slip was non-crystallographic or "banal." The physical picture of the "banal" mechanism was one of a bundle of hexagonal rods where the rod axis represented the slip direction. This accounted for the forkedness of the slip lines when viewed in a plane perpendicular to the slip direction and their more or less straight character when viewed in a plane parallel to the slip direction. An alternate mechanism where slip could occur on two (112) or (110) planes containing the same slip direction was advanced but rejected in favor of the banal mechanism because it was contrary to what had been found for other metals. The authors felt that only in certain accidental cases would specimens be oriented in such a manner that the shearing stress on two planes would be close enough to cause di-planar or cooperative slip.

Taylor's Mathematical Analysis

In a later work, Taylor[3] studied the deformation of β-brass crystals, also a body-centered cubic structure. Taylor

found that, when the slip plane did not coincide with the maximum shear stress plane containing the slip direction, it was always inclined toward the nearest (110) plane. This enabled him to construct a mechanism where the resistance to shear of any plane in the zone of the slip direction could be found as a function of the angle ψ between the slip plane and the nearest (110) plane. The stress on this slip plane could then be calculated from the following equation:

$$F = \frac{P}{A} \sin\xi \cos\xi \cos(x - \psi)$$

where F = force on the glide plane

P = yield load in axial tension or compression

A = cross sectional area of the specimen

ξ = angle between the slip direction and tensile axis

x = angle between the plane of maximum shear stress containing the slip direction and the closest (110) datum plane

ψ = angle between the glide plane and the closest (110) datum plane.

Differentiating and dividing through by F, we arrive at

$$\frac{1}{F}\frac{dF}{d\psi} = \tan(x - \psi)$$

Integrating this relation between the limits 0 and ψ yields:

$$\ln F/F_o = \int_o^{\psi} \tan(x - \psi)\, d\psi .$$

$$\ln F/F_o = \ln \cos(x - \psi) - \ln \cos x$$

Here the symbol F_o is the resistance to shear of the (110) datum plane where ψ is equal to zero. If the relationship between x and ψ is known, then the variation in shear resistance along the slip zone can be calculated as a function of ψ. The author believes that this is a confirmation of the hexagonal rod movement of the banal theory since the experimental curve of ψ vs x is of the same slope as the one predicted by the banal mechanism. For β-brass, the slip lines were wavy but not as pronounced as in α-iron. No explanation for this difference was proposed.

Fahrenhorst's and Schmid's Indirect Observations

The investigation of Fahrenhorst and Schmid[4] gave reference to several indirect methods of determining the slip mechanism of α-iron. From measurements of the yield stress of various crystals of known orientation, it was possible to calculate the critical resolved shear stress on various assumed glide planes. The four planes for which calculations were made were: (1) (110) planes; (2) (112) planes; (3) (123) planes; and (4) the plane of maximum shear containing the slip direction. This yielded four curves of a slope similar to the yield point versus orientation curve. Since the curve for assumed (123) slip best fitted the experimental curve, the authors concluded that the slip system (123): [111] was the correct one.

It becomes immediately evident, when some simple calculations

are made, that values of stress obtained from any one of the four assumptions do not differ significantly, and the scatter among these values is less than the experimental error involved in the measurements. Hence, such a method of analysis does not only not prove any of the assumptions to be correct, but it eliminates the possibility that some other correlation might exist.

The second indirect method used by Fahrenhorst and Schmid was to plot the course of the specimen axis during its migration on straining. Using the same four assumptions, Fahrenhorst and Schmid found that the migration predicted by (123) slip gave the best correlation with experimental observations. However, many specimens did not conform to this predicted behavior.

The third method employed by these investigators was to plot curves of shear stress versus shear strain for the same four assumed slip systems. Again the curve for the system (123): [111] gave the least variation from experiment; but, as in the first part of the study, significant differences do not exist and lie well within the experimental error.

Deformation of Silicon Ferrite

Barrett, Ansel, and Mehl[5] studied the behavior of single crystals of ingot iron and silicon ferrites of various compositions. The stresses for slip were only studied qualitatively and hence only broad generalizations could be made on this

subject. Tension, compression, torsion and bending were the methods used to deform the specimens. The use of thin sheet specimens necessitated the trace normal method to be used for determination of the indices of the glide plane. All 194 sets of glide traces investigated were said to be explained by slip on planes of the type (110), (112) or (123) and in the [111] direction. When the measured glide trace was found to differ from one of the three planes by more than 7°, the specimen was regarded as "no good" and the data were not recorded. When individual sets of measurements had a range of more than 10°, they again were considered to represent bad data and were not tabulated.

Silicon contents in excess of 4% were found to limit slip to (110) planes regardless of the test temperature. For finites containing less than 4% silicon, lowering the test temperature below room temperature favored (110) slip. The temperature at which (110) uni-planar slip occurred increased from -190°C at 1% Si to -70°C at 4% silicon. The waviness of the slip lines was found to decrease as the tendency for uni-planar (110) slip increased--with lower temperatures and increased silicon contents. The variation of critical resolved shearing stress with temperature is shown qualitatively in Fig. 1.

Diplanar Cooperative Slip

Chen and Maddin[6] studied deformation in single crystals of body-centered cubic molybdenum produced from exaggerated

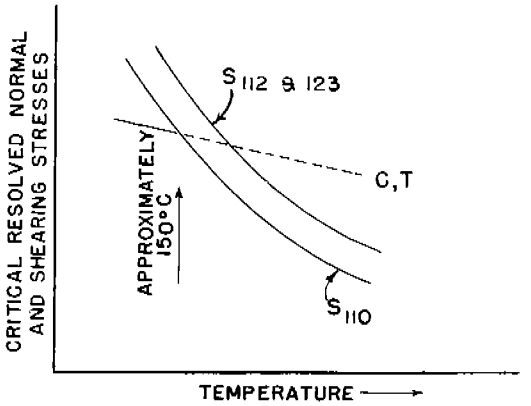

FIG. 1

INTERRELATION OF RESOLVED SHEAR AND NORMAL STRESSES FOR SLIP (S), TWINNING (T), AND CLEAVAGE (C) AS A FUNCTION OF TEMPERATURE FOR A LOW SILICON FERRITE. (AFTER BARRET, ANSEL, AND MEHL).

grain growth of sintered rods. Orientations of the five crystals studied were determined by back reflection techniques while the traces of the glide planes were determined microscopically. These data indicated that the glide ellipse could occupy any position in the [111] zone in agreement with Taylor[3] and Taylor and Elam[2]. However, Chen and Maddin chose to use the X-Ray asterism of the deformed crystals to determine the operative glide planes and chose the alternate conclusion, discarded by Taylor and Elam, that slip on two sets of (110) planes could always account for the observed position of the glide plane. For example, when the glide ellipse coincided with a (112) plane, it would actually consist of slip on equal segments of two adjacent (110) planes containing the same direction. Such a mechanism can explain the observation that the glide ellipse can occupy any position in the [111] zone and that the glide traces should be very wavy when viewed perpendicular to the glide direction and straight when viewed parallel. It is also consistent with the early proposals since the (110) plane is the most densely packed.

Opinsky's and Smoluchowski's Theoretical Treatment

Opinsky and Smoluchowski[7] in their theoretical treatment of slip in the body-centered cubic lattice divided the stereographic unit triangle into several regions which indicated the favored slip system if the axis of the specimen fell in that region.

The calculations were made on the basis that each of the planes has the same critical shearing strength which is highly improbable as the authors point out although it is as good an assumption as can be made in this case. By working backwards from the known boundaries in the basic unit triangle where slip occurs on the (110), (123) or (112) planes the resistance to shear of these planes were calculated. This is in many respects similar to the Taylor analysis, for it predicts the position of the glide plane with respect to the relative resistances to shear of the various planes in the slip zone.

In a later paper[8], Opinsky and Smoluchowski measured the ratios of shearing strengths on the three planes at various temperatures in silicon ferrite in tension and compression. These ratios are shown in Table I below.

Table I

RATIOS OF CRITICAL SHEARING STRENGTHS

FOR SILICON FERRITE AT VARIOUS TEMPERATURES

Room Temp. Tension

$$S_{(123)} = 1.07\ S_{(110)} = 0.99\ S_{(112)}$$

Room Temp. Compression

$$S_{(123)} = 1.11\ S_{(110)} = 0.99\ S_{(112)}$$

Compression at + 190°C

$$S_{(123)} = 1.06\ S_{(110)} = .99\ S_{(112)}$$

Compression at -140°C

$$S_{(123)} = 1.13\ S_{(110)} = 1.16\ S_{(112)}$$

The significant contribution of this work was that a method of calculation was developed whereby the slip behavior of a specimen could be predicted by its orientation. This had not been accomplished for a metal where several slip systems could operate simultaneously.

New Observations on Non-Crystallographic Slip

Vogel and Brick[9] studied the plasticity of single crystals of ingot iron in tension and compression at various temperatures. The traces of the glide planes were measured optically and superimposed on the stereographic projection of the specimen orientation. The authors concluded that the glide plane may occupy any position in the [111] zone and that its identity is determined by two criteria:

(1) The orientation of the stress axis with respect to the crystal axis;

(2) The variation in shearing strengths of the various planes of the slip zone. The interrelation of these is a function of temperature and direction of stress (tension or compression).

The data indicated that the slip plane deviates toward the $(\bar{1}01)$ in tension at elevated temperatures and towards the $(\bar{1}01)$ in compression at low temperatures. This was the first experiment to yield a quantitative relationship between critical resolved shear stress for slip and the testing temperature. (See Fig. 2). There is some scatter in the data, but the trend is quite evident.

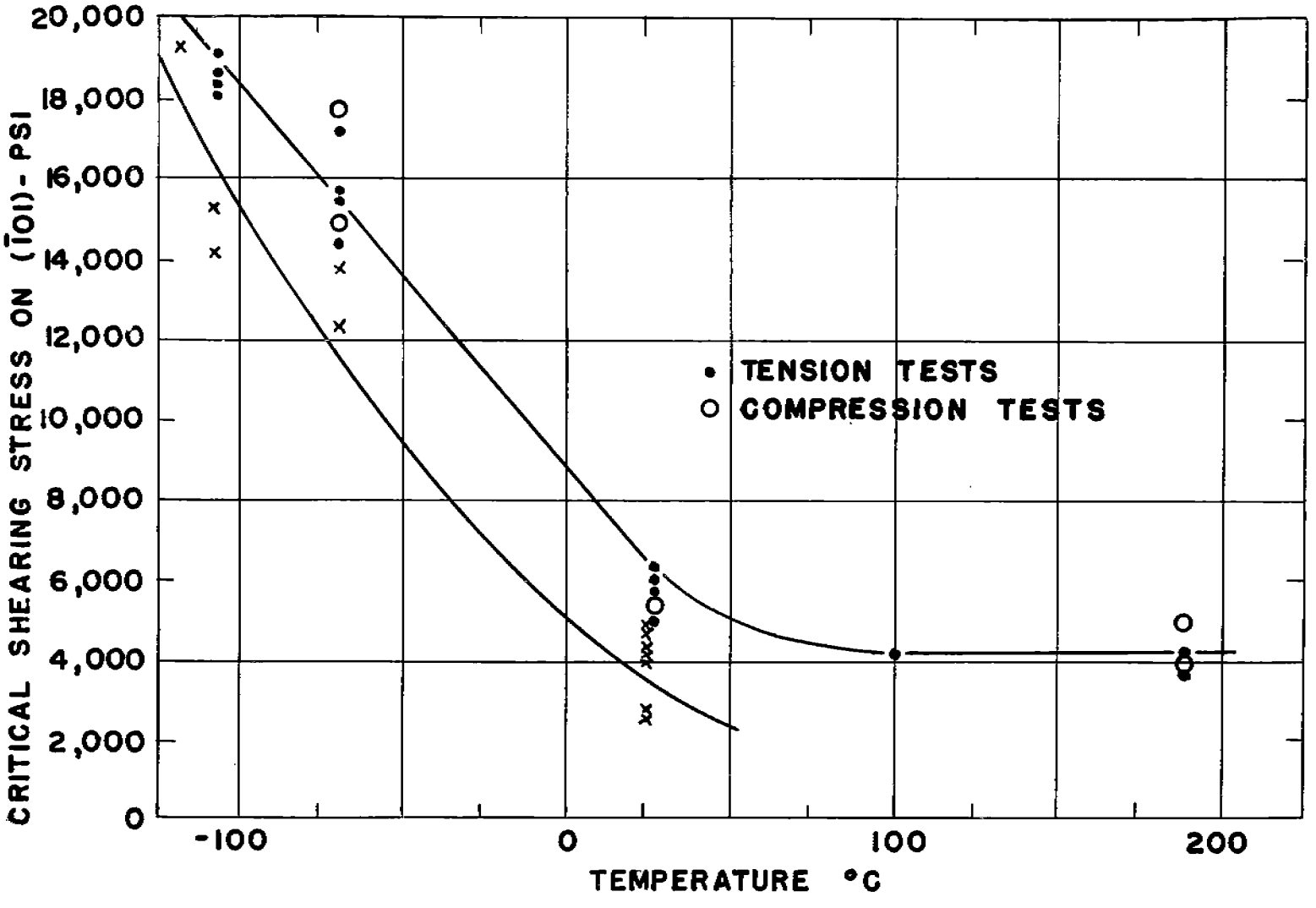

FIG. 2

TEMPERATURE DEPENDENCE OF CRITICAL SHEARING STRESS ON (1̄01) PLANE.
• ○ (AFTER VOGEL AND BRICK (9)).
× (AFTER STEIJN AND BRICK (14)).

Dislocations and Slip

The literature contains voluminous references to the slip behavior of metals as reconciled by dislocation theory, but none of these works has revealed a mechanism which could clearly account for body-centered cubic slip behavior. Chalmers and Martius[13] have simply (simple in contrast to the complex mathematics of most dislocation theory) determined a parameter which could predict the slip systems in various metals. The parameter, designated as $\mathscr{E}$, is defined as the ratio of the Burgers vector to the interplanar distance. According to this theory, slip should occur on the planes and in the direction for which $\mathscr{E}$ is a minimum. For body-centered cubic metals slipping in the [111] direction, the first choice of slip would be (110), the second (112) and the third (123). If the $\mathscr{E}$ parameters are listed for various directions, however, it is seen that body-centered cubic metals should slip on (110) and (100) planes in [100] directions rather than on (112) planes in [111] directions. Although this has never been recorded, it does not give dislocation theory a "black eye" since the approach is quite empirical as was pointed out by the author.

The Modified Taylor Analysis

The most complete investigation of slip in body-centered cubic iron is the recent work of Steijn and Brick[14]. This investigation has brought forth an analysis which will be described in detail since it pertains quite pertinently to this

investigation. Single crystals of three different alloys were studied in tension and compression at temperatures from room temperature to liquid air temperatures. It was found that no difference in slip behavior obtained for the three alloys: .0014 C, .094 Ti; .0014 C, 0.31 Ti; and .0231 C, 0.00 Ti. The slip behavior was also not affected if the specimens were polished by hand rather than electrolytically.

First the atom movements involved in this theory will be discussed, and then the correlation with the experimental data will be presented. Fig. 3 represents a projection of a [111] plane of the body-centered cubic lattice with the atoms represented as hard spheres. Although this picture is not strictly true, it is rigorous enough and yet simple enough to be handled easily. At the outset, it should be remembered that the mechanism by which the atoms move is immaterial.

In cubic lattices, the direction [hkl] is always perpendicular to the plane (hkl) and so our octahedral slip direction is represented by a line projecting out of the plane of paper in Fig. 3 and perpendicular to it. All planes having this as a common direction (those belonging to the zone) can be shown as traces on Fig. 3. The solid black lines are (110) traces, the dash-dash lines (112) traces and the dot-dash lines (123) traces. The entire gamut of planes in this zone can be represented as a series of lines radiating from o to m, n, p, etc.

To visualize (110) slip, one imagines that a stack of

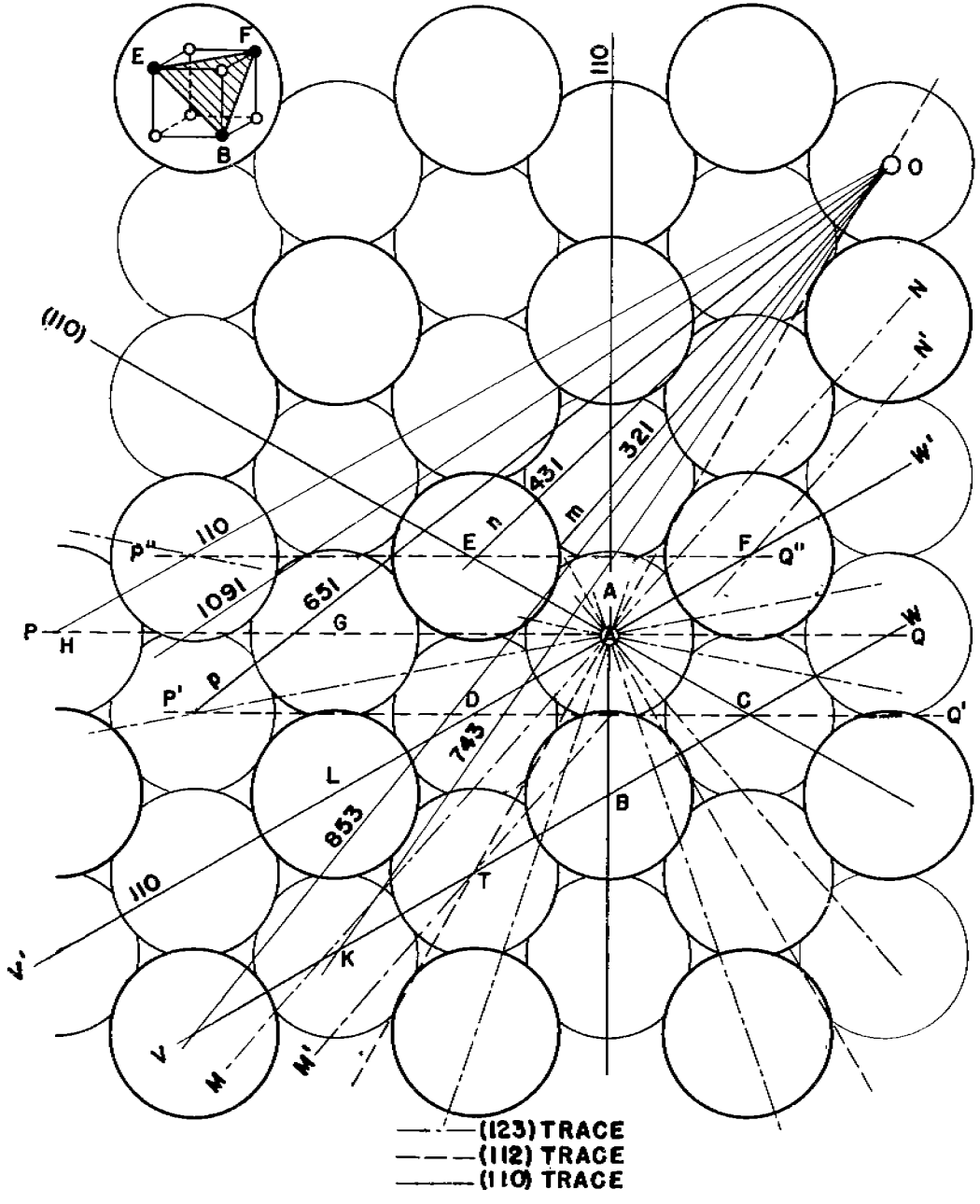

FIG. 3

PLAN OF (111) PLANE.

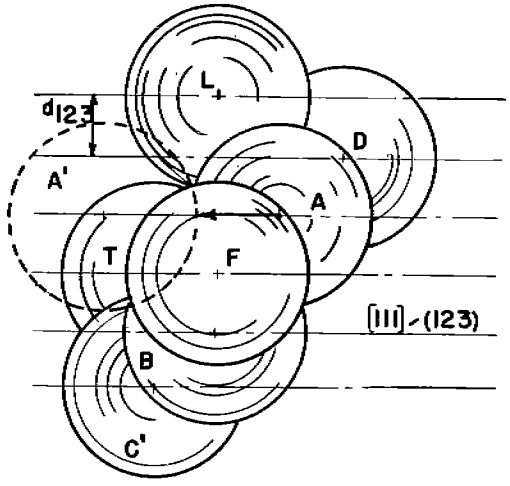

FIG. 4a

SLIP ON (123) - PLANES.

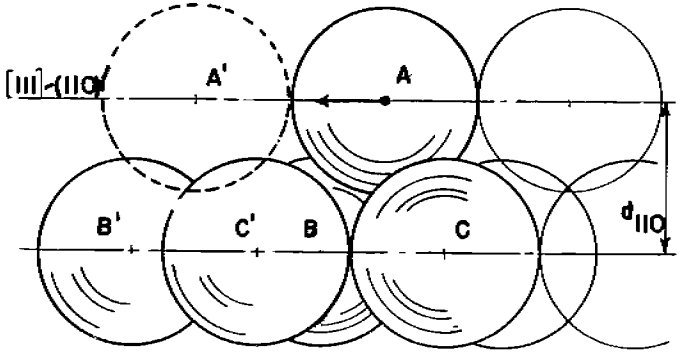

FIG. 4b

SLIP ON (110) - PLANES.

(110) planes slides as a block over the atoms on and below the trace v-w. The movement of atom A to its next position along [111] is exactly the same as the movement of atoms D, L, F, etc., since these atoms are indistinguishable. This movement is designated as an A-type movement, a side view of which is shown in Fig. 4.

In (112) slip, a stack of planes of a given thickness slides in block form over the atoms on and below the trace P'Q'. The movement of atoms A, G, and H is indistinguishable and is called a B-type movement. Although the mechanism is not important, it can be seen to involve riding up over atom B and then passing through the region bounded by atoms C x D or their equivalent in the plane immediately above the plane of the paper.

Since d_{112} is less than the radius of the atoms, it can be seen that the atoms E, F, etc. of plane P"Q" are affected by the movement of atoms A, G, and H of plane P'Q' and cannot move independently of them. This movement of atoms on plane P"Q" is called a C-type movement. Thus slip on (112) planes is composed of an equal number of B and C type movements. Figs. 5a and 5b show the side view of such movements. Although the atom movements for right- and left-handed slip are the same, the order in which they occur is reversed. Steijn postulates that this is the reason for Taylor's division of data into two groups, one for each slip direction.

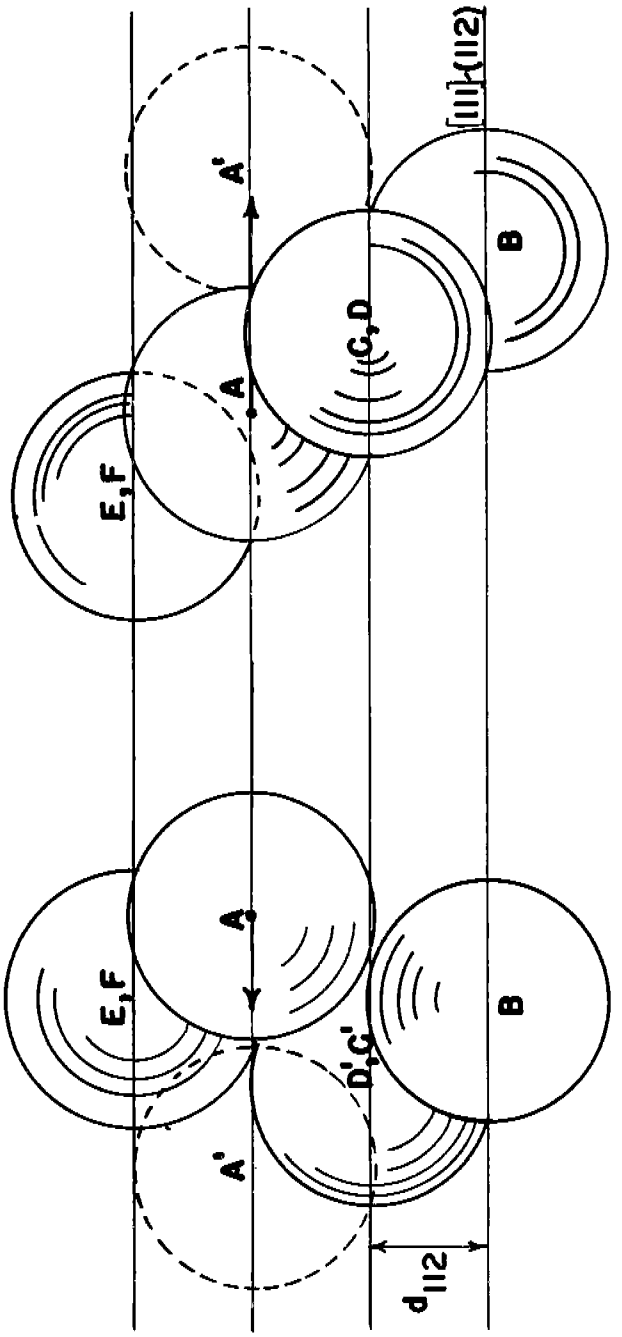

FIG. 5b

(112) SLIP "TO THE RIGHT."

FIG. 5a

(112) SLIP "TO THE LEFT."

For (123) slip, the atoms on and above the trace MN are considered to shear as a block over those atoms on trace M'N'. Again, because d_{123} is smaller than the atom radius, there is interaction. Atom A shears with a B-type movement, atom L with a C-type movement and atom D with an A-type movement. This implies that (123) slip can occur with the addition of no new atom motions, but rather is composed of A and (B + C) type movements. This explanation can be extrapolated to include any plane in the [111] zone and the relative proportions of these movements are listed in Table II below where L represents the width of a given plane.

Table II

(110): $\frac{L}{1/3\ a\sqrt{6}}$ x 1 A movement

(1091): $\frac{L}{1/3\ a\sqrt{546}}$ x 8A + 1 (B + C) movements

(651): $\frac{L}{1/3\ a\sqrt{186}}$ x 4A + 1 (B+ C) movements

(431): $\frac{L}{1/3\ a\sqrt{78}}$ x 2A + 1 (B + C) movements

(321): $\frac{L}{1/3\ a\sqrt{42}}$ x 1A + 1 (B + C) movements

(853): $\frac{L}{7/3\ a\sqrt{6}}$ x 2A + 3 (B + C) movements

(743): $\frac{L}{1/3\ a\sqrt{6}}$ x 1A + 3 (B + C) movements

(211): $\frac{L}{a\sqrt{2}}$ x 1 (B + C) movements

If the shearing force required to cause slip on a (112) plane of width L be over a unit interatomic distance F_{112} and that for a (110) plane be F_{110}, the shearing forces on the various planes can be calculated by the weighted averages method. For example, if slip on a unit area (110) plane requires M type-A movements and that of a unit area (112) plane N type (B + C) movements, and the numbers of A and (B + C) movements required for a unit shear of a high index plane (hkl) are respectively m and n, then the force required to shear the high index plane can be calculated from the relation:

$$F_{hkl} = \frac{m}{M} \cdot F_{110} + \frac{n}{N} \cdot F_{112}$$

or, since unit areas are involved

$$S_{hkl} = \frac{m}{M} \cdot S_{110} + \frac{n}{N} \cdot S_{112}$$

Letting $\frac{S_{112}}{S_{110}} = \gamma$

$$\frac{S_{hkl}}{S_{110}} = \frac{m}{M} + \gamma \cdot \frac{n}{N}$$

The results of these calculations by Steijn are given in Tables III and IV.

Table III

$$F_{(1\ 9\ 10)} = \frac{a\sqrt{2}}{1/3\ a\sqrt{546}} \cdot F_{112} + \frac{8/3\ a\sqrt{6}}{1/3\ a\sqrt{546}} \cdot F_{110}$$

$$F_{(516)} = \frac{a\sqrt{2}}{1/3\ a\sqrt{546}} \cdot F_{112} + \frac{4/3\ a\sqrt{6}}{1/3\ a\sqrt{186}} \cdot F_{110}$$

$$F_{(431)} = \frac{a\sqrt{2}}{1/3\ a\sqrt{78}} \cdot F_{112} + \frac{2/3\ a\sqrt{6}}{1/3\ a\sqrt{78}} \cdot F_{110}$$

$$F_{(321)} = \frac{a\sqrt{42}}{1/3\ a\sqrt{42}} \cdot F_{112} + \frac{1/3\ a\sqrt{6}}{1/3\ a\sqrt{42}} \cdot F_{110}$$

$$F_{(853)} = \frac{3a\sqrt{2}}{7/3\ a\sqrt{6}} \cdot F_{112} + \frac{2/3\ a\sqrt{6}}{7/3\ a\sqrt{6}} \cdot F_{110}$$

$$F_{(743)} = \frac{3a\sqrt{2}}{1/3\ a\sqrt{222}} \cdot F_{112} + \frac{1/3\ a\sqrt{6}}{1/3\ a\sqrt{222}} \cdot F_{110}$$

Table IV

$$S_{(10\ 9\ 1)} = (.1816\gamma + .8386)\ S_{110}$$

$$S_{(651)} = (.3111\gamma + .7184)\ S_{110}$$

$$S_{(431)} = (.4804\gamma + .5547)\ S_{110}$$

$$S_{(321)} = (.6547\gamma + .3780)\ S_{110}$$

$$S_{(853)} = (.7423\gamma + .2857)\ S_{110}$$

$$S_{(743)} = (.8542\gamma + .1644)\ S_{110}$$

By assuming various values of γ, Steijn obtained the series of curves shown on Fig. 6. The significance of the γ parameter is quite evident, and it would be extremely helpful if this ratio could be theoretically calculated. All that is known concerning it is that alloying elements should affect the parameter differently, depending especially upon atomic radius and perhaps upon other factors which govern alloying behavior. Temperature should also affect the γ ratio quite markedly. A summary curve by Steijn shows the quantitative lie of the data of various investigators (Fig. 7). The difference in behavior of crystals in tension and compression is manifest on a different S_{γ}/S_{110} ratio. Why this should be changed by changing the stress direction is not known although Steijn postulates that the elastic deformation which always precedes plastic flow affects it greatly. Perhaps if a lattice is elastically compressed by alloying elements, then behavior in tension is affected.

A Summary of the Various Theories

In general, two points of view can be distinguished in the literature concerning body-centered cubic slip.

The one is that slip occurs on the (110), (112) and (123) planes or combinations of these and in the [111] direction. It is obvious that the extreme waviness of the slip lines as always observed cannot be accounted for, and certainly cannot be designated, as slip on true crystallographic planes--at

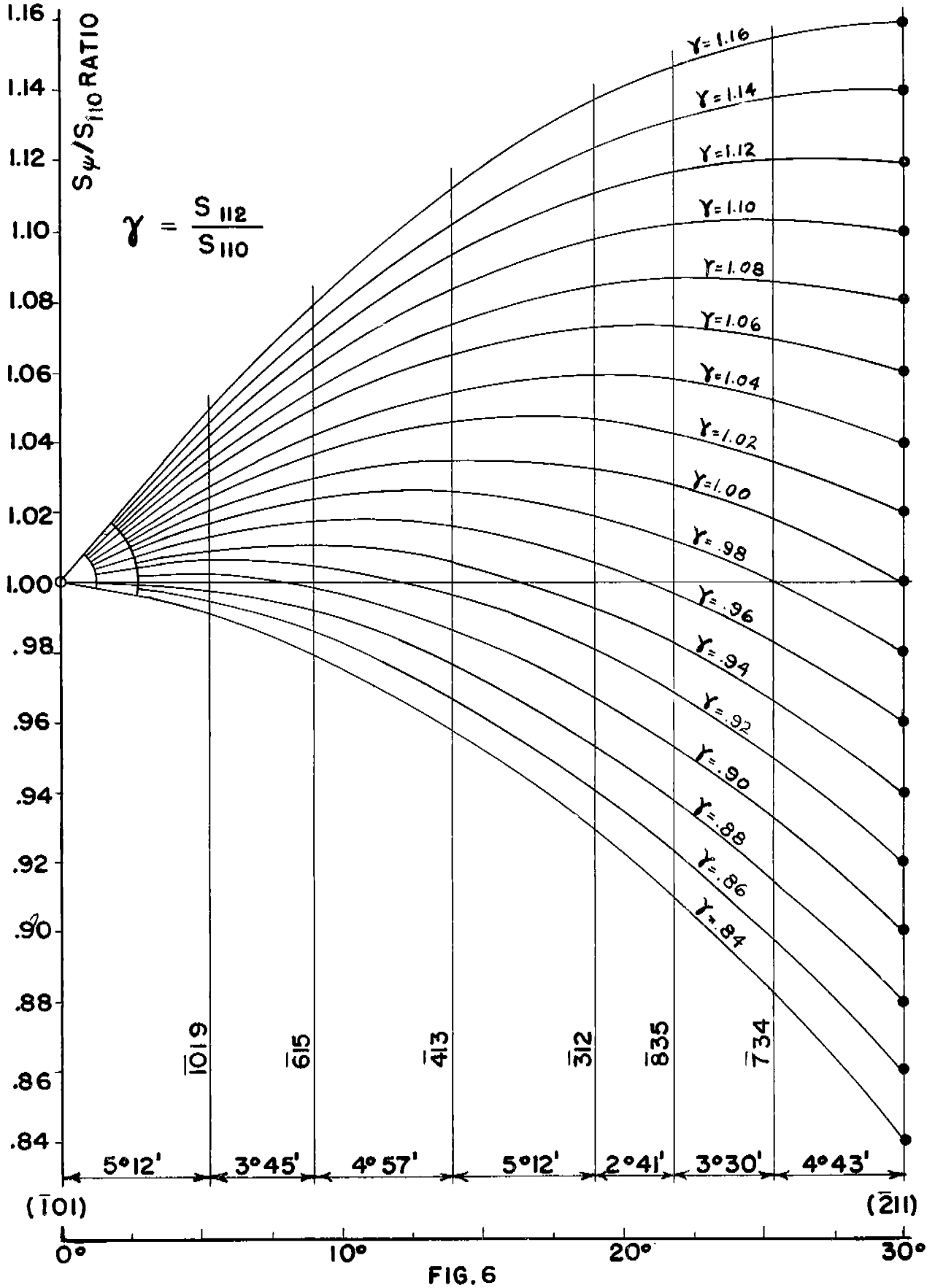

FIG. 6
HYPOTHETICAL S_ψ/S_{110} - CURVES FOR ASSIGNED γ VALUES.
(AFTER STEIJN AND BRICK (14))

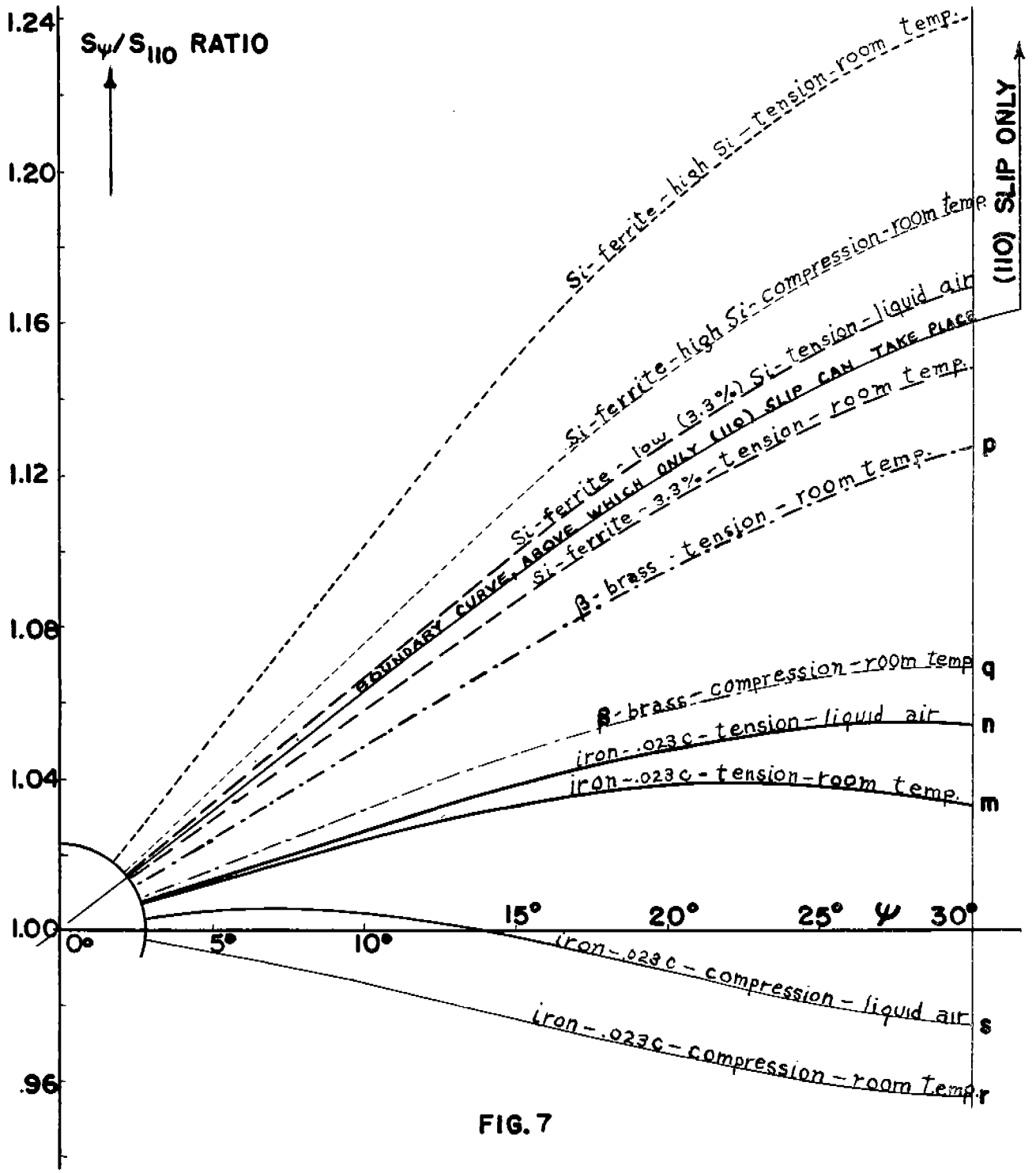

FIG. 7

A QUALITATIVE PICTURE OF SLIP IN B.C.C. - METALS.
(AFTER STEIJN AND BRICK (14))

least within the resolving power of our present-day measuring equipment.

The second viewpoint, which is in direct opposition to the first, is that of Taylor wherein it is postulated that slip occurs in an octahedral direction but not necessarily on low index crystallographic planes. In other words, the pole of the integrated glide ellipse, which will be defined as the pole representing the average slope of the wavy slip lines, can occupy any position in the [111] zone depending upon the variation of the resolved shear stress. The glide plane favored in compression is not the same as that one favored in tension and hence the concept of opposite slip direction necessarily caused the data of Taylor to be grouped into tensile behavior and compressive behavior.

The work of Steijn and Brick has reanalyzed the Taylor method and built, using the Taylor work as a foundation, a theory which allows slip to occur on any "integrated plane" in the [111] zone by combinations of three types of atom movements. The data for compression and tension were resolved into one group on the basis of a normal stress affecting the active slip plane. The waviness of the slip lines was also explained by using the various combinations of the three atom motions involved.

Dislocation theory was found not to clear the picture and was not discussed. Likewise the methods using X-Ray

asterism were found not to be of consequence in obtaining insight into the mechanism of slip in α-iron.

B. Twinning

Introduction

The study of twinning and the criteria for its occurrence comprises the second part of this review. Evans[15] has defined a twinned crystal as follows:

> If in a compound crystal made up of two structures of the same form there is a co-linear common plane, but the two structures are not co-directional, the common plane is termed a twin plane, and the common line which is its normal, a twin axis; and the two structures together constitute a twin crystal and its parent. (Underscoring added by the author.)

The physical conditions necessary for twinning have been set forth by Preston[16]:

1. "The twinning plane can only be such that the operation of twinning does not bring atom centers closer than the closest approach of atoms in either component of the twin."
2. "The components of the twin must have in common at least one plane of atoms."

The plane of atoms between the twin components is known as the composition plane. This may be the twinning plane, another plane, or in some cases a non-crystallographic surface. In this common plane, there is an array of atoms that belong to both the twin and its parent crystal and necessarily a distortion of this boundary region caused by the differences

in interatomic spacing necessary to promote coherency across the twin interface. When the twinning plane coincides with the composition plane, this distortion becomes a minimum.

Types of Twins

Plastic theory allows for two distinct types of deformation: slip and twinning. They are best differentiated by reference to a sketch of the lattice such as shown in Figs. 8a and 8b. It is readily seen that in twinning, as opposed to slip, the displaced portion of the lattice has assumed a distinctly different orientation from its parent. Metals, in general, exhibit two separate types of twins: growth, or congenital twins, and deformation twins. Since we are concerned with the body-centered cubic lattice, let it suffice to say that only growth twins have been proved to exist in face-centered cubic metals while hexagonal metals exhibit both growth and deformation twins. The body-centered cubic metals, however, exhibit only deformation twins.

Atom Movements in Body-Centered Cubic Twinning

In 1928 Mathewson and Edmunds[17] first proved that Neumann bands produced by low temperature shock on α-iron were true deformation twins. The twinning plane was of the (112) type and the direction [111]. It can be shown that on the body-centered lattice the sense of direction in a twinning movement is of utmost importance and must be defined if the

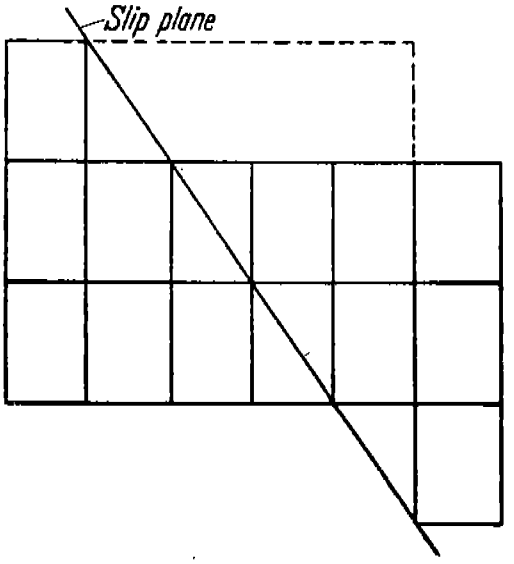

Fig. 8a. Classical picture of slip in two dimensions showing lattice after slip to be a mirror image (18).

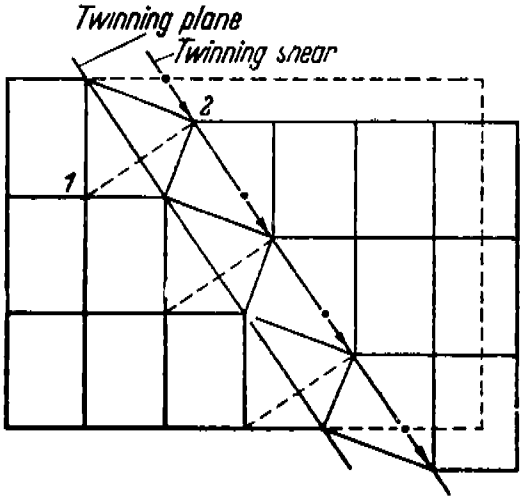

Fig. 8b. Classical picture of twinning showing new orientation of twin. Mirror image relationship exists across twinning place (18)

twin system is to have meaning. Clark and Craig[18] have described the "easy and hard" senses of twinning direction by means of various projections of the twinning plane upon other lattice planes. Fig. 9 shows the twinning plane (112) in perspective with respect to the body-centered cubic unit cell. Fig. 10 is a projection of a (110) plane with the (112) plane illustrated as a diagonal trace. Here the dark circles are atoms in the plane of projection, while the light circles give the position of atoms above and below the datum plane.

If the upper right-hand portion of the block of atoms is shifted upwards along the twinning plane until the first twin position is found, the configuration appears as shown in Fig. 11. Fig. 12 illustrates the movement applied to the second layer of atoms. The shearing distance for each layer can be described by the relation

$$d_{\bar{1}11} = n\frac{\sqrt{3}}{6} a_o$$

where d = shear distance

n = order of the plane in question with respect to the twin plane

a_o = the lattice parameter

For the first (112) plane above the twin plane n=1, for the second n=2, etc.

It can be seen that the twin orientations could have

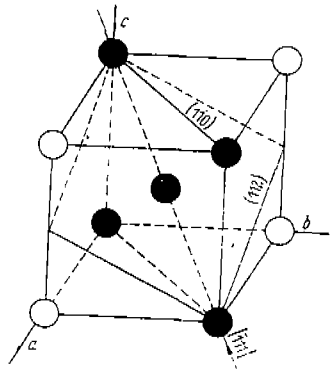

Fig. 9. Body centered cubic unit cell showing a twin plane (112) and a twinning direction $\bar{1}11$.

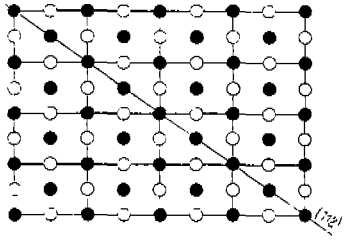

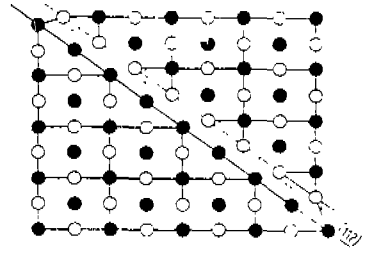

● Atoms in plane of projection
Atoms adjacent to the projection plane

Fig. 10. (110) projection showing position of twin plane and direction (18).

Fig. 11. (110) projection showing twinning shear in $\bar{1}11$ direction of the 1st atom layer (18).

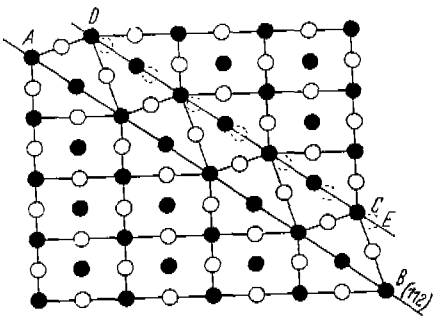

Fig. 12. (110) projection showing twinning shear in 111 direction applied to two atom layers (18)

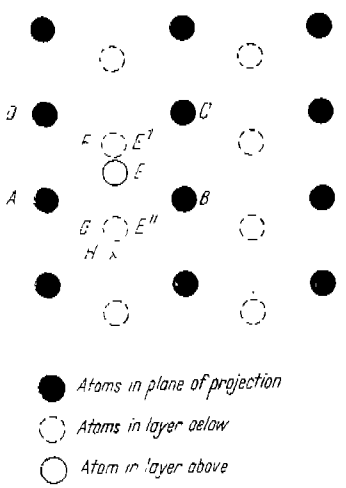

Fig. 13. Plan view of (112) plane (18).

been produced by the movement of the upper right-hand block of atoms downward and to the right in the $[11\bar{1}]$ direction, but in this case the shearing distance is twice as great or

$$d_{11\bar{1}} = n \frac{\sqrt{3}}{3} a_o$$

A plan view of a (112) plane makes this readily visible (See Fig. 13).

The movement of E to E' represents twinning in the easy or $[\bar{1}\bar{1}1]$ direction. Here the motion of atom E is guided by the atom pairs BC or AD. The movement of atom E to position E" represents $[11\bar{1}]$ or hard twinning. In this instance, atom E must ride up and over the barrier presented by the atom pair AB. Barrett[19] has postulated that the E-E" movement should require more energy than the E-E' movement and that, if this energy were supplied to atom E, it could possibly carry it further to position H. This movement of atom E to position H is that of slip on the (112) plane. Barrett also believes that the movement of only one layer of atoms from E to E' positions would not relieve the applied stress; hence, other layers would move. These secondary stress relieving movements should occur on adjacent planes since they would not create new twin interfaces.

Barrett[1] has shown that, although $\{111\}$ or $\{112\}$ twinning in face-centered cubic metals produces the same orientation, $\{112\}$ twinning forces certain atoms to become 0.048 a_o distant instead of the normal 0.707 a_o. $\{111\}$ twinning causes no change

in interatomic distance. In the body-centered cubic lattice {111} twinning would cause a 30% decrease in spacing while {112} twinning involves a decrease of only 5.8%.

Critical Resolved Shear Stress as a Twinning Criterion

There is no conclusive evidence for the existence of a critical resolved shear stress for twin formation. Barrett[1] believes that one exists since an increase in the resistance to twinning with decreasing temperature has been reported. Schmid and Boas[20] feel that such a critical twinning stress has not been defined. They believe that there are four reasons for this; namely, (1) twinning is discontinuous, (2) crystal faults affect the twinning stresses by factors of two or three, (3) the process of slip may accompany twinning and affect the measurements, and (4) the work of Gaugh and Cox[21,22] indicates that a single stress law does not govern twinning.

Yakovlera and Yokutovitch[23] found that decreasing the diameter of cadmium crystals from 0.7 mm to 0.1 mm increased the twinning stress ninefold but only the stress for slip by a factor of two. More recently, King[24] has reported a critical resolved shear stress for twinning in cadmium crystals of various purities. Vogel and Brick[9] and Steijn and Brick[14] have concluded that no critical resolved shear stress for twinning in α-iron exists even though it preceded fracture in all tests at -150°C and below. The support offered for this conclusion is that twinning occurred on certain (112) planes that

bore resolved shear stress considerably lower than the maximum. Also twins occurred in the shoulder of the test specimens where the area was approximately four times as great as the minimum section.

Energy Criteria for Twinning in Metals

The rapid rates of loading encountered in impact testing favor the formation of twins. An immediate release of this shock load seems to promote twin formation also. On the contrary, the slip process is retarded by shock loading, thus giving the impression that the movement or diffusion of dislocations through the lattice requires the application of the stress causing these movements over a critical period of time; the extent of the time depending upon the testing temperature. While slip is prone to cause small amounts of shear on large numbers of adjacent planes, twinning usually occurs over a stack of planes of greater height but in a lesser number of sites. These considerations led to a great deal of postulations that an energy change was the driving force for twin formation.

The energy asscciated with twin formation is released as heat except for a small amount retained in the twin interfaces and some lost by sound wave propagation. Chalmers [25] found the predicted temperature rise in β-tin to agree with experiment; however, it was not sufficient to cause localized melting. Attempts have been made to correlate the

width and number of twins formed with the energy supplied in hopes that a constant energy per unit volume would result. At present, no data are reported.

Miscellaneous Observations

Low[26], working with large grained polycrystalline specimens of pure and recarburized α-iron, found that in the carbon-free specimens twinning occurred only during fracture. This was evidenced by the observation that twins were found only adjacent to the fracture. The specimens containing small amounts of carbon twinned both previous to and during fracture. From this he concluded that twinning was not the cause of the low temperature brittleness of iron.

Paxton[27] measured the shear angles of twins in α-iron by optical reflection methods and proved conclusively that the (112) plane and the [111] directions were correct. For the two specimens investigated, he found eight sets of twins, three of which could not be expected to appear in tensile deformation. These he termed "accommodation twins" and cited that they probably occurred to relieve localized strains set up by the other twin systems.

As for slip, there are two main groups of thought as to the criterion for the initiation of twinning. The first, the critical resolved shear hypothesis, has received the most comment and appears to be favored although much conflicting data is reported. The unfavorable aspects are the lack of a

truly constant resolved shear stress and the discontinuous nature of the process.

The second viewpoint is that of energy association. This appears to have some basis for being correct, but the experimental work is scant, and no conclusions can be drawn concerning its validity. All in all, it can be stated that twinning is an extremely complex process, affected by so many variables that few reliable investigations have been performed that do not include the measurement of other phenomena with twinning.

C. Cleavage

The literature on the general problem of fracture of metals is perhaps the most voluminous of any metallurgical subjects, and yet almost nothing is known about the fundamentals of metallic fracture. The particular type of fracture known as cleavage has been investigated to a small extent in polycrystalline metals of all crystal systems and for single crystals of certain hexagonal metals such as zinc, cadmium, etc. A search of the literature reveals almost no work on the cleavage of the body-centered lattice. This section of the literature review will be composed of a short dissertation on the rules that apply generally to single-crystal cleavage and the few inconsequential bits of experimental data.

General Considerations of Cleavage

Under certain experimental conditions, low temperatures,

high strain rates, and special orientations, single crystals will fracture by cleavage on low index crystallographic planes. The yield point, elastic limit and fracture point may be coincident in which case the term "true brittle behavior" may be used; however, plastic deformation in the form of slip or twinning may precede cleavage.

The concept of a critical resolved shear stress was proposed as a criterion for the initiation of slip and twinning and a similar theory, the critical resolved normal stress theory, has been proposed for cleavage failure. This theory applies only when the fracture is a flat plane surface, and the stress for cleavage may be calculated from the relation

$$N = \frac{F}{A} \cos^2 \phi$$

where N = resolved normal stress

F = axial load at fracture

A = cross sectional area of the crystal

ϕ = angle between the stress axis and the cleavage plane.

Barrett[1] has stated that the variations of N with temperature, in the very few cases that have been reported, is insignificant. The matter of the variance of N with previous deformations are a good deal more uncertain. Early experiments on single crystals of zinc indicated that prior deformation lowers N.

Studies by Ludwik[28] on polycrystalline materials led various observers[29--32] to postulate curves of fracture stress versus amount of plastic flow that showed increasing fracture

strength with increasing prior deformation. Zener[33] points out that this concept should be re-examined. The flow stress curve was defined as the plot versus strain of the tensile stress necessary for continued plastic flow. The fracture stress was then defined as the plot against strain of the tensile stress which would be needed to produce fracture if plastic flow did not occur. Zener says that "according to our present viewpoints regarding the initiation of fracture in metals, fracture cannot occur independently of deformation, and therefore there is grave danger that the concept of the fracture stress curve is purely a figment of our imagination."

Theories of Cleavage Strengths

The theoretical strength of metallic perfect crystal has been calculated from the energy required to form the two surfaces of the cleavage planes and been found to be 10^2 to 10^3 times greater than observed. The reasons for the lack of metal crystals to achieve theoretical strength have been attributed to pre-existent microcracks, cracks formed during deformation, and other inhomogeneities such as grain boundaries, inclusions, etc.

In cubic crystals, particularly body-centered cubic ones, it has been often proposed that the problem of fracture can be resolved by studying the relative stresses for slip, twinning and cleavage. Barrett[1] states that "when a stress is applied to a crystal, it should cause slip, twinning, or cleavage, depending on whether the resolved stress on the slip plane in the

slip direction, or on the twinning plane in the twinning direction, or normal to the cleavage plane is first to exceed the critical value for the process concerned."

Experimental Work on α-iron Crystals

Schmid and Boas[20] show a macro-photograph of a cleavage plane of α-iron which exhibits a rough striated appearance. Paxton's[27] crystals fractured with almost no plastic flow and he recorded the fracture stress to be ≈27 kgm per sq. mm. Steijn and Brick pulled several single crystals to fracture at various temperatures. The results of their investigation are shown in Fig. 14. It can be seen that the cleavage stress increases with the amount of strain at constant temperature. This curve does not tell anything of the effect of orientation, and even worse the authors did not report whether their "fracture stresses" were critical resolved normal stresses or tensile stresses. It appears from the text of their work that the stresses are true stress (load at fracture divided by the area of the fracture cross section.)

II. EXPERIMENTAL PROCEDURE AND TECHNIQUES

In a fundamental investigation one would desire, as a starting material, a quantity of the metal being studied in its "purest" and "cleanest" form. With this in mind, the first attempts to grow single crystals of iron were made with

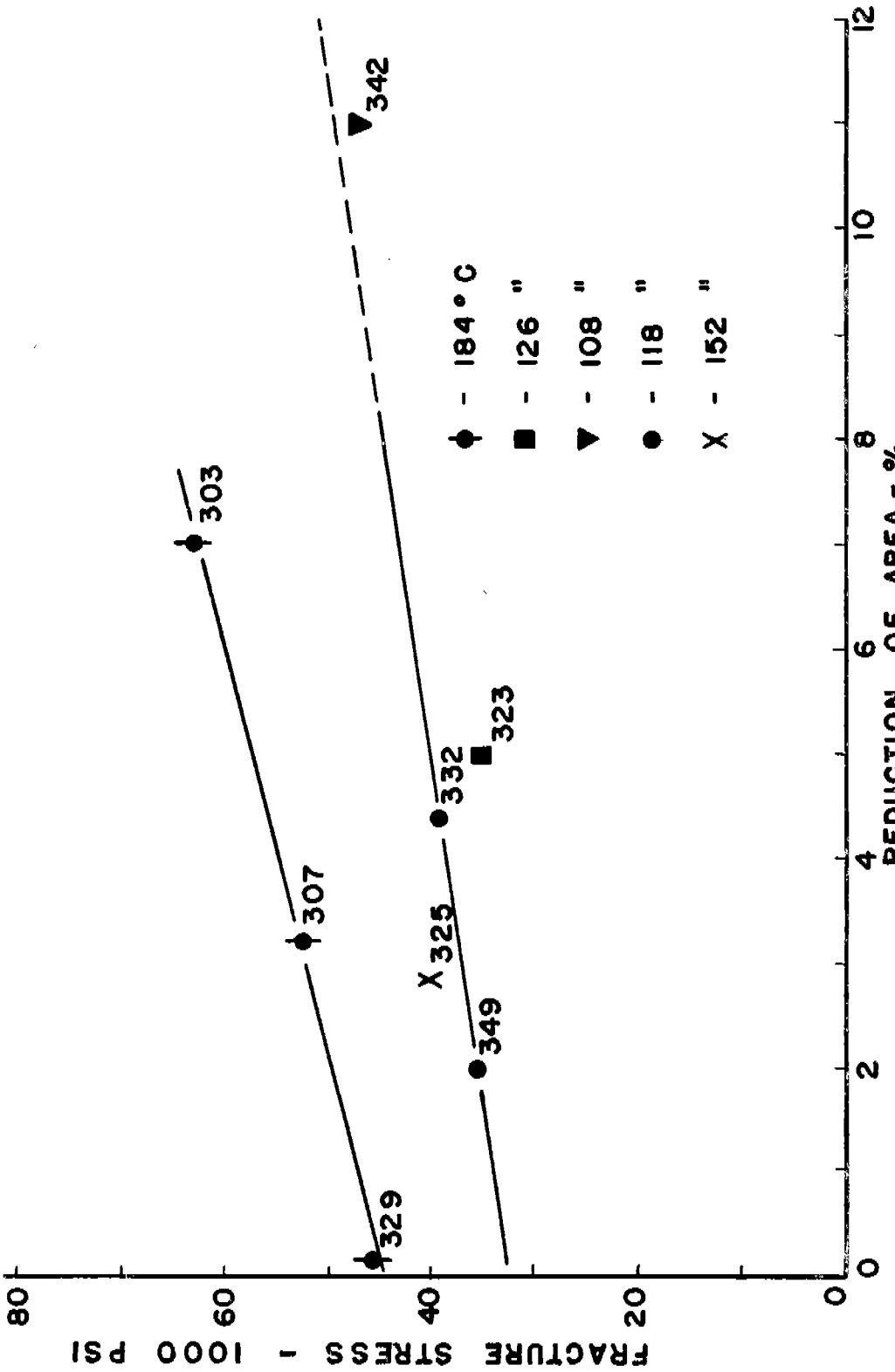

FIG. 14
FRACTURE STRESS VS. STRAIN FOR CLEAVAGE AT VARIOUS TEMPERATURES.
(AFTER STEIJN AND BRICK (14)).

various "high-purity" irons available commercially.

Westinghouse Puron was investigated and discarded despite its relatively high purity because of the prohibitive number of inclusions. Carbonyl iron was eliminated from consideration because no adequate vacuum melting facilities were available to cast it into usable form. National Research Corporation vacuum melted iron appeared to be the best choice both with respect to purity and inclusion count.

Attempts at Growth by Various Methods

Several ten-pound ingots were purchased and cut into specimens of various shapes. It was decided that three methods would be investigated to find a satisfactory means of mass producing single crystals long enough for test purposes. These methods were: (1) strain-anneal; (2) strain-temperature gradient; and (3) transformation.

In simple terms, the strain-anneal method consists of plastically deforming a series of test specimens in varying amounts and then allowing them to recrystallize at some temperature below any phase change; for iron, this would be the α to γ transformation at 910°C. The strain-temperature gradient method is really just a modified form of the strain-anneal method where, instead of allowing the whole specimen to heat to some subcritical temperature at a low rate, the specimen is drawn through a furnace with a temperature gradient. Usually the specimens

used in this method are deformed by rolling, drawing, or other methods of severe plastic deformation. The transformation method uses the technique of the strain-temperature gradient method but a different principle. Here the specimen is held in a part of the furnace where the temperature is higher than 910° (Ae_3). It is then drawn through the gradient, and supposedly a nucleus forms when the end of the specimen passes through the $\gamma \rightarrow \alpha$ transformation and grows at the rate at which the specimen is being pulled.

For the strain anneal experiments, ten series of twelve specimens each were strained in tension from 1.75 to 4.0 per cent elongation in two inches in increments of 0.25 per cent. Each series was heated at 5°F per hour to a temperature of 880°C, held for ten hours and cooled to room temperature. The series having a strain of 3.25 per cent elongation yielded two single crystals about one and one-half inches in length. These crystals were bounded by other very large crystals that extended to the ends of the test specimen. When the same strains were used on a similar series from a second N.R.C. ingot no single crystals were produced.

For the strain-temperature gradient work, again ten series of twelve specimens each were machined into rectangular bars 1/2 inch by 1/2 inch by 10 inches long. These were rolled from 30 to 75 per cent reduction in thickness in increments of five per cent. Each series was heat treated by drawing

through the gradient furnace at various speeds. Rates from 0.1 inch per hour to 10.0 inches per hour were used without success. Recently, Low[34] has grown long single crystal wires of N.R.C. iron by this method. Perhaps the section size is the critical parameter.

The transformation work was initiated with cylindrical rod specimens 1/2 inch round and six inches in length. At first, draw speeds were on the order of six inches per hour, and then were decreased until the first noticeable change in grain size was produced. It was found that, as slower and slower draw speeds were used, the grain size increased to a maximum and then leveled off. The greatest grain size produced was about 10 millimeters of length and extended completely through the cross section. Tapering the specimens so that the section where the first nucleus formed was small, had no beneficial effects.

These initial experiments indicated that the strain-anneal method prossessed the most possibilities of producing large crystals, but that reproducibility among the various ingots of National Research Corporation Iron was not to be expected. Since larger heats of this material were not available, it was decided to abandon it in favor of another. The other alternatives were Armco Iron and decarburized mild steel. These were compared with respect to purity and inclusion rating and SAE 1008 steel, silicon killed, was chosen on the

basis of its cleanliness and availability.

Specimen Preparation

The starting material was received in the form of a 400-foot coil of 3/4 inch round hot-rolled stock. The "as-received" grain size was ASTM #7-8. A representative photomicrograph of this material is shown in Fig. 15. An unetched sample showed the material to contain fewer inclusions, especially FeO, than even the "high purity" laboratory irons previously described. The heat analysis accompanying the steel listed the impurities as follows:

C	Si	Mn	P	S	Cr	Ti	Mo	Ni	Cu
0.09	0.14	0.46	0.010	0.027	0.08	0.01	0.01	0.07	0.05

Specimens were machined from the stock to the dimensions shown in Fig. 16. It was believed that the radius of the shoulder portion would be a critical factor in determining the critical strain. Later results from specimens of radically different design showed this to be incorrect. The long gauge section was used in order that the ratio of gauge length to gauge diameter should always exceed the usual minimum accepted value of four to one. The diameter was maintained as large as possible with respect to the over-all geometry of the specimen so that the radius of curvature would not be so great that experimental errors in the optical measurements would be excessive.

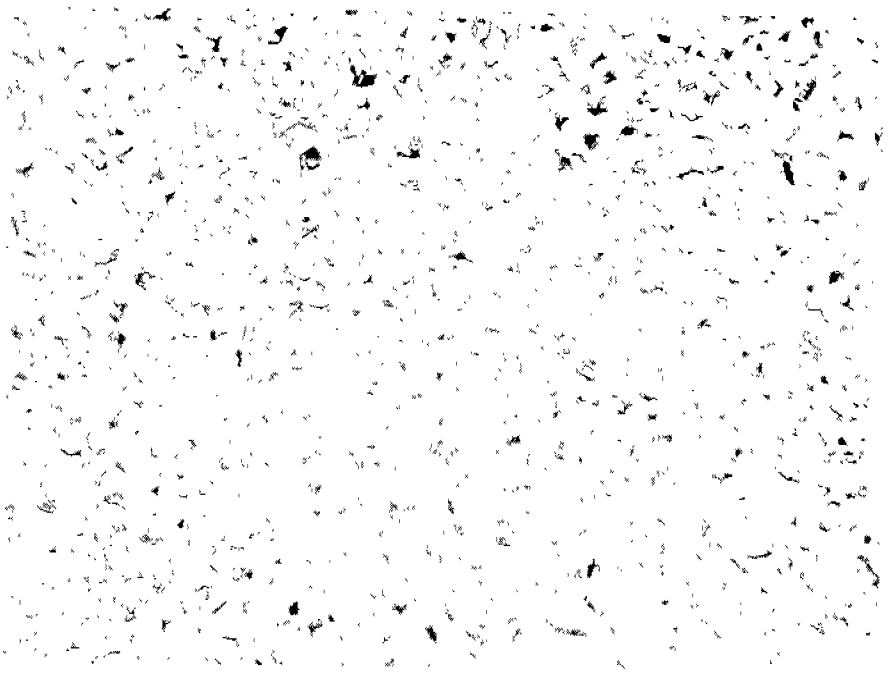

Fig. 15. SAE 1008 stock as received. (X100)

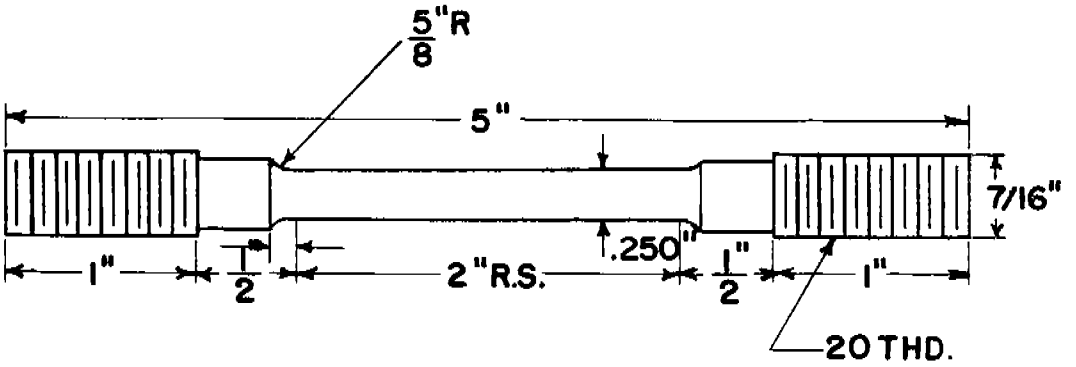

LONG SPECIMENS FOR SLIP AND TWINNING STUDIES.

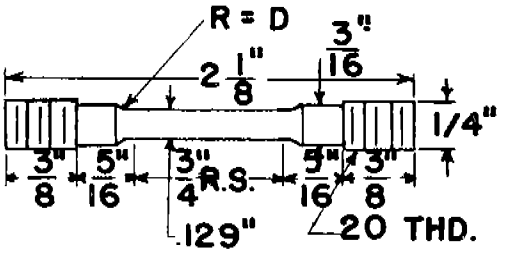

SHORT SPECIMENS FOR FRACTURE STUDIES.

FIG. 16

Decarburization: Equipment and Technique

The decarburization of specimens occupied an important phase of the investigation and hence should be dealt with in some detail. The mechanism of the water saturated-hydrogen decarburization of metals is not well known, but the techniques involved have been studied extensively.

Furnace Construction

The heat treating furnaces were constructed about a 3 1/2-inch Inconel tube, 48 inches long. This tube was wrapped in mica sheet to insulate it from the resistance windings. Many high temperature "burn-outs" led to the belief that the organic binding material of the mica sheet was embrittling the resistance wire. To prevent this, a burning-out treatment was used which consisted of inserting a high-pressure blow torch first into one end of the tube and then the other and allowing the binding material to ignite. An eight-hour treatment proved sufficient to remove the sulfurous binder and prevent subsequent embrittlement.

Next, the first layer of windings of #9 Kanthal wire was placed on the tube directly over the mica sheet. The spacings are shown in Fig. 17a and must be determined empirically from the heat flow characteristics of the furnace geometry. The tube was then painted with several coats of special "low-silica" alundum cement. This special adhesive again prevents attack

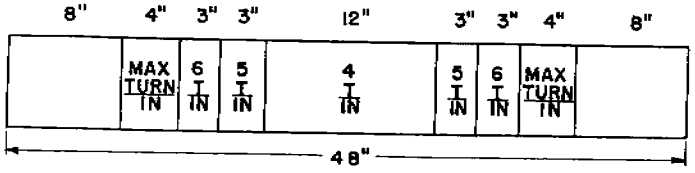

FIG.17a

INSIDE WINDING
COLD RESISTANCE 11 Ω

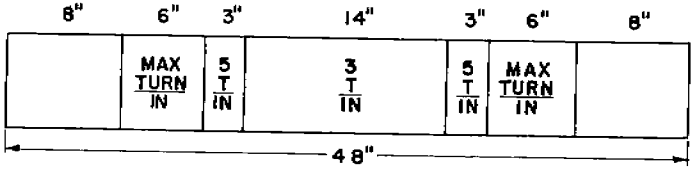

FIG. 17b

OUTSIDE WINDING
COLD RESISTANCE 11 Ω

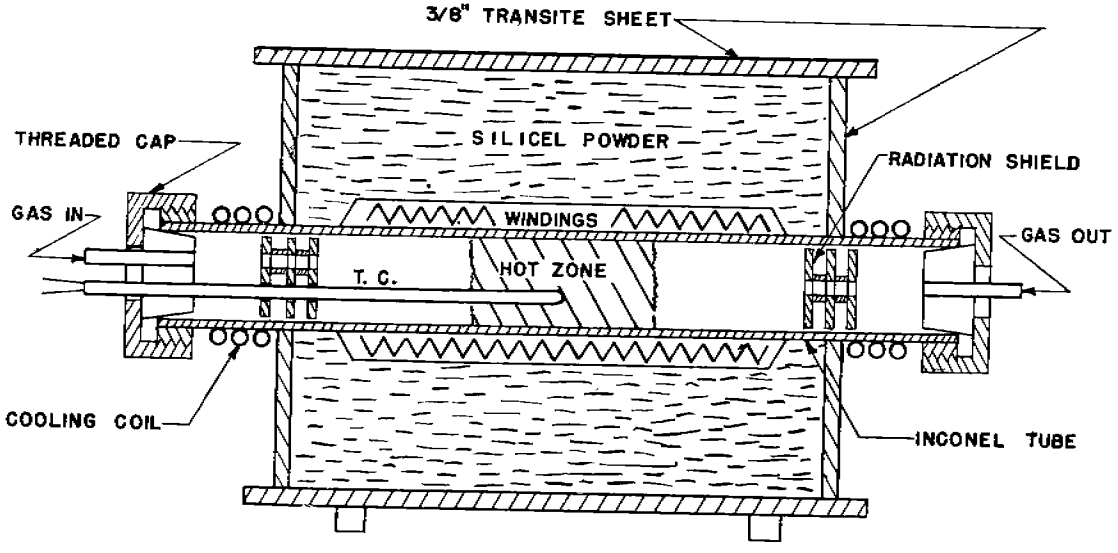

FIG. 18

CROSS SECTION OF DECARBURIZATION AND ANNEALING FURNACE

by silica on the resistance windings. Sauereisen electrical resister cement was applied as a pasty mixture until the outline of the wire windings could not be seen and then a few more coats were applied for added strength. Next, a few more thin coats of the low silica cement were applied to protect the next winding from silica attack. The second layer of windings is spaced according to Fig. 17b. More alundum cement and then a final thick coating of Sauereisen cement completed the heating element assembly.

In metallic tube furnaces, some method of cooling must be provided for the ends of the furnace to prevent burning of the seals. For this purpose, three coils of 3/8 inch copper tubing were wound around the extreme ends of the Inconel tube and soldered to effect good conductivity. Water was circulated through these tubes and extracted enough heat to protect the end seals.

Sealing was accomplished through the use of threaded cap screws with hollow centers and a flange that forced the tapered rubber stoppers into the end of the furnace tube. Glyptal was used around the stoppers as a precautionary measure. This arrangement proved quite satisfactory both with respect to leakage and easy accessibility to the interior. Such a furnace is suitable for use with negative or positive pressures and under various atmospheres. A cutaway view of the complete furnace assembly is shown in Fig. 18.

Gas Purification, Saturation and Distribution

Since one furnace was designated as a decarburization furnace and the other as a growth or annealing furnace, it was advisable to construct a universal gas purification, saturation, and distribution system. This arrangement is shown schematically in Fig. 19 and pictorially in Fig. 20. In decarburizing, a saturated gas is necessary, the degree of saturation depending upon the decarburization temperature. The per cent saturation was controlled by the temperature of the gas being saturated. This is best regulated by bubbling the carrier gas through the saturating liquid which is held at some predetermined temperature.

Ideally, decarburization should be done with iron in its α-form since the rate of diffusion of carbon in alpha iron at 700°C is about one hundred times as great as in gamma iron at 920°C. However, since power fluctuations caused the furnace to rise into the alpha and gamma phase field on occasion, it was decided to increase the decarburization temperature to 950°C where any fluctuations would not affect the diffusion characteristics appreciably. Knowing the temperature of decarburization, the iron-oxygen equilibrium diagram (see Fig. 21), and the vapor pressure of H_2O as a function of temperature (Fig. 22), one can easily calculate the correct saturation temperature for a given H_2/H_2O ratio. Very good control of this temperature was

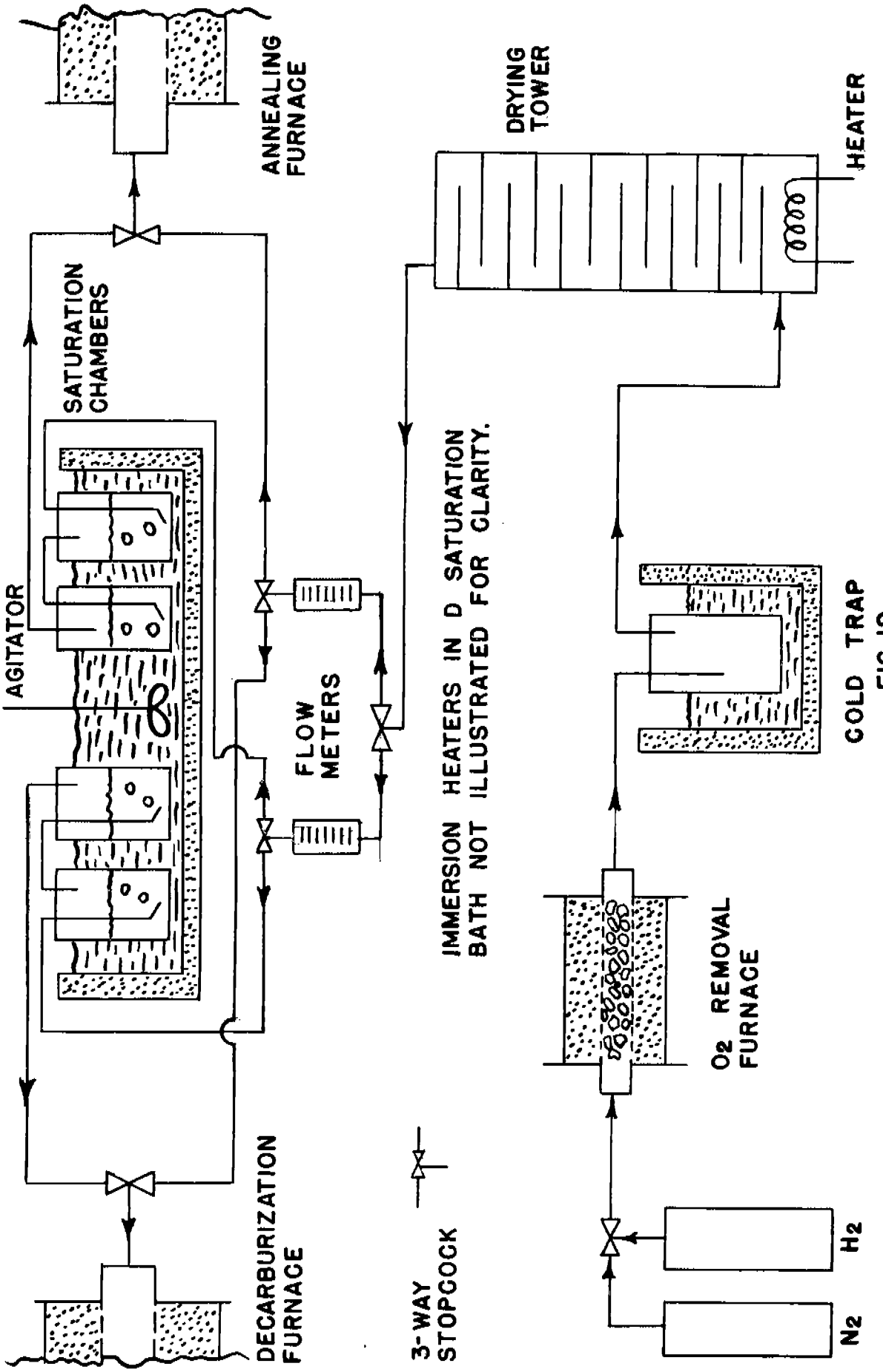

FIG. 19
GAS PURIFICATION, SATURATION, AND DISTRIBUTION SYSTEM.

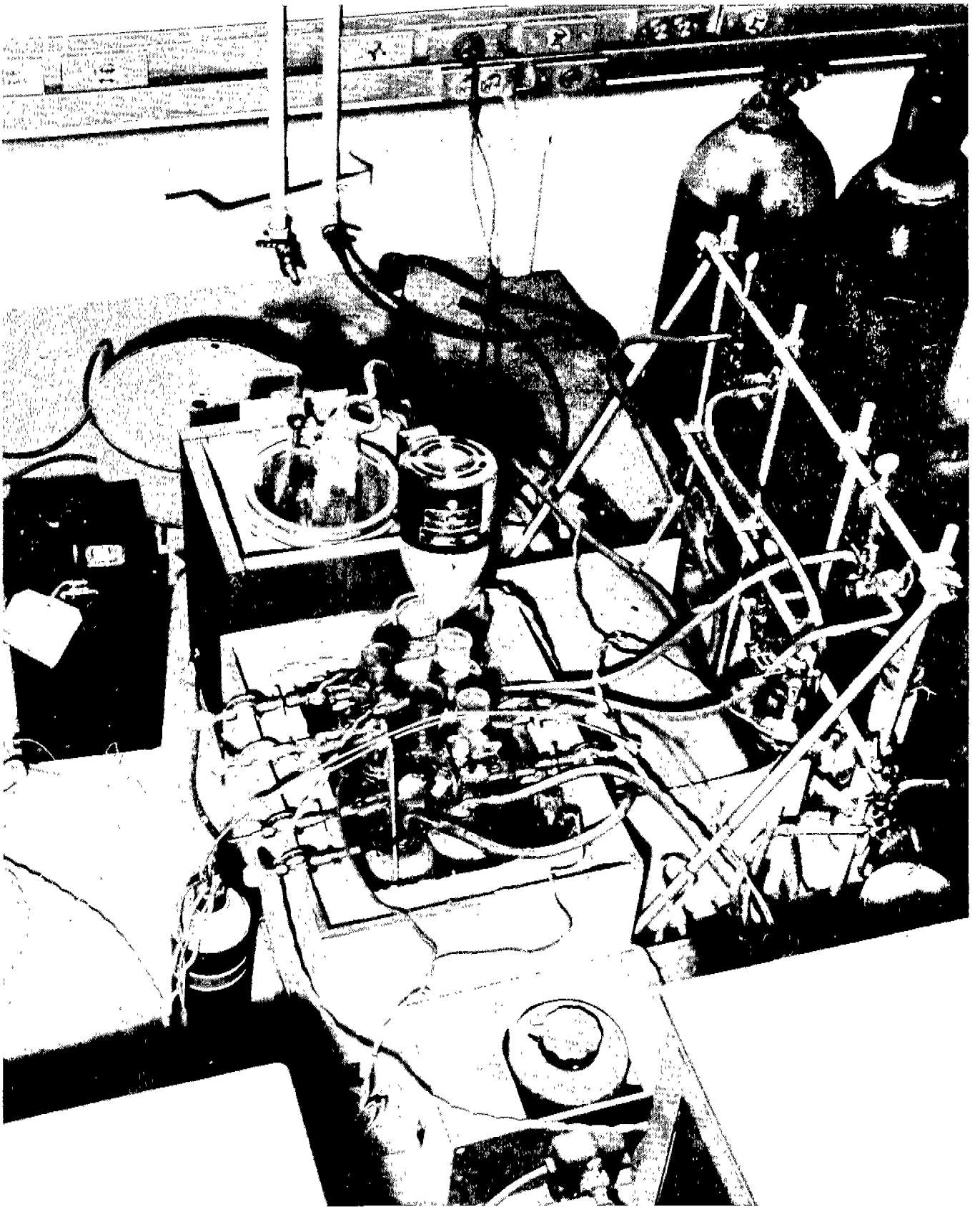

Fig. 20. Gas purification, saturation, and distribution system.

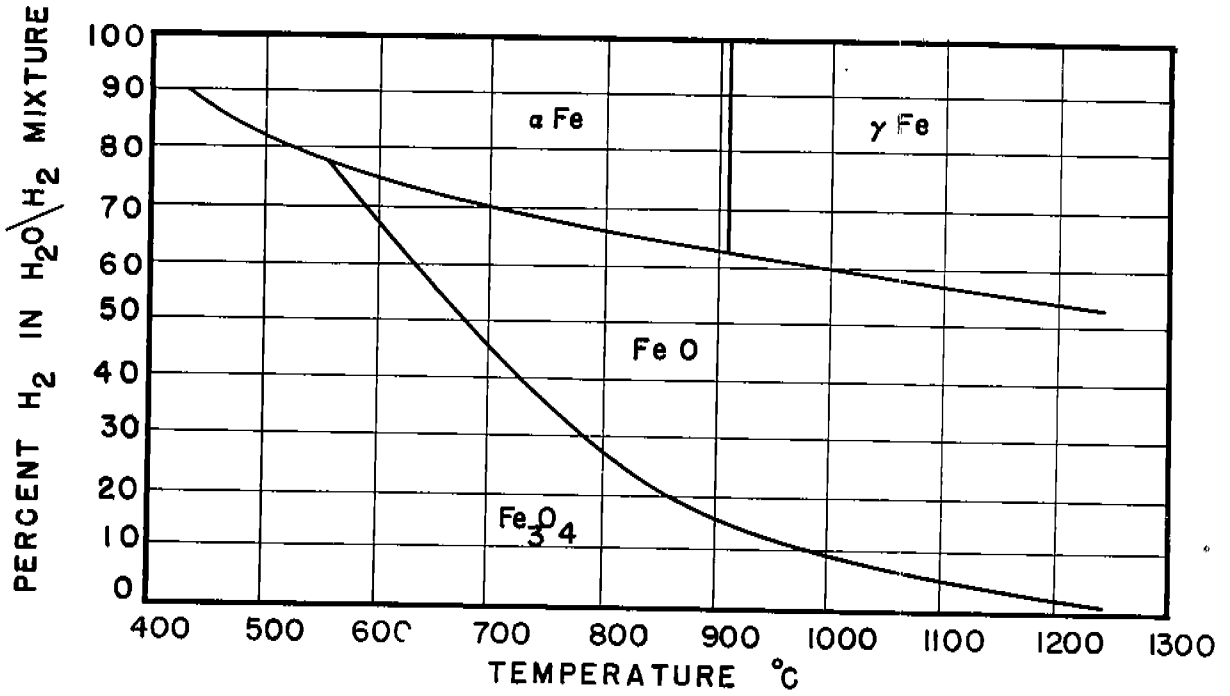

Fig.21 The H_2-H_2O Iron oxide equilibrium diagram.

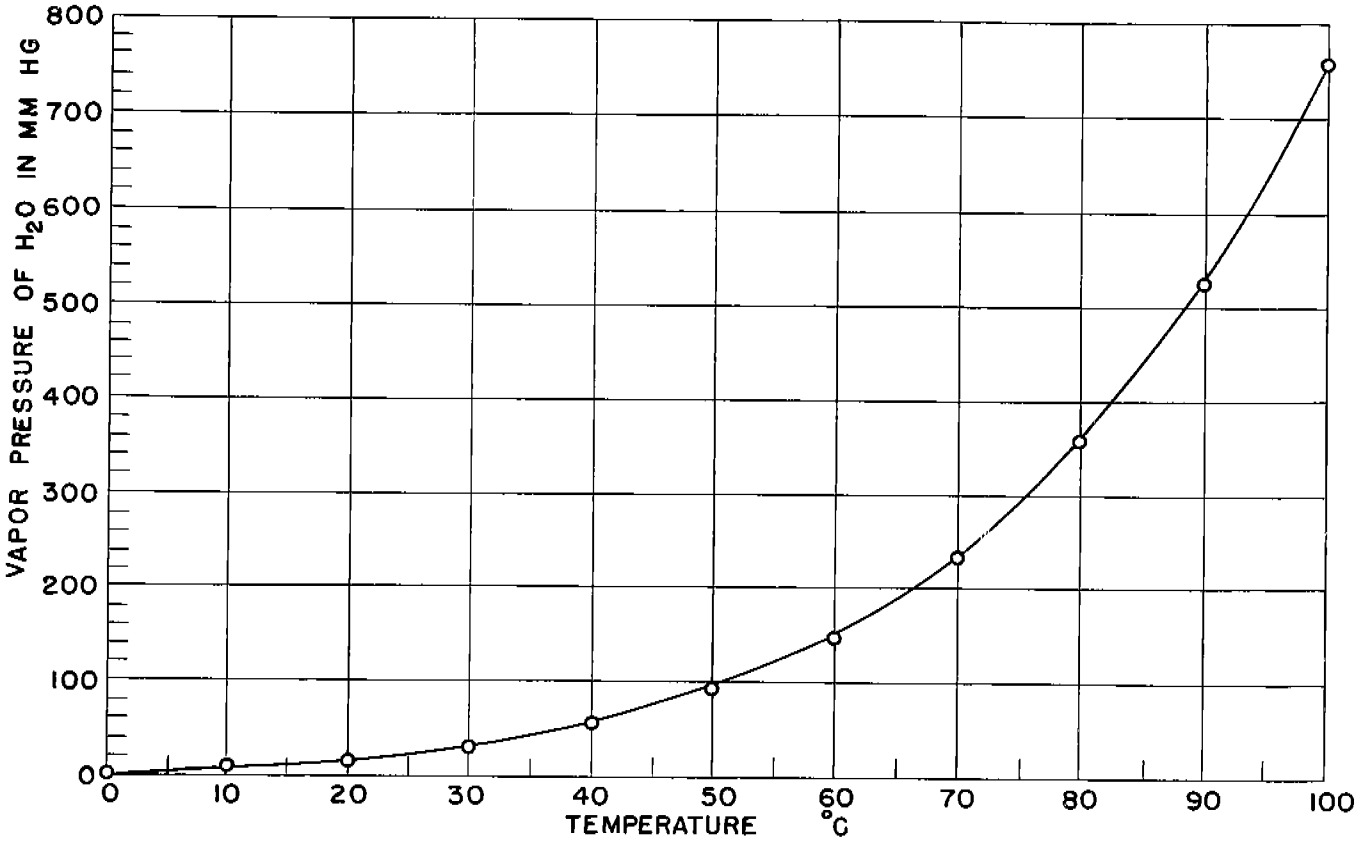

FIG. 22

DIAGRAM OF VAPOR PRESSURE OF H_2O VS. TEMPERATURE.

obtained with two immersion heaters, a mercury thermoregulator, and a bath of light-weight paraffin oil kept in motion with a mechanical stirrer. The current supplied to one heater was regulated until the equilibrium temperature of the bath was one to two degrees below the desired temperature. The second heater in conjunction with the thermoregulator controlled only the range between the equilibrium temperature of the first heater and the control temperature. Temperatures may be controlled within ± 0.02°C in this manner. The tube leading from the saturators to the furnace was kept above the saturation temperature to prevent precipitation of water from the carrier gas. The flow rate was regulated until a small flame could be struck and maintained at the exit end of the furnace.

Technique

A series or batch of specimens consisted of a group of thirteen placed in two racks as illustrated in Fig. 23. These racks were placed on either side of the exact center of the furnace tube. Constancy of temperature was maintained ± 2°C in a 15-inch region of the furnace, so all portions of the specimens were at the same temperature. The furnace was first flushed with nitrogen to remove any air, then dry hydrogen was used until the specimens reached the decarburization temperature. After reaching temperature, the furnace was switched to the wet hydrogen mixture. Caution must be exercised

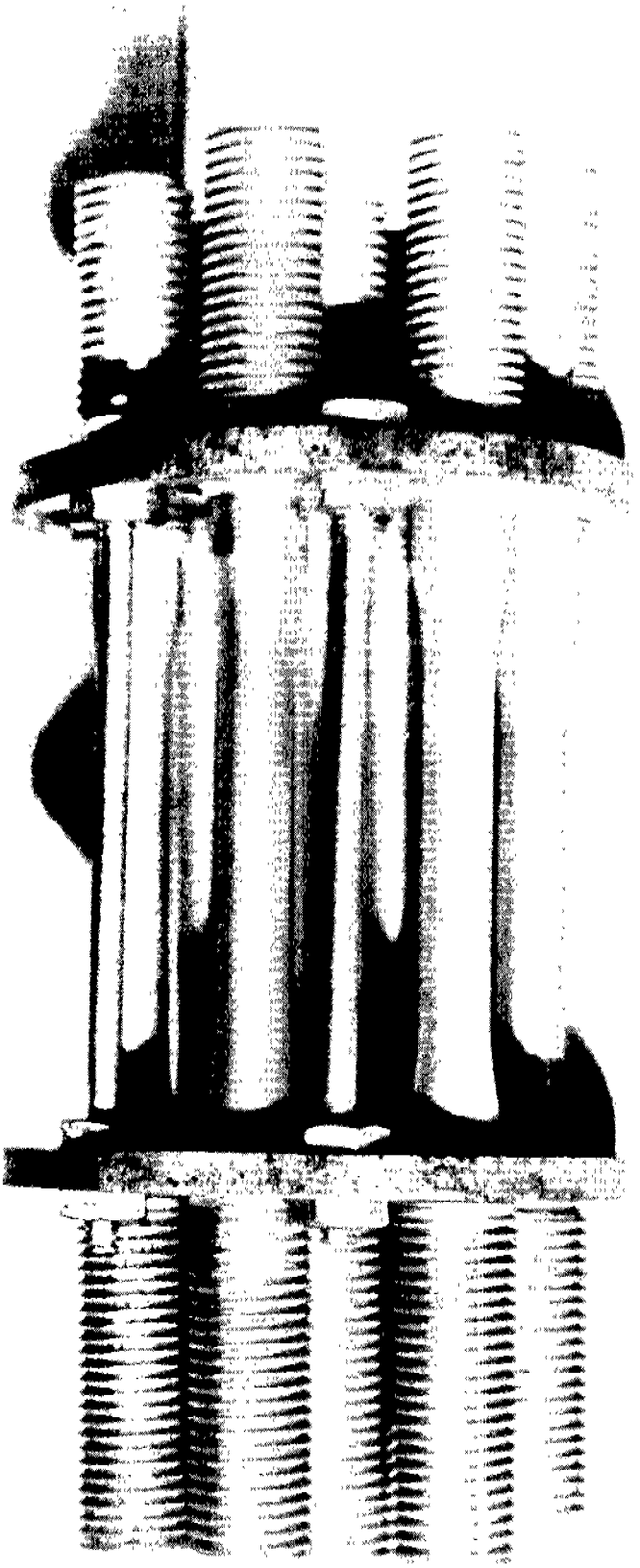

Fig. 23. Specimens in rack for decarburizing or annealing.

that no wet gas be allowed to contact the specimens while they are in the two phase ($\alpha+\gamma$) region or else columnar grains will grow from the surface of the specimen inward as a result of diffusion in a two-phase region. These grains are impossible to refine into an equiaxed structure and therefore void the specimens for further use.

After decarburization had occurred for one hundred hours, a resistance of four ohms was inserted in series with the windings. This resistance was sufficient to decrease the equilibrium temperature of the furnace to about 840°C and hence cause it to cool to this temperature at a rate slow enough to produce a grain size of ASTM #3-4. This grain size is ideal for straining. It is big enough to permit critical strains which are large enough to be measured easily and yet small enough to permit a homogeneous strain. The atmosphere was changed to dry hydrogen for the cooling treatment so that no bluing of the specimens would occur. A representative photomicrograph of the structure is shown in Fig. 24. A typical analysis of the decarburized material is 0.019% carbon, .009% oxygen, .0003% hydrogen, and .0018% nitrogen. The analyses of the other elements remains the same as in the original steel.

Determination of the Critical Strain for Exaggerated Grain Growth

After decarburization, the specimens were prepared for

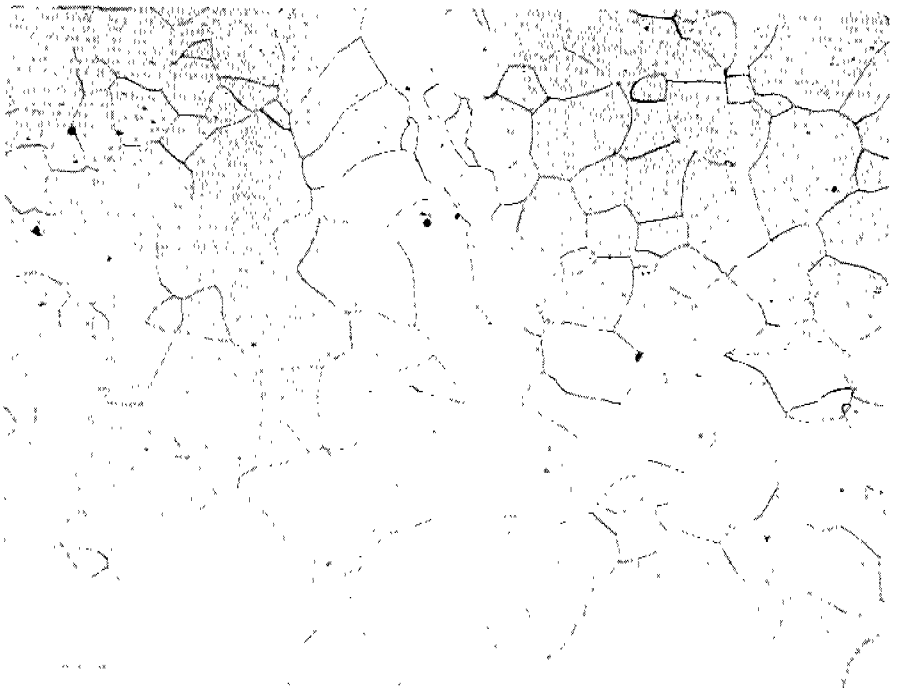

Fig. 24. SAE 1008 "as decarburized." (X100)

straining by marking with one inch gauge scratches. The marking device is shown in Fig. 25. This tool was clamped in the tool rest of a metal working lathe, and the specimen placed between the centers. The jig was advanced until it touched the gauge section, and the specimen rotated until a scratch of about ten degrees of arc length was produced. Very light pressure of the jig was used since the soft material of the specimen was easily indented. The gauge marks were one inch in length plus or minus a fraction. The accuracy was not important since individual specimens were measured before straining.

Straining was performed on the 2400-lb. range of a Baldwin Southwark Universal Hydraulic Testing Machine. All elongations were measured with a Gaertner optical cathetometer having a sensitivity of ± .00005 inch. This is greatly in excess of that needed for such measurements. The first series was strained from 2.0 to 4.0 per cent elongation in one inch, measured in the relaxed state, in increments of 0.2 per cent elongation. The series was then placed in the annealing furnace and heated rapidly to 350°C under dry hydrogen. Upon reaching 350°C, the program controller was activated and a heating rate of 5°F per hour was applied. This heating rate was maintained until the bars reached 880°C at which temperature the furnace was maintained for 80 hours and then allowed to furnace cool to room temperature.

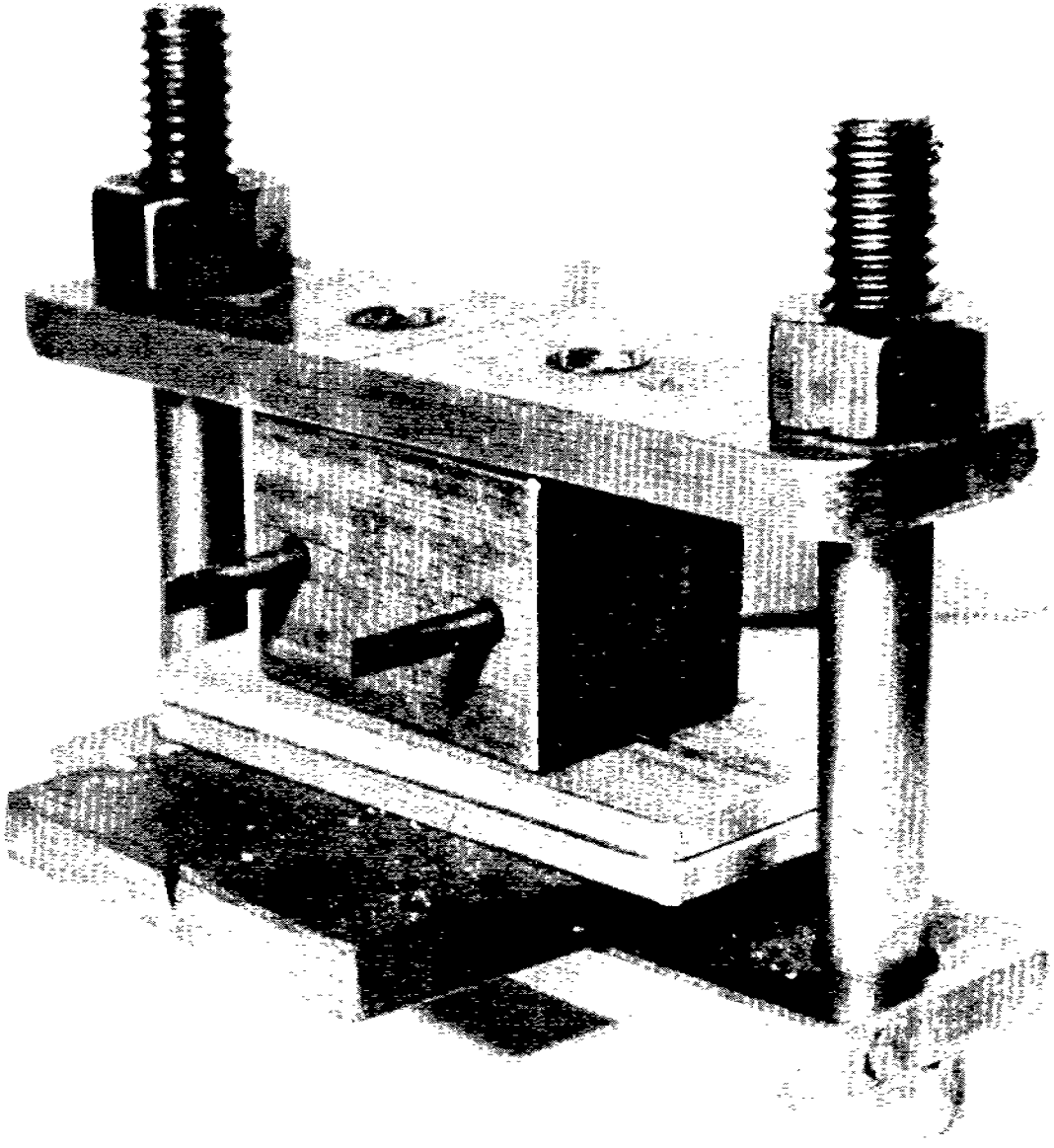

Fig. 25. Tool for making gauge marks on strain anneal specimens.

After removal from the growth anneal, the bars were found to have a coarse-grained surface made visible by heat etching. They were then sectioned longitudinally through the mid-section, polished through #000 metallographic paper and etched in 3% Nital. The complete series of specimens is shown superimposed on the theoretical grain size--deformation plot of Fig. 26. It can be seen that the critical strain lies at 3.2% elongation. The dotted lines indicate that this may be a range as subsequent tests have indicated. The single crystal extended throughout the gauge section and well up into the shoulders where it was bounded on both ends by a fine grained polycrystalline aggregate. It was thought that this would provide a single crystal which could be tested under conditions where the influence of the grips would be at a minimum.

The 3.2% strain was used for all subsequent series yielding about 50% usable single crystals. Later experiments on specimens of a one-inch gauge length gave yields of 95% single crystals. This indicated rather conclusively that the yield depended upon the length to which the crystals were required to grow. All specimens which were not single crystals were bi- or tri-crystals with their boundaries very nearly perpendicular to the specimen axis.

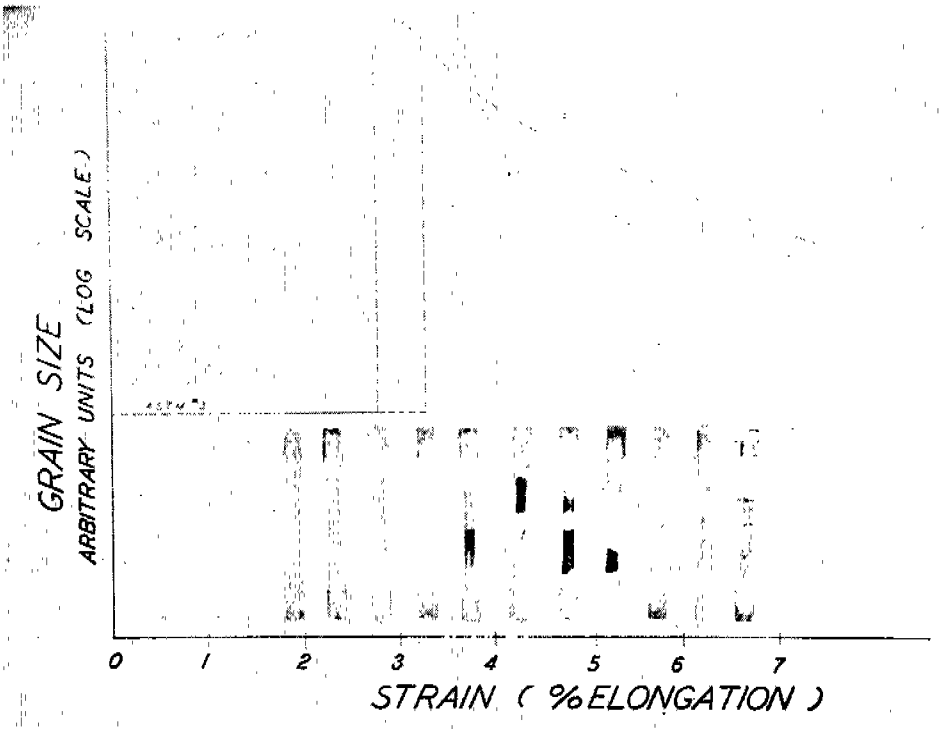

26. Grain size after annealing as affected by prior deformation. (Reduced approximately 4 times.)

Electropolishing

Needless to say, the cutting in half of a specimen to inquire of its "single crystalness" ruins it for test purposes. The technique of electropolishing seemed to lend itself admirably both to the removal of the fine grained surface layer and to preparation of the surface for X-ray and metallographic examination.

Although electropolishing has become widespread in its use, it is to be regarded more as an art than a science. What produced good results for one produced disastrous results for another. It was therefore found necessary to develop a procedure for the decarburized steel used in this investigation, and it will be described in detail. There are many hundreds of references to electropolishing techniques but none will be cited here. Any of the papers by Jacquet[35] serve as references to particular electropolishing procedures, as he has devoted his life to such studies. The following information may be regarded as a successful alloy of hearsay and experience:

For iron, the three electrolytes that have received most usage are perchloric acid-acetic anhydride, perchloric acid-ethyl alcohol, and chromic acid-ortho phosphoric acid. The perchloric acid is best for metallographic specimens where a uniform circulation of electrolyte across a comparatively small surface is possible. However, to polish the entire

gauge section of a cylindrical tensile specimen, the control of agitation necessary to prevent pitting and chalking is quite impossible. For this reason, the perchloric mixtures were discounted.

Various mixtures of chromic and orthophosphoric acids were investigated including those with additions of a few per cent of sulfuric acid. The composition which gave the best results was 10 per cent of dry chromic acid and 90 per cent, by weight, of orthophosphoric acid (85% strong). The sulfuric acid produced no visible benefits and was therefore omitted.

When a curve of voltage versus current is plotted for most electrolytes, a leveling off or plateau is found where, over a small range, an increase in current produces no change in voltage. The current values corresponding to this plateau are the ones chosen for polishing. No such effects were found for the electrolyte used in this work. Consequently, the method of trial and error was used until the correct value of 10 amperes per square inch was found to give the optimum results. The resulting voltage drop which depends on the cathode to anode distance was about 25 volts.

Most proponents of the chromic-orthophosphoric electrolyte suggest heating the bath to 70-80°C. In this work, it was found better to cool the bath so that the temperature was

never greater than room temperature. The large currents needed for the relatively large surfaces, and the rather low electrical conductivity of iron contribute to heating of the specimen. This heat was conducted away as rapidly as possible by a circulating water bath which surrounded the electrolyte container. A high-speed stirrer was used to prevent local overheating at the specimen-electrolyte interface.

A photograph of the electropolishing apparatus is shown in Fig. 27 and illustrates the relative position and size of the various components. The throwing power--or perhaps better, the throwing-off power--of this electrolyte is very low. Thus a cathode of similar geometry to the surface being polished must be used. In this apparatus, a stainless steel beaker served both as a cathode and a container for the electrolyte. A specimen can be seen mounted in its swiveling bracket, ready for immersion into the polishing bath. The ends of each specimen were protected from electrolytic attack by a coating of Halowax (chlorinated form) supplied by the Fisher Scientific Company. This wax has a melting point of 100°C and is easily peeled from the specimen after polishing.

The cooling bath of circulating tap water and crushed ice proved insufficient to conduct away the necessary amount of heat. Overheating of the specimen accompanied by severe pitting resulted. This could be stopped by turning off the current for one minute out of every two, but such an arrangement

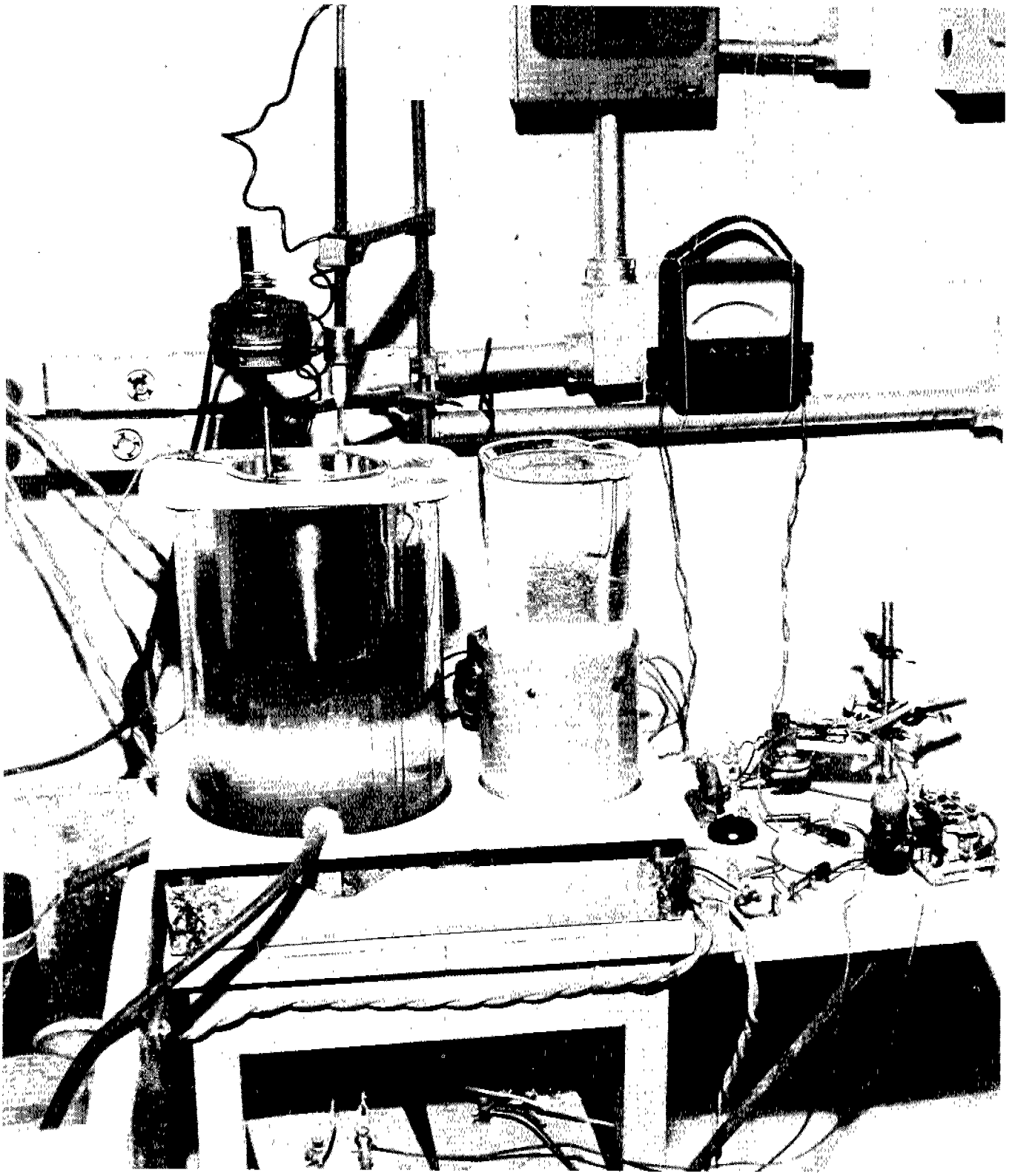

Fig. 27. Electropolishing apparatus.

requires careful attention and much time since about two hours are required to completely polish one specimen. An automatic switch was designed which permits current to flow for any desired time and then breaks the circuit for any arbitrary time (see Fig. 28). The timer consisted essentially of a synchronous motor attached to an elliptical bakelite cam. This cam activates the lever arm of a microswitch which in turn activates the main current relay. A cycle of 30 seconds polishing and 30 seconds rest was used, but any desired ratio could be obtained by varying the cam shape and the motor speed. This method reduced the polishing time to about 75 minutes.

A typical specimen after electropolishing and etching is shown in Fig. 29. The usual procedure was to lightly polish the crystal with #000 metallographic paper after removal from the growth treatment, then polish electrolytically to remove .01 to .02 inch of surface. Etching in .3% Nital revealed the grain structure and, if some small "grain islands" remained in the single crystal portion, the specimen was electropolished a little more and re-etched until an "island free" surface obtained. It was then given a very light touch with #0000 metallographic paper and a three-minute electropolish which readied it for X-Ray, and metallographic analysis.

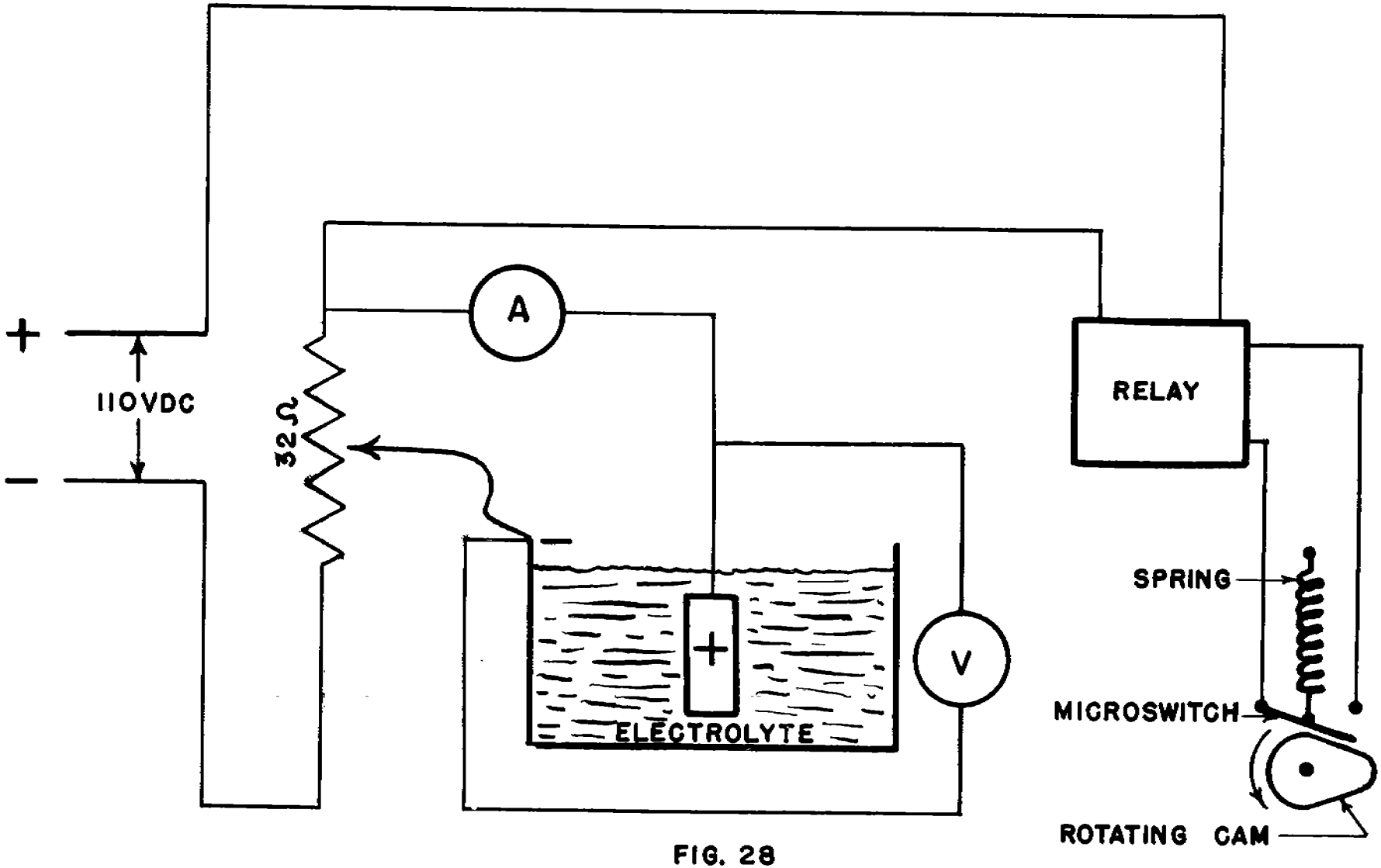

FIG. 28
SCHEMATIC REPRESENTATION OF ELECTROPOLISHER.

Fig. 29. Single crystal test specimens:

X-Ray Determination of Crystal Orientation

The orientation of a single crystal or an individual grain in an aggregate can be determined most conveniently and accurately by means of the back reflection Laue method[1]. This technique, which was developed by Greninger[36], has been summarized by Barrett[1] and described in detail by Opinsky[37].

There are essentially four steps in the determination of the angle between any crystallographic direction and a given geometric direction in a specimen. They are:

(1) To take a back-reflection Laue pattern of the specimen;

(2) To plot on a Wulff net, with the aid of the Standard Greninger chart, the stereographic projections of the specimen axis and the zone axes responsible for all the prominent hyperbolae on the X-Ray pattern;

(3) To draw all the great circles which are 90° away from the projections of the zone axes and examine them for the basic stereographic unit triangle, the vertices of which give the positions of the $\{100\}$, $\{110\}$, and $\{111\}$ projections;

(4) For complete indexing of all the intersecting points of the great circles, change the stereographic projection of step 3, by rotation, into one of the three standard forms, $\{100\}$, $\{110\}$, or $\{111\}$. By comparison of the pattern with the corresponding known standard pattern, these indices can be determined.

The angle between any crystallographic plane and direction, and the specimen axis can then be ascertained.

The radiation used in this work was that from a tungsten, targeted tube operated at 40 kilovolts and 20 milliamperes. Exposure times averaged two hours per specimen. Each film was developed in MQ Universal developer for five minutes, then fixed for 20 minutes and washed for one hour.

The complete camera assembly is shown in position on the X-Ray machine in Fig. 30. It consists of the X-Ray source, collimating tube, goniometer film holder, and protective lead sheathing. The film holder is that one designed by Opinsky[37] and permits only very small errors to be introduced from inaccuracies in specimen to film distance, warpage of the film, etc. There are four steel points inside the cassets which puncture the film and describe its position with respect to the specimen axis and the X-Ray source. This prevents confusion after development, and also permits accurate determination of the center of the X-Ray beam. The film size was always 5 inches by 7 inches and was covered by a piece of thin aluminum foil to reduce the effect of background scattering.

The goniometer-specimen holding jig is the most important part of the apparatus. It is illustrated in the horizontal or picture-taking position in Fig. 30, and a more detailed photograph is shown in Fig. 31. This jig allows the specimen to be

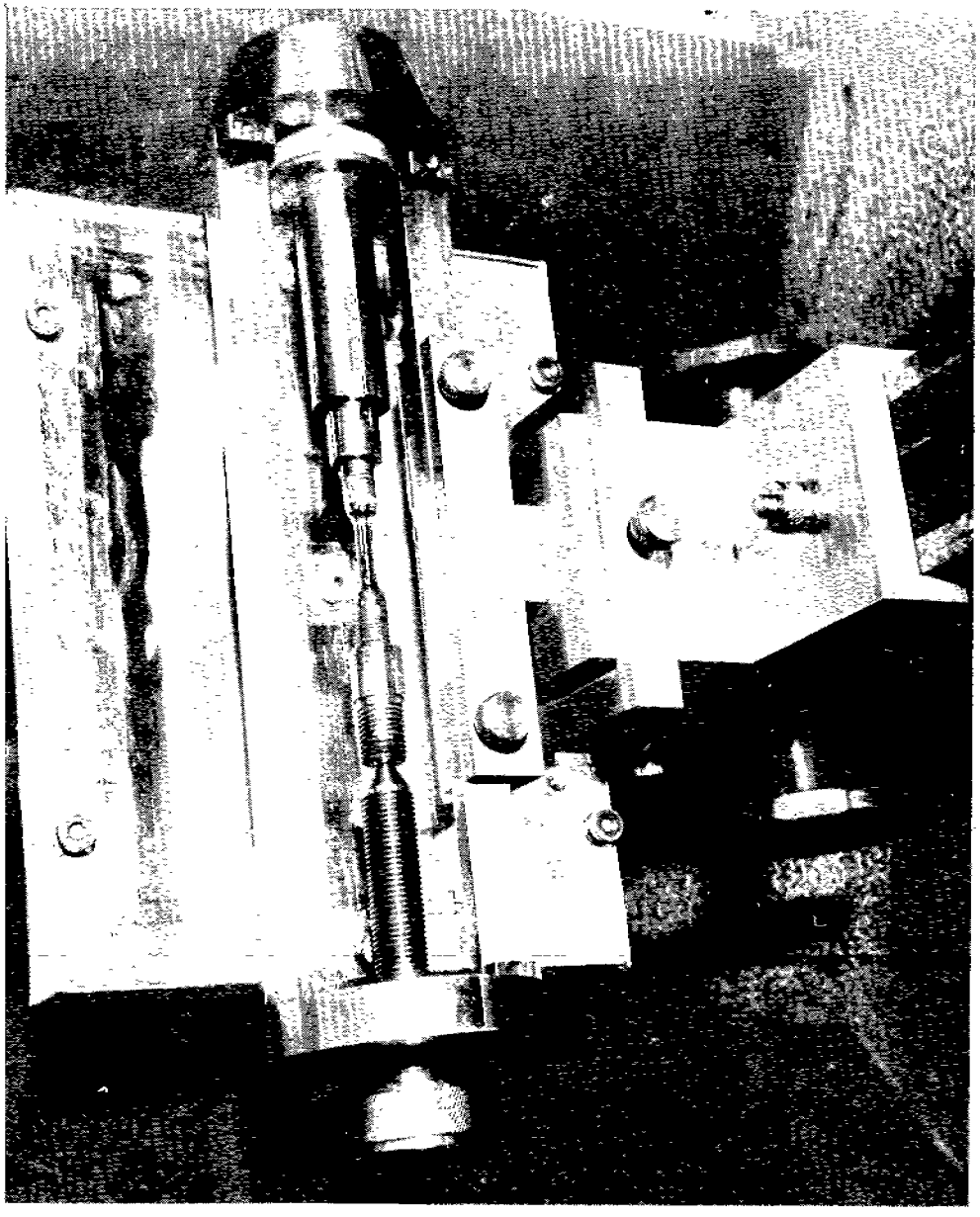

Fig. 30. Goniometer and precision Laue back reflection camera in position on X-ray machine.

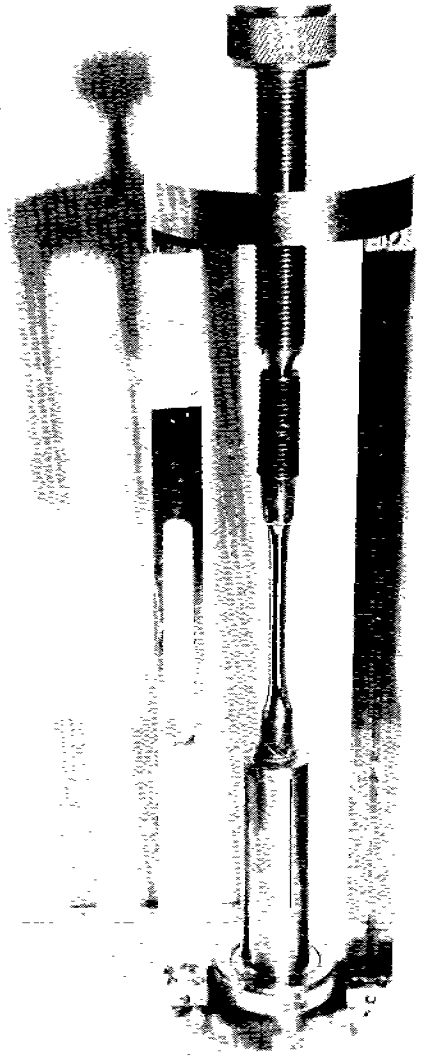

Fig. 31. Goniometer-specimen holder with long specimen inserted.

moved horizontally or vertically in the X-Ray machine as well as to be rotated about its longitudinal axis. The exact position of the specimen for each X-Ray exposure was determined by noting the readings on the horizontal, vertical, and rotational scales, hence the same point on the specimen could be reached by duplicating these readings.

The stereographic projections were always rotated to bring the specimen axis into the stereographic unit triangle of a $\{100\}$ standard projection bounded by the planes (001), (011) and $(\bar{1}11)$. Sometimes two rotations were necessary to do this. If the specimens were of such an orientation that this was very complicated, the opposite end of the specimen designated as F' was rotated into the unit triangle with vertices (001), $(0\bar{1}1)$, and (111). A typical standard projection showing the specimen axis as F is illustrated in Fig. 32.

Determination of the Glide Planes and Fracture Surfaces by Optical Trace Methods

An experimental study of the planes of deformation in a crystal lattice requires a method of detecting the orientation of the deformation marking on the specimen surface and then translating these data to the orientation of the crystal lattice. When the crystal orientation, the slip (or twin)

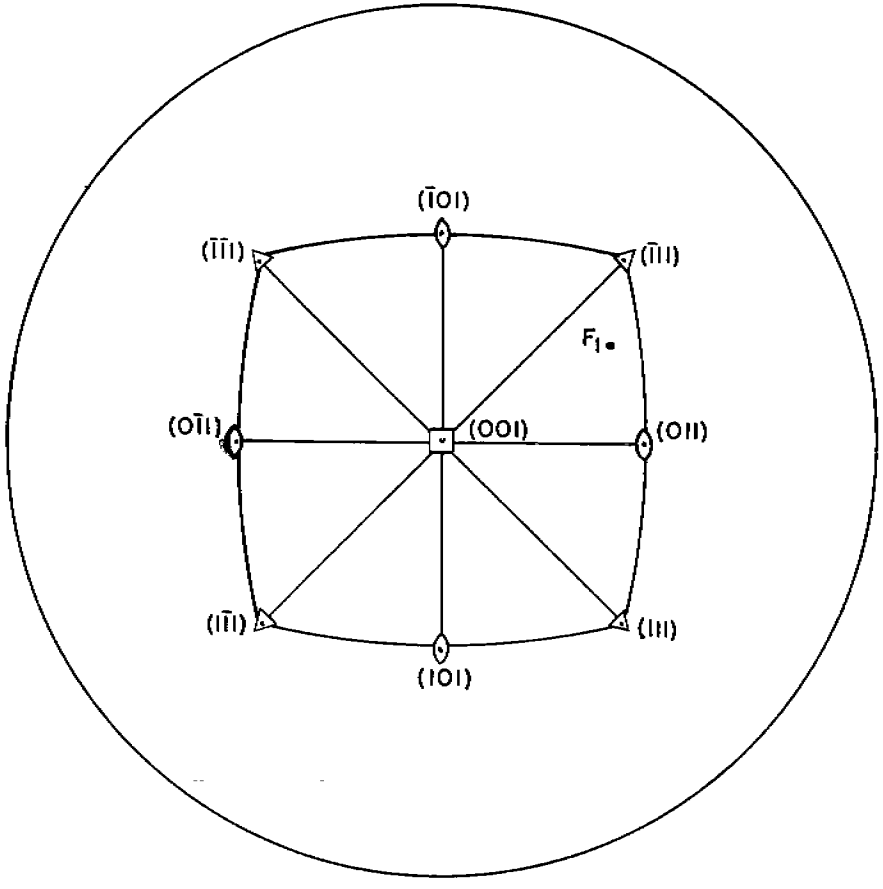

FIG. 32
STANDARD {001} PROJECTION SHOWING POSITION OF TENSILE AXIS (F).

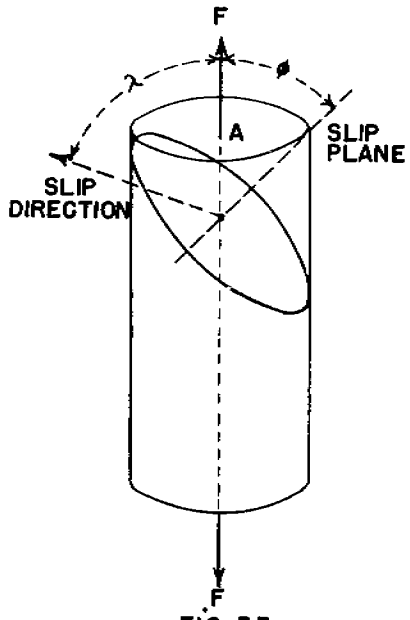

FIG. 33

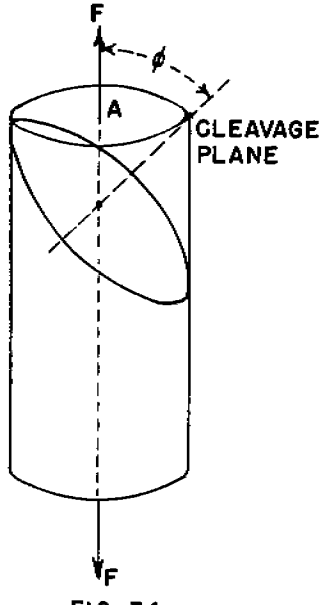

FIG. 34

COORDINATES FOR CALCULATING RESOLVED STRESSES.

direction and the slip (or twin) plane are known, the resolved shear stress for slip (or twinning), S_{shear} can be calculated from the equation:

$$S_{shear} = \frac{F}{A} \cos \phi \cos \lambda \qquad \text{(See Fig. 33)}$$

where F = applied force along the stress axis

A = cross sectional area of the specimen

ϕ = angle between the normal to the slip (or twin) plane and the stress axis

λ = angle between the stress axis and the slip (or twin) direction.

Also, the resolved normal stress for cleavage, $N_{(cleavage)}$, can be calculated from the equation:

$$N_{cleavage} = \frac{F}{A} \cos^2 \phi \qquad \text{(See Fig. 34)}$$

where the terms are defined as above. The values of ϕ and λ therefore must be evaluated from the stereographic projections.

The various pros and cons of square specimens instead of cylindrical ones were studied. The square specimen has the advantage of having flat surfaces which are easily focused on the microscope. However, the angles between the faces of the specimen must be accurately known. Also, since the ability to see the slip lines depends on the direction of slip, the ability to see the trace of the glide plane when it coincided with one edge of the specimen would be severely lessened. For these reasons, and many others, the choice of cylindrical

specimens was made.

A schematic representation of a specimen is shown in Fig. 35. A reference mark R.M. is drawn on the cross section at one end of the cylinder (i.e. a diameter). F is the cylindrical axis and also the stress axis. The original X-Ray photogram was taken along the line R.M. and perpendicular to F.

After being deformed in some fashion, the specimen was placed in the goniometer and fitted on the top of the metallograph stage as shown in Fig. 36. An eyepiece was used which had one reference line, and this line was adjusted parallel to the longitudinal or tensile axis. The rotating head of the goniometer was then adjusted to the "zero" position. The specimen was rotated about the cylindrical axis, F, and the angles β_1, β_2, β_3, etc. between F and the traces of the slip lines were recorded every 10° of the azimuth around the bar. This procedure was repeated four times, two counterclockwise passes and two clockwise. The angular readings β_1, β_2, etc. were averaged. These angles were plotted on the original stereographic projection of the orientation of the specimen as shown in Fig. 37. The pole 90° away from this great circle is the crystallographic plane of deformation (i.e., the slip or twin plane).

A second X-Ray photogram was taken after deformation, and the position of the specimen axis at this stage is shown in Fig. 37 as F_2. In all cases this second orientation,

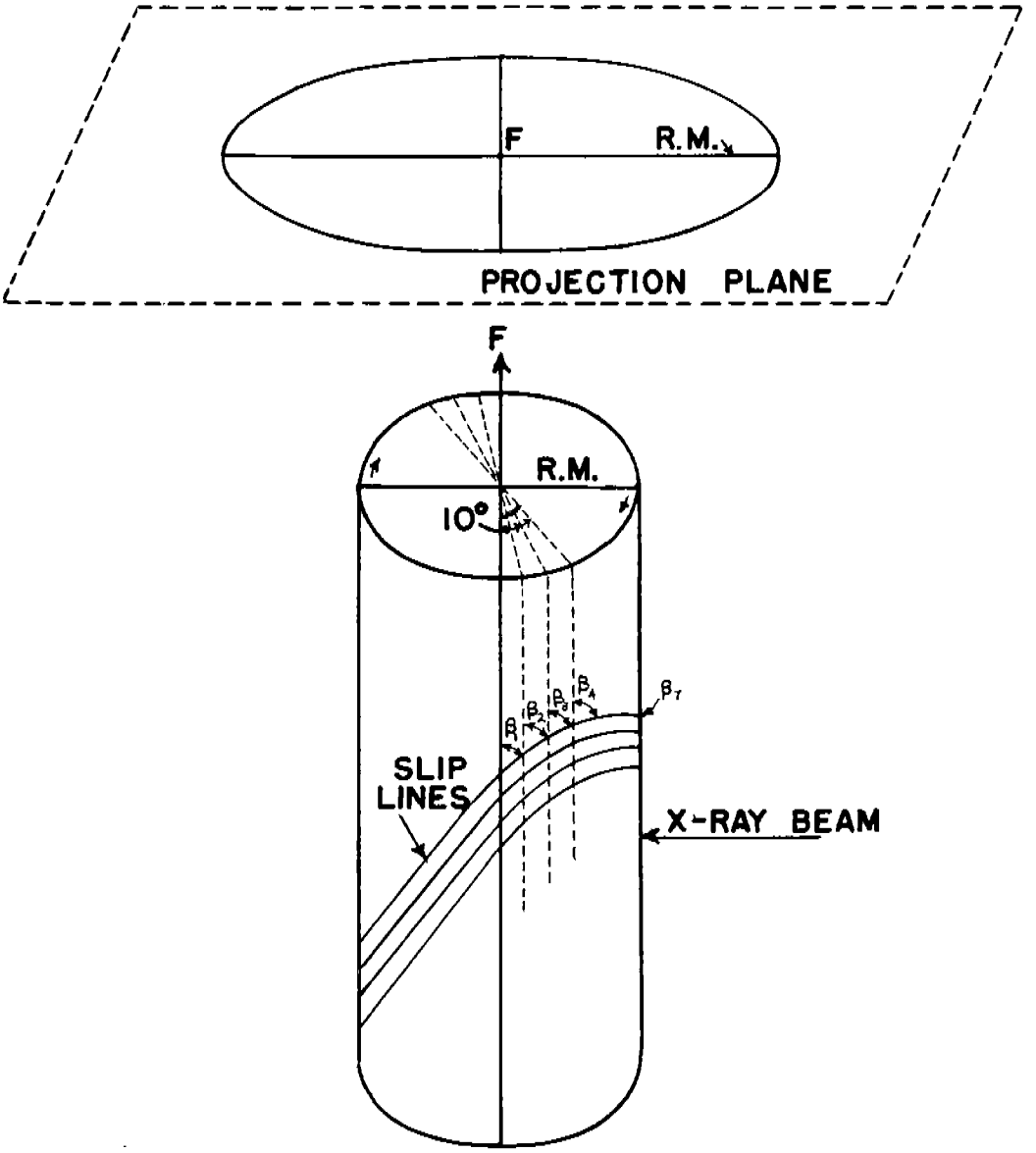

FIG. 35

THE DIAGRAM OF THE SPECIMEN WITH TRACES OF SLIP LINES SHOWN ON THE SURFACE.

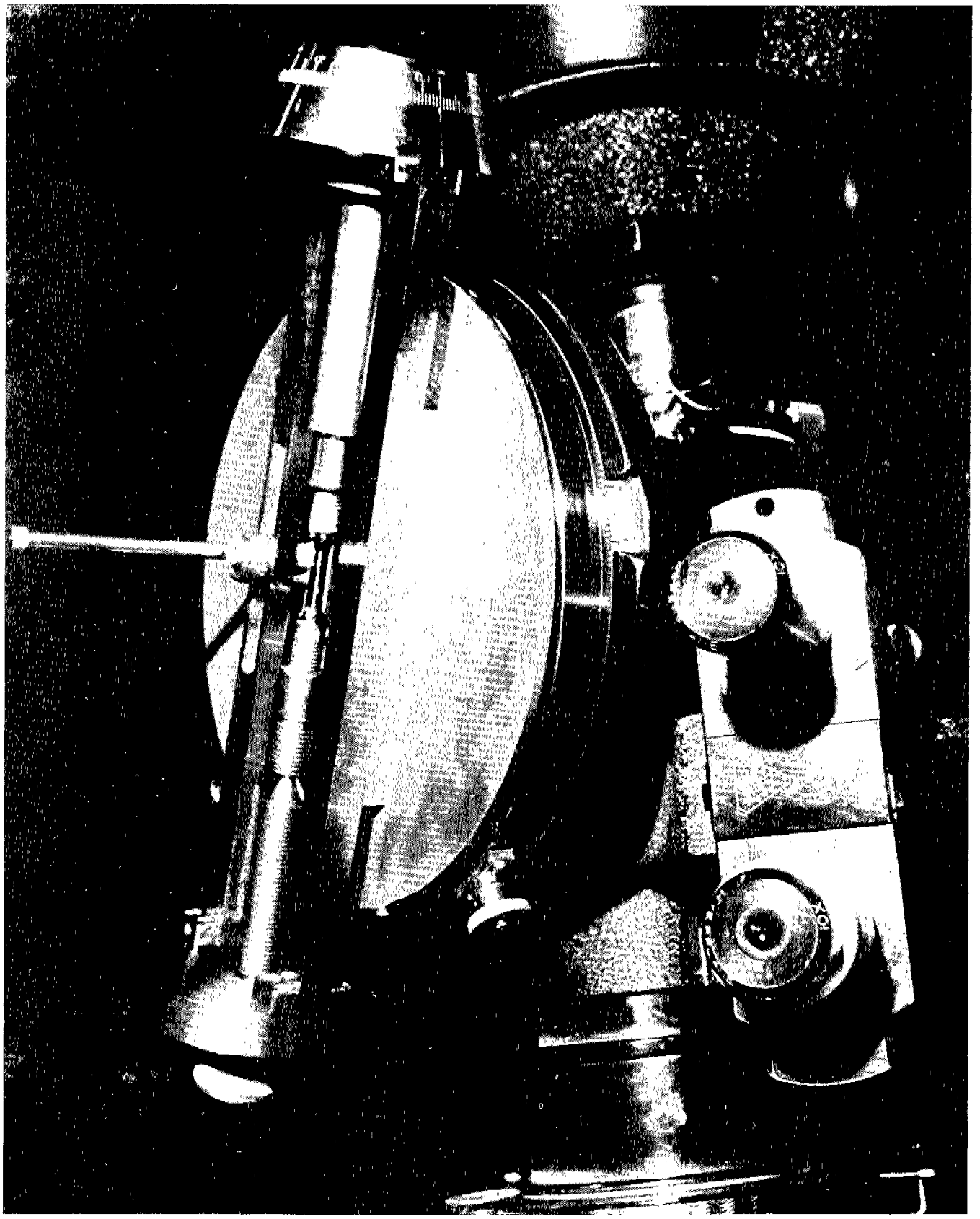

Fig. 36. Goniometer and specimen on metallograph for optical measurements.

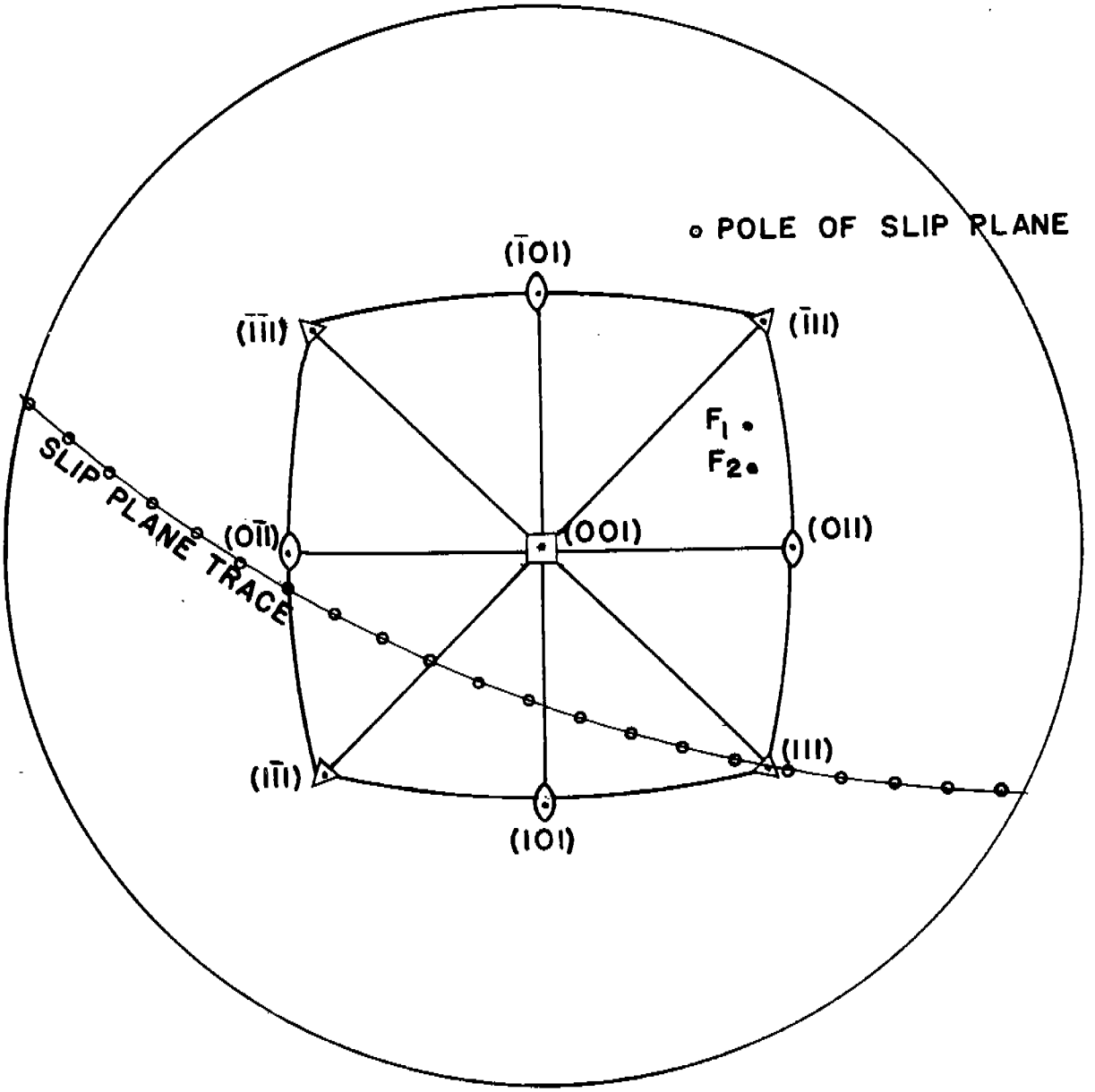

FIG. 37

STANDARD (001) PROJECTION

F_2, was used for the measurement of the angles ϕ and λ.

The measurements for twinning and cleavage were made in exactly the same way. In fact, the slip measurements were the most difficult since they were made on a series of wavy lines which were at times almost impossible to see. When the lines became quite wavy, the average slope of the trend of the slip lines was recorded as accurately as possible and is referred to as the trace of "integrated" glide ellipse.

Tensile Testing of the Single Crystals

The simplest form of mechanical deformation is the axial tensile test. It can be performed with a minimum of effort and may yield all the basic information of the plasticity of bodies of smooth contour (without notches or stress raisers). Since the yield point and fracture point were the two important values to be obtained, the simple axial tensile test was used to deform all specimens.

The Tensile Machine

A Dillon chain-driven tensile machine of 5000 pounds capacity was used. The chain drive was constructed to give a constant head speed of 0.01 inch per minute. This speed is about as slow as one would desire without trying to approach creep conditions. The grips were threaded steel rods that screwed over the threaded ends of the

specimen. They were kept as light as possible to reduce the possibility of bending the delicate crystals when inserting them in the machine. The complicated universal jointed grips that have been designed to give true axiality of loading are quite massive and not too satisfactory. A chain was chosen instead to give axial loading conditions. This chain was attached to a swivel socket which was in turn attached to the top cross head of the machine through a 0-5000 pound Baldwin type U-1 SR-4 load cell. A load cell is simply a bar of high quality steel with four SR-4 electrical resistance strain gauges attached to its sides. Since the modulus of the steel is accurately known, the load is proportional to the elastic strain in a linear fashion. Hence, a given load produces a given strain which in turn produces a given change in resistance of the strain gauge network. The strain gauges are connected in parallel to average any inhomogeneous strain from bending, twisting, etc.

The bottom grip was rigidly connected to the lower, or movable, crosshead of the machine. The cooling container was soldered directly to this bottom grip and could only be removed with the grip. It was constructed of two concentric shells of heavy gauge sheet iron with fiberglass insulation in between. The complete tensile assembly is shown in Fig. 38.

Stress and Strain Measurements

The Baldwin load cell was chosen so that the load could

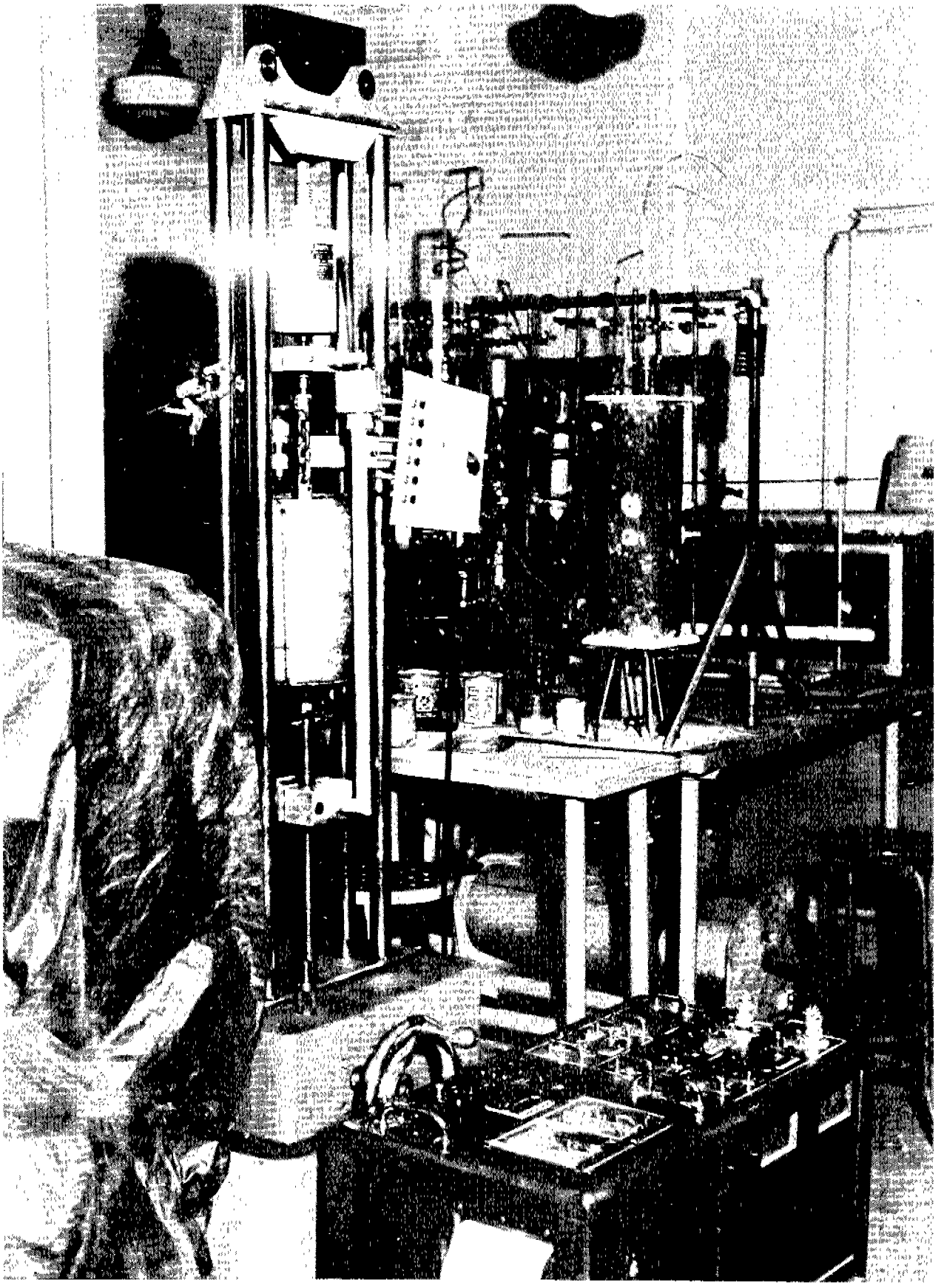

Fig. 38. Tensile testing machine, accessories, and recording apparatus

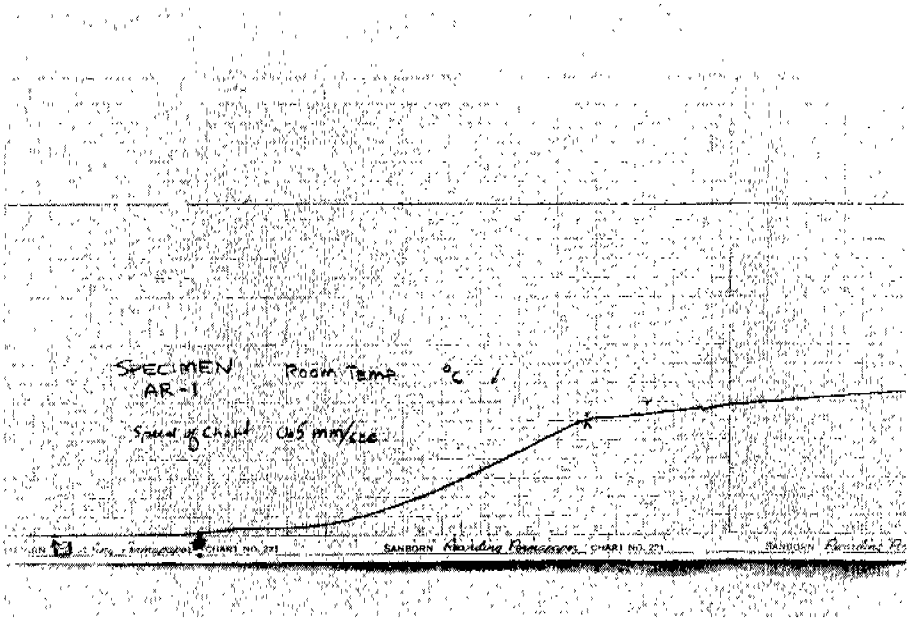

Fig. 39. Load (vertical) versus time (horizontal) for a specimen A-1 tested at 31°C.

be recorded on a self-balancing wheatstone bridge circuit. This circuit was provided in a Sanborn Twin Viso electrical strain gauge amplifier and recorder shown in the bottom of Fig. 39. It was designed from the principles of the electrocardiograph used to detect the heart beat patterns of the human body. Two separate, independent channels are provided so that the simultaneous recording of two phenomena is possible. It was originally intended that SR-4 electrical resistance strain gauges would be used for strain measurement, and these could be recorded on one channel with stress recorded on the other channel.

The principles of its operation are quite simple. An oscillator with a frequency of 2500 cycles per second is provided to supply current to the strain gauge. Inputs are provided for either single strain gauges using the internal transducer to balance the network or else from an external transducer such as the strain gauge bridge of the load cell. The current returning from the outside sensitive element (strain gauge or transducer) is superimposed upon the standard 2500 cycle output of the oscillator. As long as these two voltages are in phase (as they are for a purely resistive circuit), their amplitudes are additive. This superimposed voltage is applied to a galvanometer with a recording pen. Such an electronic circuit is phase sensitive; that is, it can detect both negative and positive

changes in voltage above the 2500 cycle reference voltage. The recording system is, in itself, quite novel. The scribing portion of the "pen" is a heated stylus which decomposes a plastic backing on the recording tape as it moves under the pen. Such a record is permanent and cannot be smudged by moisture. The width of the line is controlled by the current through the stylus. If the tape speed is increased at any time during a test, the current to the stylus is increased in proportion to the tape speed so that the line width remains constant. An attenuator is supplied with each channel so that scale magnifications of 4, 20, 40, 100, 200 and 400 may be made during the test.

For this work, a paper speed of .25 millimeters per second was used to record the load. The full-scale deflections were adjusted to give the following load values:

Attenuator Setting	Full Scale Load
x1	500 pounds
x4	1900 pounds
x	8340 pounds

A typical example of a load time curve for a room temperature test is shown in Fig. 39. The initial or elastic portion of the load time curve is not a straight line but rather a smooth curve. The yield point loads were easily determined by placing a French curve along the line and

noting the first deviation from the constant curvature of the elastic portion.

As previously mentioned, SR-4 electrical strain gauges were originally intended for use as strain indicators. There were two main difficulties which were of sufficient magnitude to discredit them. First, the adhesives and pressure needed to apply these gauges to the test section would ruin the surface of the single crystals so that further metallographic examination would be impossible. Secondly, these gauges are not satisfactory for low temperature use since they also measure temperature fluctuations. Of course a "dummy" or temperature compensating gauge is always used, but the temperature fluctuations near the dummy gauge are not always the same as those near the measuring gauge. Also, the adhesives are very brittle at low temperatures and will often crack before much elastic deformation of the specimen occurred. For these and other reasons a strain measuring element which lay outside the temperature bath was used.

The most satisfactory arrangement was found to be one involving the measurement of total crosshead motion by means of a linear differential transformer. This transformer consists of a spiral wound primary coil and a secondary coil, half of which is wound clockwise and half counterclockwise. As the iron of the transformer moves through the windings, the change in inductance is recorded as a linear function of

the position of the metal core. If a similar transformer is attached to the temperature scale of a Brown Temperature Recorder, it will follow the motion of the measuring transformer exactly. Any fluctuations in line voltage will affect both transformers in the same fashion and hence be canceled out. The strain gauge is represented by the long aluminum tube connected to the lower and upper screws of the tensile machine of Fig. 38. The core is fastened to the upper head and the transformer to the lower.

Experience with this arrangement indicated that there was so much play in the mechanical system of the tensile machine that accurate determinations of the yield strain were impossible. Since these were unimportant, the strain gauge was used merely to record the approximate plastic strain.

Temperature Baths

Tests at temperatures other than 25°C were conducted by pouring suitable equilibrium mixtures into the metal container and allowing the specimen to come to temperature. The temperature media used are listed in Table V.

Table V

Approximate Temperature	Media
+ 200°C	Russian Mineral Oil
+ 100°C	Boiling Water
Room	Stagnant Air
0°C	Crushed Ice + Water
-68 to -71°C	Dry ice and acetone
-196°C	Liquid Nitrogen

An air-driven stirrer was used to keep good circulation in the bath. Temperatures were measured with a glass thermometer in all tests except those at -196°C where an iron-constantan thermocouple was used. The two specimens pulled at -130°C and -170°C were tested in a controlled cooling apparatus of the Westinghouse Research Laboratories under the same rate of loading as all other specimens.

EXPERIMENTAL RESULTS AND DISCUSSION

Introduction

In keeping with the division of the literature review into three sections (slip, twinning and cleavage), the experimental results are so divided. At times it was found necessary to include some observations from one part of the study in the section devoted to another part in order that a complete picture could be obtained.

It should be remembered that the original aim of this study was an investigation and measurement of the stresses for slip, twinning and cleavage at various temperatures. However, mechanistics have crept into several parts of this work and necessarily so, for their importance may outweigh, and in many cases overshadow, the importance of quantitative measurements of stresses. The data which enable one to discuss mechanisms in this work are not complete, yet the author believes that they are of sufficient importance to be discussed

in light of the support they may offer to various theories of deformation in iron. For similar reasons, many observations of anomalous or "strange" behavior of the crystals during deformation are reported with little or no discussion as to their interpretation. Perhaps if some reader of this dissertation should have opportunity to reflect, then these scattered bits of information may serve a useful purpose.

Slip

The orientations of all specimens tested for behavior during slip appear in the stereographic unit triangle of Fig. 40a. The positions of the specimen axes in the unit triangle are represented by dots (.): the usual manner of presenting a series of orientations. It is quite evident that the complete gamut of orientations was not studied; but, of course, since the specimens were tested as they were manufactured, no prediction as to the orientation of future specimens was possible. Again it should be stressed that mechanistics were originally intended to be of secondary importance.

Fig. 40b shows the orientations with respect to the slip systems of maximum resolved shear stress for the orientations in question, as calculated by Opinsky and Smoluchowski. Although it was believed at the outset of the work that the Opinsky theory was correct and study would

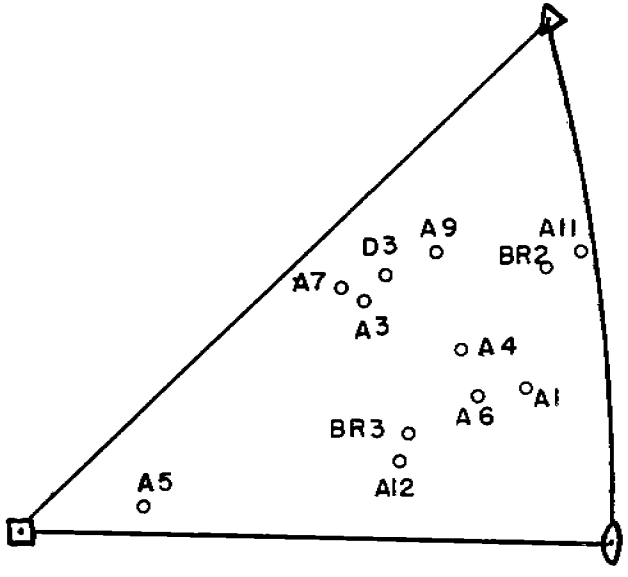

FIG. 40a

Orientations of slip specimens

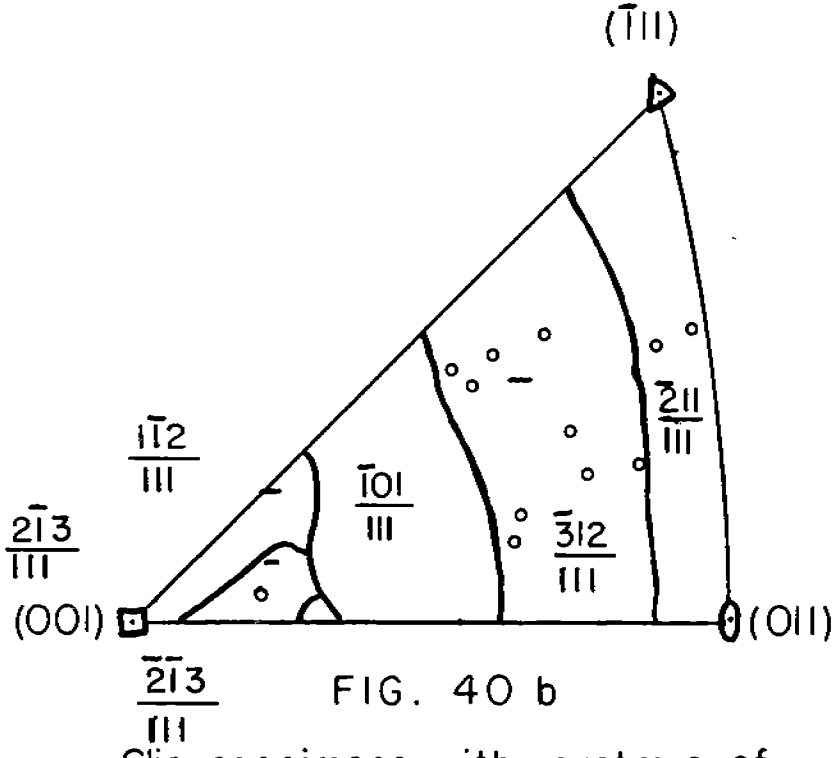

FIG. 40 b

Slip specimens with systems of maximum resolved shear stress. as calculated by Opinsky & Smoluchowski

proceed with it as a basis, the data indicated marked deviations from predicted behavior. It was then decided to record the data and to correlate it with whatever explanation seemed most nearly correct.

Behavior of the Glide Ellipse at Various Temperatures

Fig. 41 pictures the angular relationships among the integrated glide ellipse, maximum shear stress plane and various low index crystallographic planes of the [111] zone. The angular distance along this zone is set out horizontally with the ($\bar{1}01$) plane as the origin. This type of drawing clearly indicates the relative positions of the various planes and summarizes the data for all the slip specimens. Glide ellipses are represented by crosses (x) and maximum shear planes by dots (.).

The integrated glide ellipses do not usually coincide with any of the three planes ($\bar{1}01$), ($\bar{3}12$), or ($\bar{2}11$), although in some cases they are very nearly coincident. It is believed that these are not due to experimental error but are representative of a real effect. If error was the cause of the deviation from "crystallographicity" then the pole of the slip planes should deviate anywhere around the crystallographic pole and not just along the [111] zone. For only one specimen (A-3) did the pole of the glide ellipse fall more than one degree off the [111] zone. This is in direct accord with the theory advanced by Steijn and Brick where the glide ellipse was found to occupy

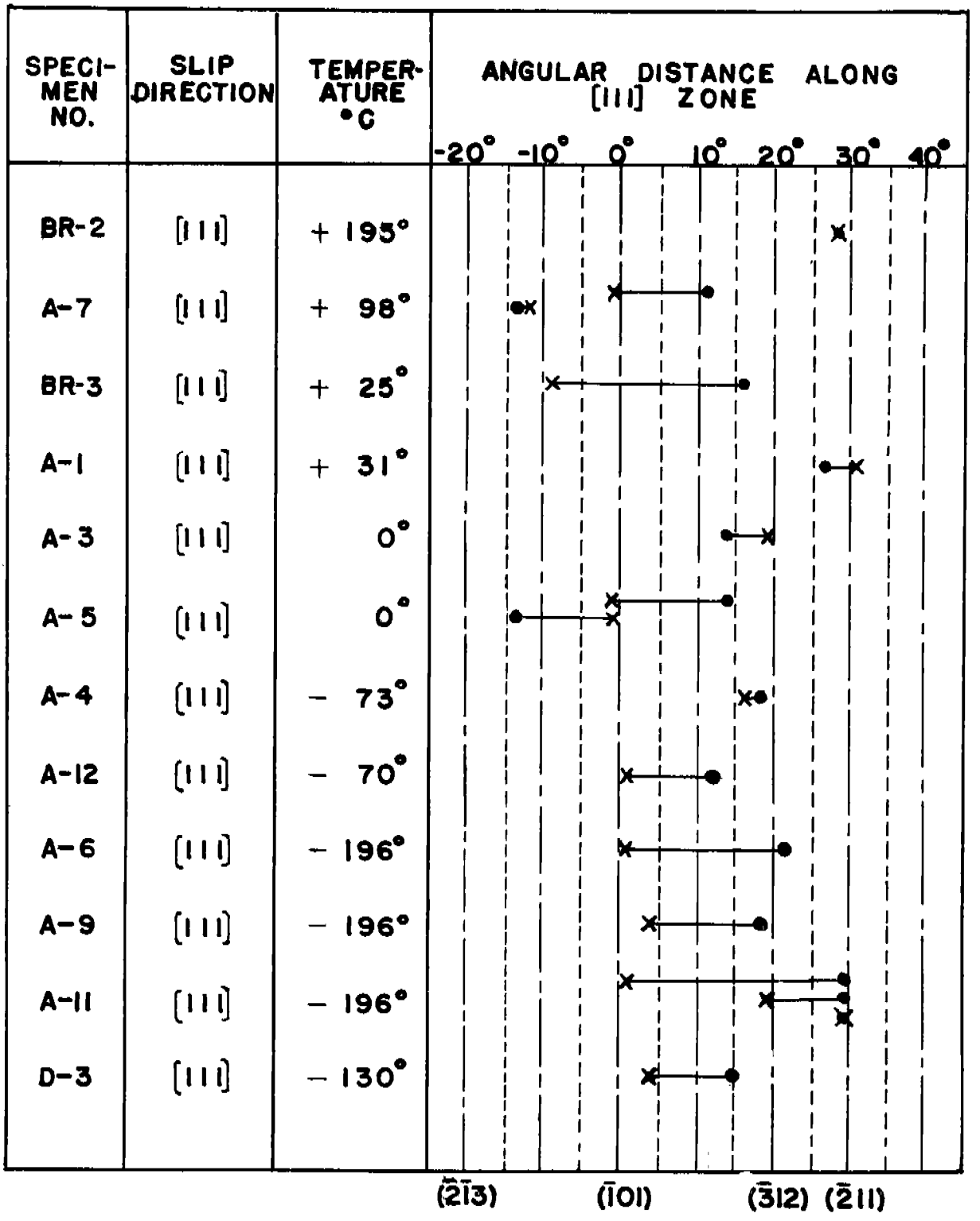

FIG. 41

RELATIVE POSITIONS OF M.S. POLES (•) AND INTEGRATED GLIDE ELLIPSE POLES (X) ALONG THE [111] ZONE. THE ' MARKING MEANS A SECONDARY OR TERTIARY SET OF PLANES.

any position in the [111] zone. To check the correlation more closely the angles ψ and χ were measured for specimens A-1 and BR-3 tested at room temperature and superimposed on the ψ versus χ plot of Steijn for an alloy of similar composition (.023% C). (See Fig. 42). These data fall exactly on the curve drawn through the values obtained by Steijn. Unfortunately, these were the only specimens tested at a temperature comparable to Steijn's.

Change in the Behavior of the Glide Ellipse with Temperature

As the temperature was decreased below room temperature, the glide ellipse tended toward the $(\bar{1}01)$ plane regardless of the position of the maximum shear stress plane. At intermediately low temperatures (0°C and -70°C) the glide ellipse did fall near the $(\bar{2}11)$ when the maximum shear pole fell in that position; however, at -196° the deviation was always toward (101). Specimen A-11 was interesting in that three separate sets of traces were present. One coincided with $(\bar{1}01)$, one was very nearly $(\bar{3}21)$, and the third was coincident with $(\bar{2}11)$. The maximum shear plane coincided with $(\bar{2}11)$. Such a behavior is not to be expected on the basis of any theory which predicts only primary slip. However, if other factors are considered, then the behavior appears more logical.

If specimen A-11 was not homogeneous with respect to included particles or foreign atoms such as carbon or silicon, the slip behavior could vary along the gauge length of the

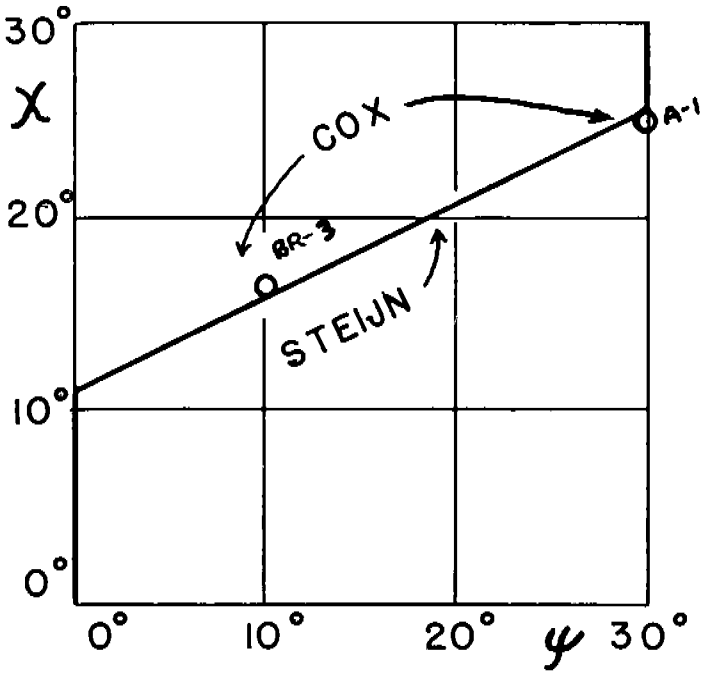

FIG. 42

ROOM TEMP. SLIP

crystal. The theory of Steijn would predict a slip trace near $(\bar{1}01)$ since the resistance to shear of this plane in relation to the $(\bar{2}11)$ is quite low at low temperatures. However, if foreign matter hindered certain A type movements, then $(\bar{2}11)$ slip would predominate. As pointed out later, the variation in shear stress along the $[111]$ zone is not significant at lower stresses but it may be of sufficient magnitude at -196°C to affect the selection of the glide ellipse.

Another possible explanation is that the first slip may have been $(\bar{1}01)$ but that the occurrence of twinning, strain hardening, and other such lattice distortions invalidate the criterion of critical shear stress as originally intended. In reality any of the theories of slip were only meant to apply to the first slip and not that after severe plastic flow had taken place.

At higher temperatures, room temperature and above, the glide ellipses fall nearer to the maximum shear poles. This indicates that the shearing strengths of the $(\bar{2}11)$ and $(\bar{1}01)$ planes are approaching each other. In fact, if the maximum shear pole is close to $(\bar{2}11)$, then the integrated glide ellipse pole may tend toward this plane. (See specimens A-1 and BR-2.) This means that the ratio of $S\psi/S_{110}$ decreases toward unity with increasing temperature, which indicates a weakening of planes in the vicinity of $(\bar{2}11)$. Phenomenologically, then, one can say that the γ ratio, S_{112}/S_{110}, is

the factor which determines the slip behavior for a given set of test conditions, excluding, of course, orientation. The $S\psi/S_{110}$ curve for the room temperature tests in this work is equivalent to Steijn's for the .023% C alloy. (See curve m in Fig. 7).

The migration of the tensile axes of the specimens are, in general, as predicted by Opinsky and Smoluchowski in their maximum shear stress theory. Of course, since they had assumed equal shearing strengths for all planes and this author has chosen to assume different ones, it may seem incongruous to correlate these results with theirs. However, the predictions based on non-equal shearing strengths would be indeed most complicated. Perhaps for some of the specimens in which the Opinsky predictions did not suffice to explain the observed migrations, the differences in shearing strengths were sufficiently important to complicate the matter. Specimens in the region near the (001) vertex of the unit triangle are the ones for which axis migrations are most complex. These should be strained in small increments and X-rayed to determine the incremental migration. Figures 43 to 54 are the complete stereographic data for all specimens used in this part of the research. All azimuthal slip trace data, axis migrations, etc., are clearly indicated with the following symbols:

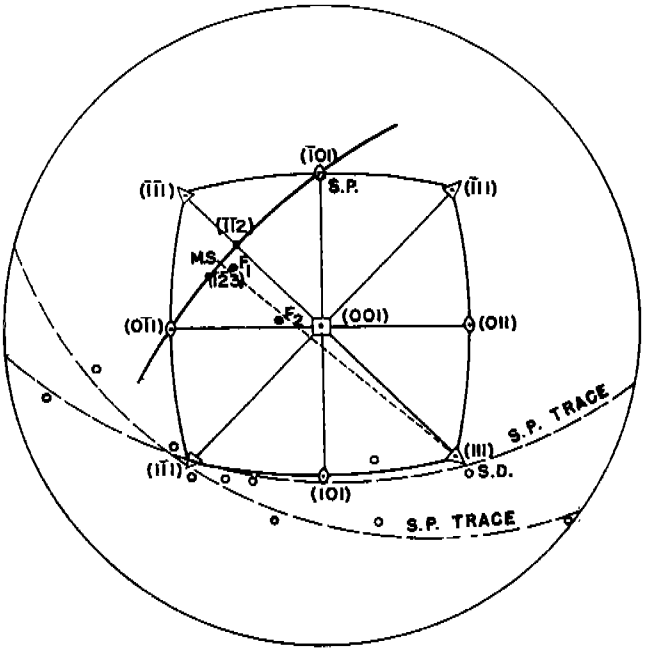

FIG. 43
SPECIMEN A-7

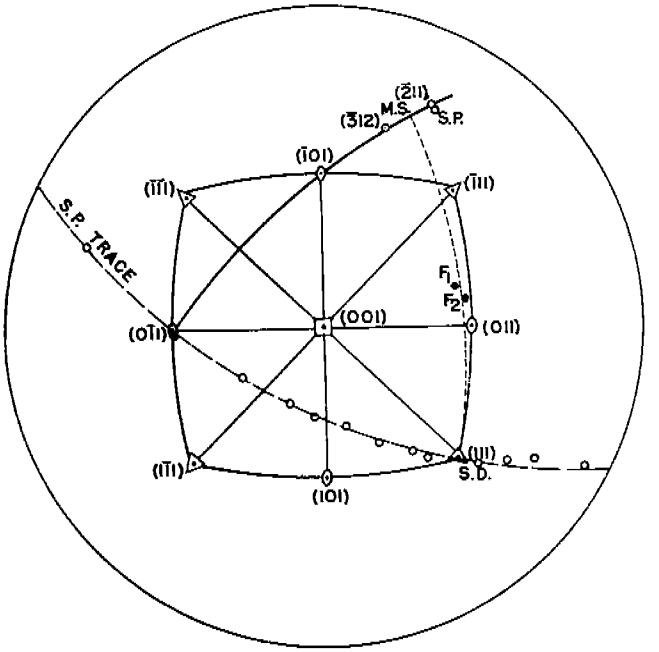

FIG. 45
SPECIMEN A-1

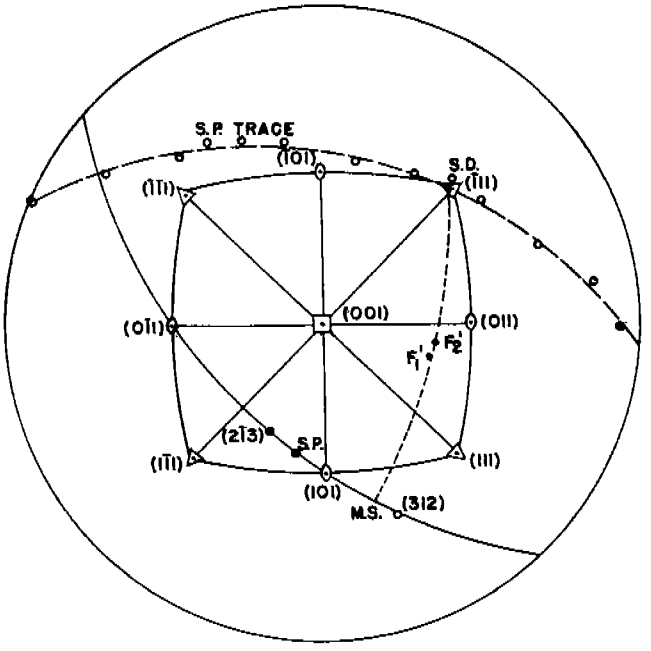

FIG. 44
SPECIMEN BR-3

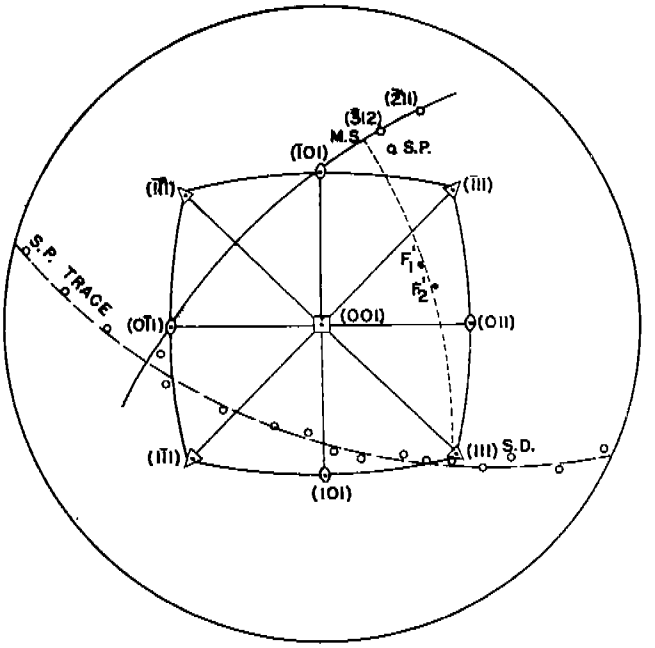

FIG. 46
SPECIMEN A-3

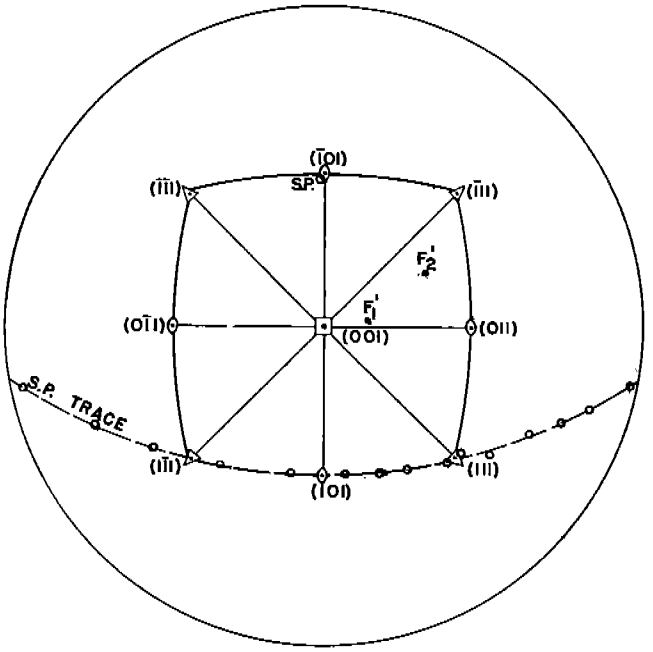

FIG. 47
SPECIMEN A-5

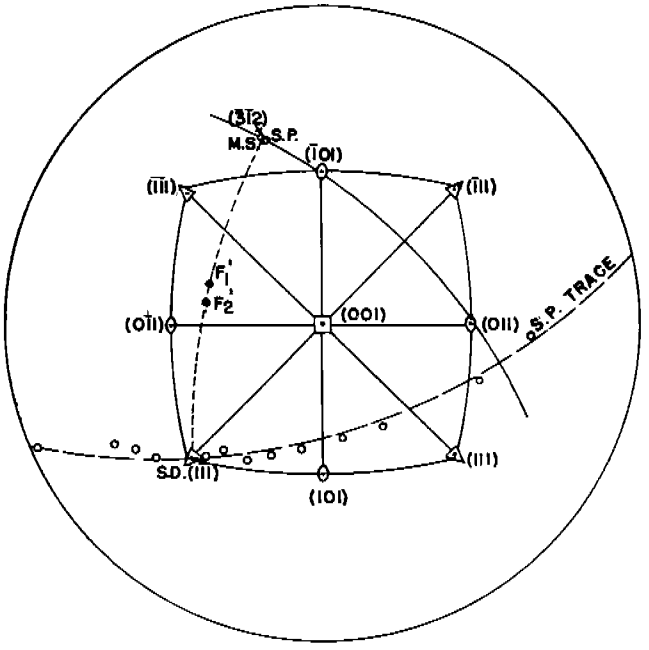

FIG. 48
SPECIMEN A-4

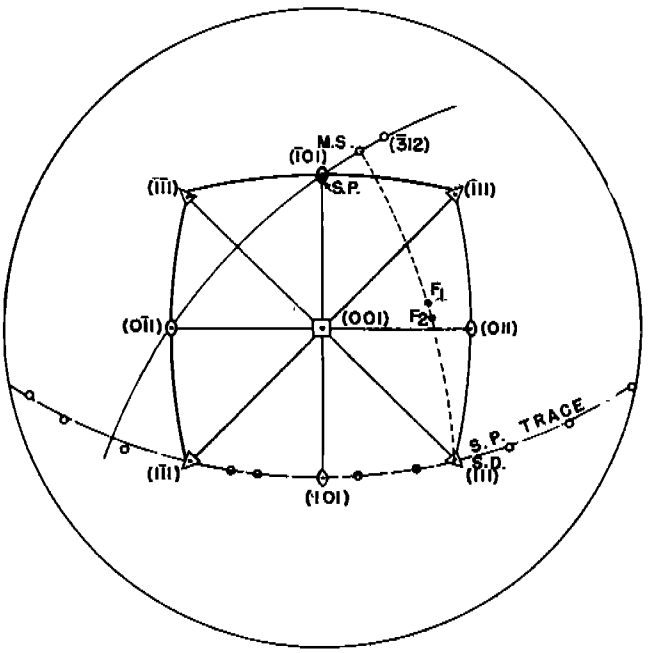

FIG. 49
SPECIMEN A-12

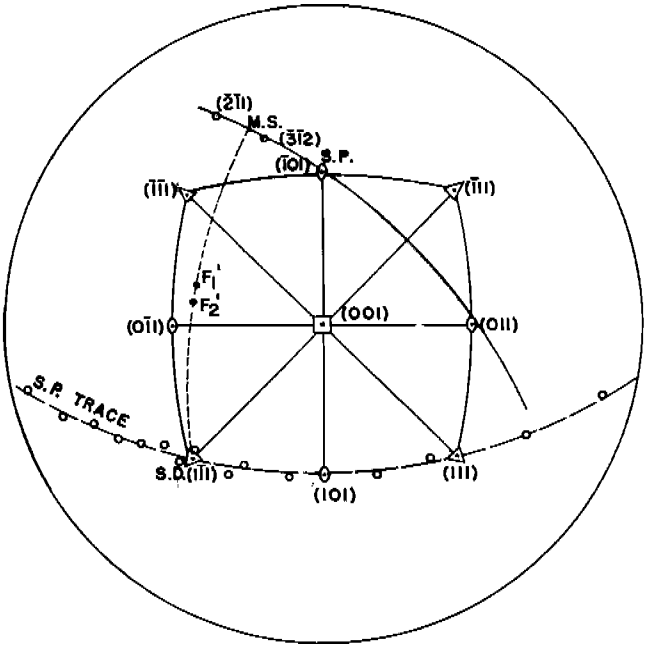

FIG. 50
SPECIMEN A-6

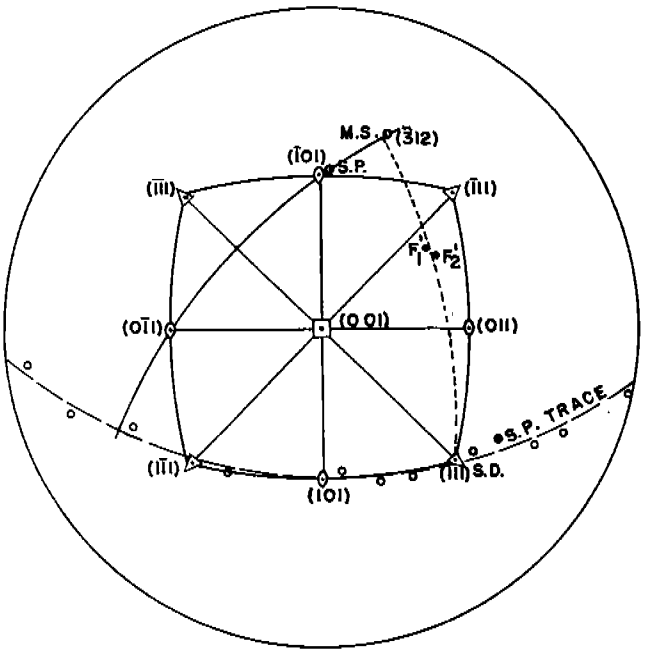

FIG. 51
SPECIMEN A-9

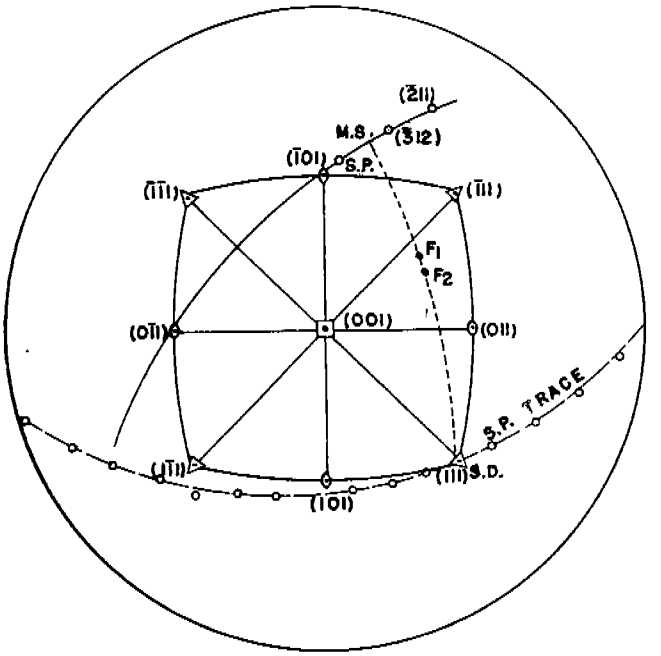

FIG. 53
SPECIMEN D-3

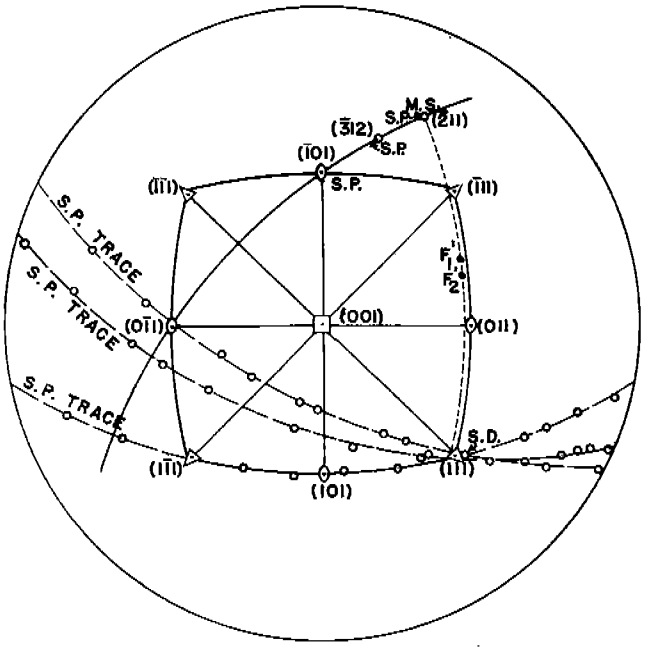

FIG. 52
SPECIMEN A-11

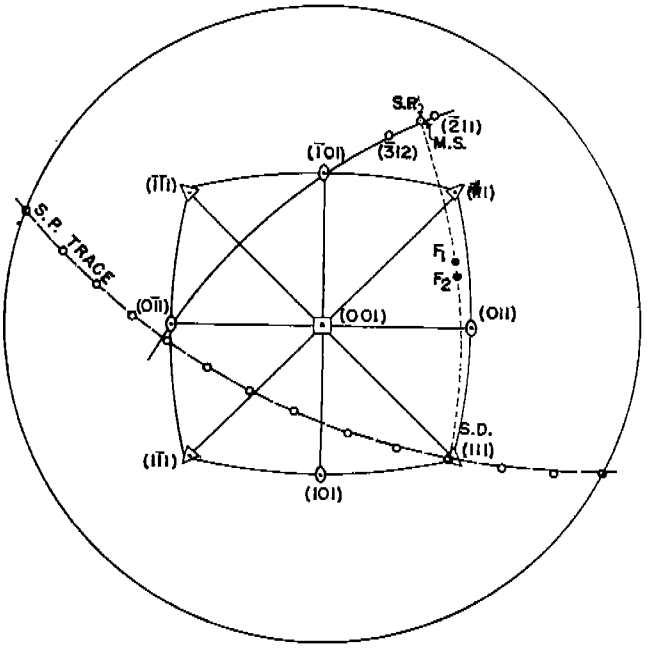

FIG. 54
SPECIMEN BR-2

S.D.	Slip direction
S.P.	Slip plane
M.S.	Maximum shear plane containing slip direction
F_1 or F_1'	Specimen axis before deformation
F_2 or F_2'	Specimen axis after deformation

Variation in the Critical Resolved Shear Stress for Slip with Temperature

The results of the quantitative stress measurements at various temperatures are plotted in Fig. 55. The results of the twelve tests are compatible with those of Steijn and Brick and Vogel and Brick (See Fig. 2). Whereas Fig. 2 is a plot of shear stress resolved onto the (110) plane, the shear stresses of Fig. 55 are those resolved upon the plane of the integrated glide ellipse. Graphically, the differences are almost insignificant. To illustrate the point more clearly, the yield stress resolved onto various planes in the [111] zone were calculated and are given in Table VI. The symbols used are the same as those for the stereographic projections.

Table VI

YIELD STRESS (psi)

RESOLVED ONTO VARIOUS PLANES OF THE [111] ZONE

SP	MS	$(\bar{1}01)$	$(\bar{3}12)$	$(\bar{2}11)$
2735	2735	2432	2735	2735
4411	4411	4023	4411	4336
5676	5484	5414	5484	5275

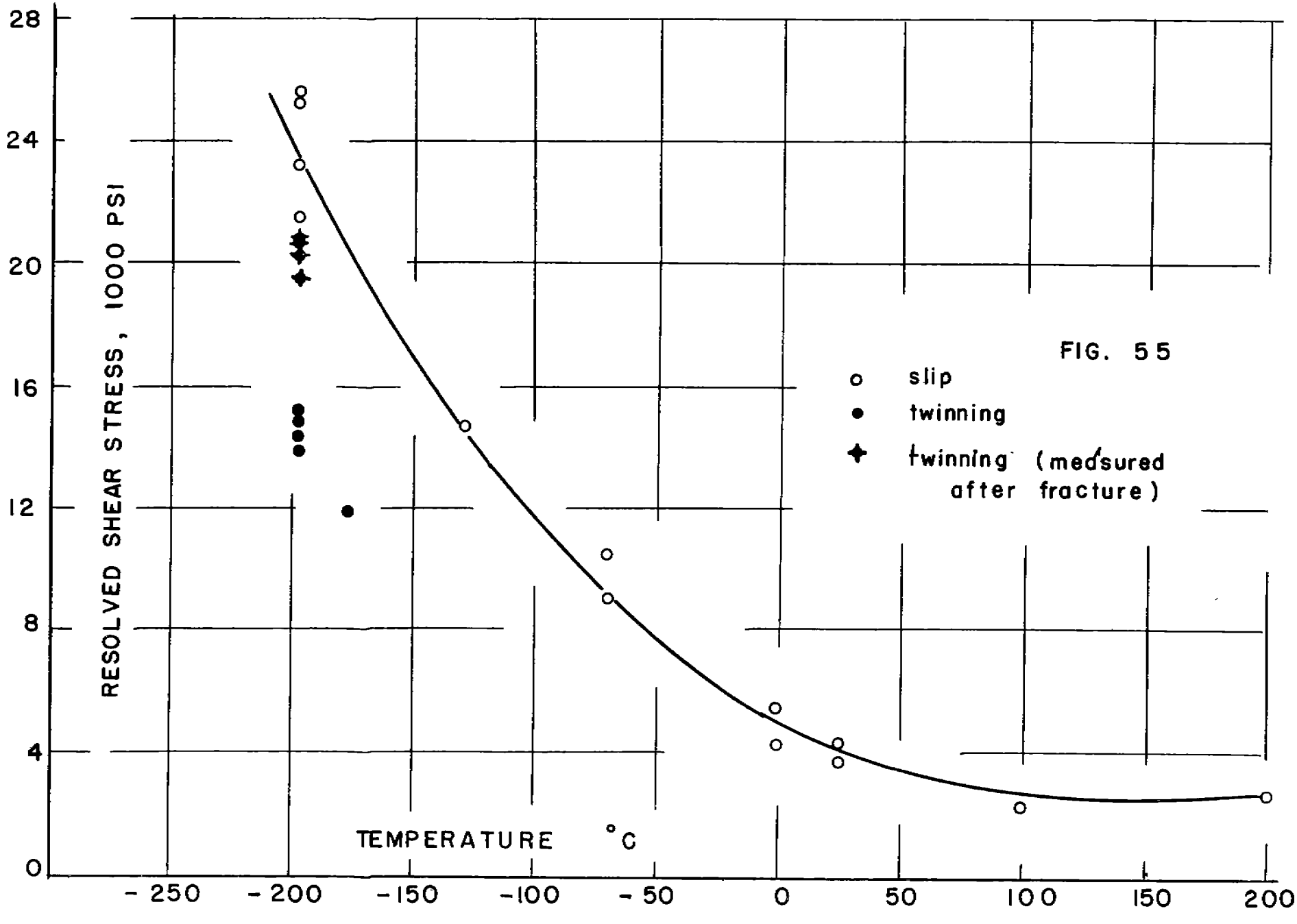
28
24
20
16
12
8
4
0
RESOLVED SHEAR STRESS, 1000 PSI
8
TEMPERATURE °C
- 250
- 200
-150
-100
- 50
0
50
100
150
200
slip
twinning
twinning (measured after fracture)

FIG. 55

Table VI (Continued)

SP	MS	$(\bar{1}01)$	$(\bar{3}12)$	$(\bar{2}11)$
10570	10570	10070	10570	10410
9000	9173	8825	9000	8646
17270	18530	17270	18530	18220
21200	21690	20690	21690	21200
23150	26150	23150	25800	26150
25800				
26150				

It can be seen that the values for any plane in the zone do not vary more than a few per cent. In fact, the variation for any specimen is less than the scatter between two specimens tested at the same temperature. The values of critical resolved shear stress at any temperature are found to be slightly lower than those of Fig. 2 even though the decarburized mild steel is much less pure than the vacuum melted ferrites used by Steijn. No explanation is advanced for this difference.

It should be brought to mind that the data at -196°C were not obtained rigorously. No marked yield point was observed in these specimens, but rather the first deviation from elastic behavior was a loud bang accompanied by a drop in load caused by twin formation. When the specimens were examined metallographically, both slip lines and twins were present. No methods were available to check whether slip or twinning had occurred first, or both simultaneously. Perhaps twinning was the initial process, and then the heat liberated by twinning caused enough local temperature rise to permit slip. Regardless of the order of these processes, the value of stress at

the first load drop was resolved both onto the twin and slip planes. If slip and twinning occur close to each other in the strain history of the specimen, then this is not a bad assumption. When specimen D-3 was tested at -130°C with no twinning and the data fell on the curve previously extrapolated to -196°C, the validity of the low temperature data were confirmed. Fig. 56 illustrates the presence of twins (straight lines) and slip lines (wavy lines) in Specimen A-11, tested at -196°C.

Surface Manifestations of Slip

The appearance of slip lines, bands, traces or whatever in iron is quite different than that in other materials. The extreme waviness of the lines when viewed in a plane perpendicular to the slip direction is shown in Fig. 57. The straighter appearance of Fig. 58 was photographed parallel to the slip direction. This has been reported often in the literature. Paxton (38) has found that in most instances these lines appear as undulations rather than discrete displacements of the lattice. This is in agreement with this work. Specimens that have been mechanically polished with alumina and Selvyt cloth show clear, discrete lines while electropolished specimens tend to exhibit these undulations or striations. Since Paxton regarded the fine striations as the true structure, mechanical polishing was never used.

Fig. 56. Slip lines (wavy) and twins (heavy straight lines, in specimen A-11 tested at -196°C (X150)

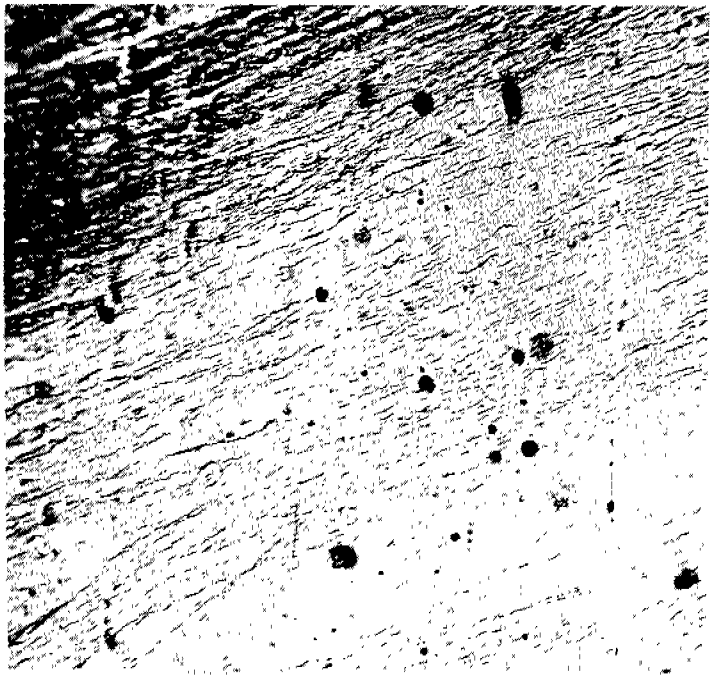

Fig. 57. Wavy slip lines viewed in plane perpendicular to slip direction (X150)

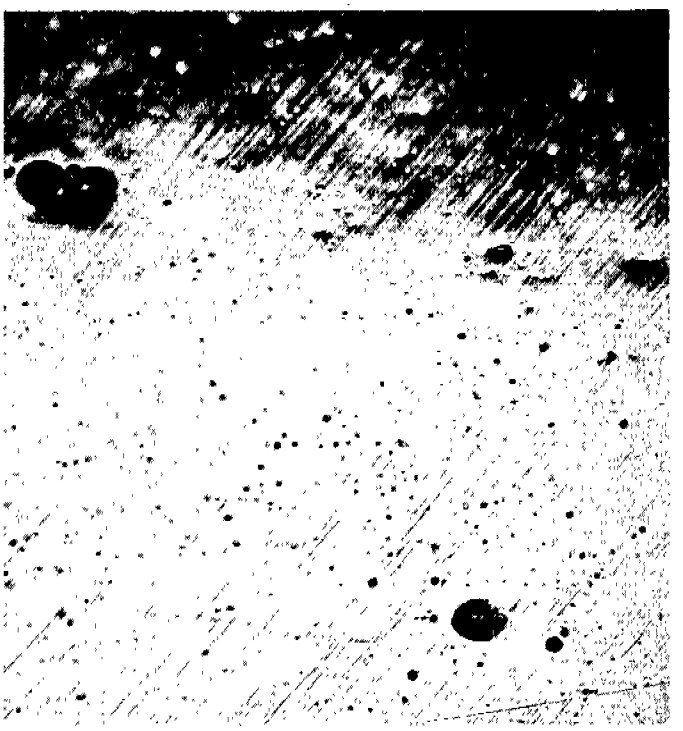

Fig. 58. Straight slip lines viewed in plane parallel to slip direction (X150)

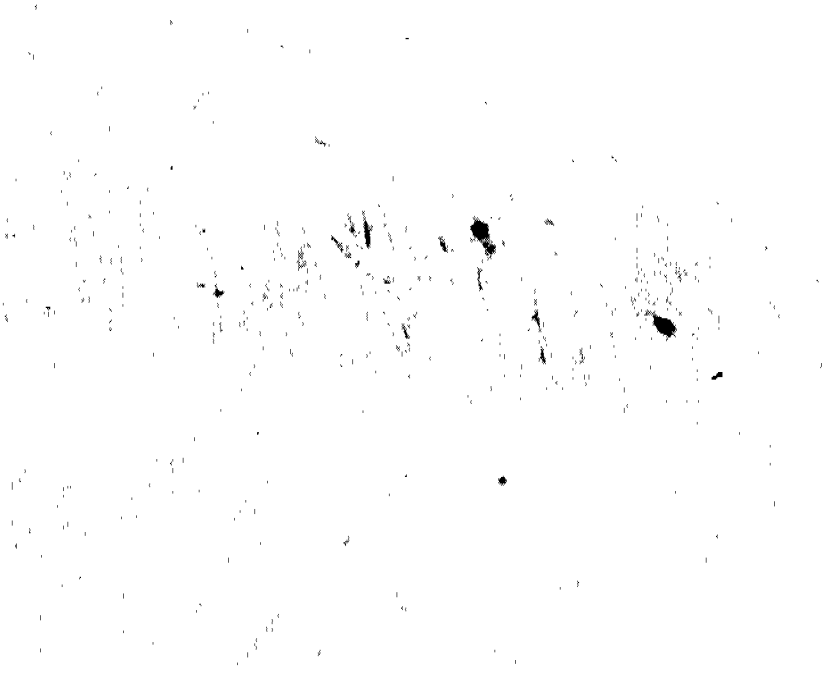

Fig. 59. Slip lines in scratch (X1000). Vertical illumination.

A check experiment was performed on a single crystal cylinder, containing a longitudinal scratch in the surface. After being deformed in compression, this specimen was found to exhibit heavy discrete slip lines across the width of the scratch but nowhere else. Figures 59 and 60 show this specimen under light and dark field illumination respectively. The structure is not an artifact since placing the light source at different angles to the surface did not make the effect vanish.

There are two possible explanations for this. The first is that certain residual stresses are introduced by the scratch which tend to make the surface more susceptible to being broken up. The second is that strain hardening of the metal near the scratch forces the dislocations to leave the metal surface at specific places; e.g. the slip lines. Neither of these proposals was verified since to differentiate between residual stresses and strain hardening would be most difficult.

Deformation in these specimens is not homogeneous. Fig. 61 illustrates clearly the clustering of the slip lines along a portion of the gauge length of Specimen D-3. This could be due to inhomogeneities in chemical composition, inclusions, or many other things. No attempts were made to measure the spacing of these clusters or to correlate them with other test variables.

Asterism and Lattice Distortion During Deformation

Figures 62 and 63 are typical Laue back reflection photographs before and after testing. The spots of Fig. 62 are sharp

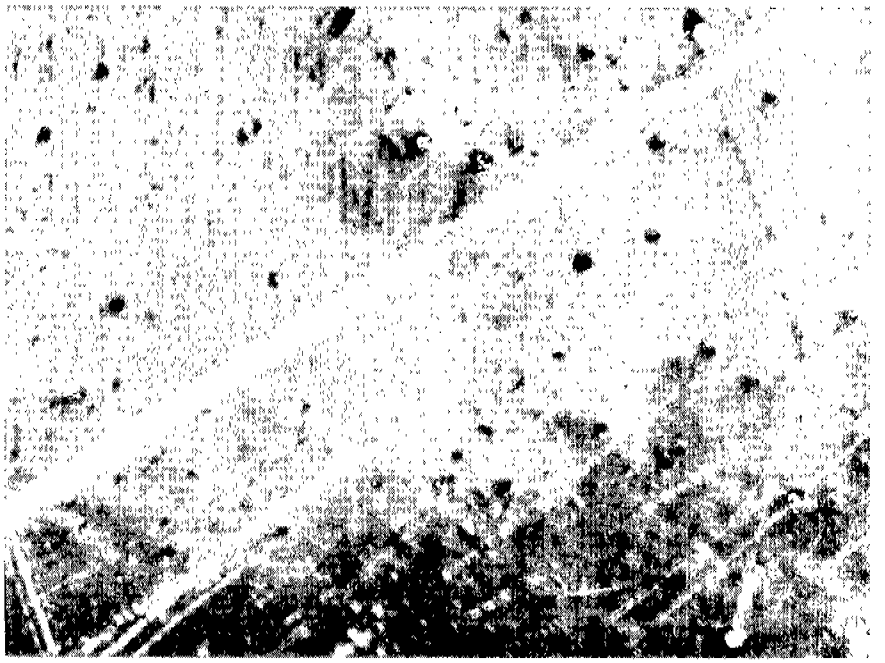

Fig. 60. Slip lines in scratch (X150). Dark field illumination.

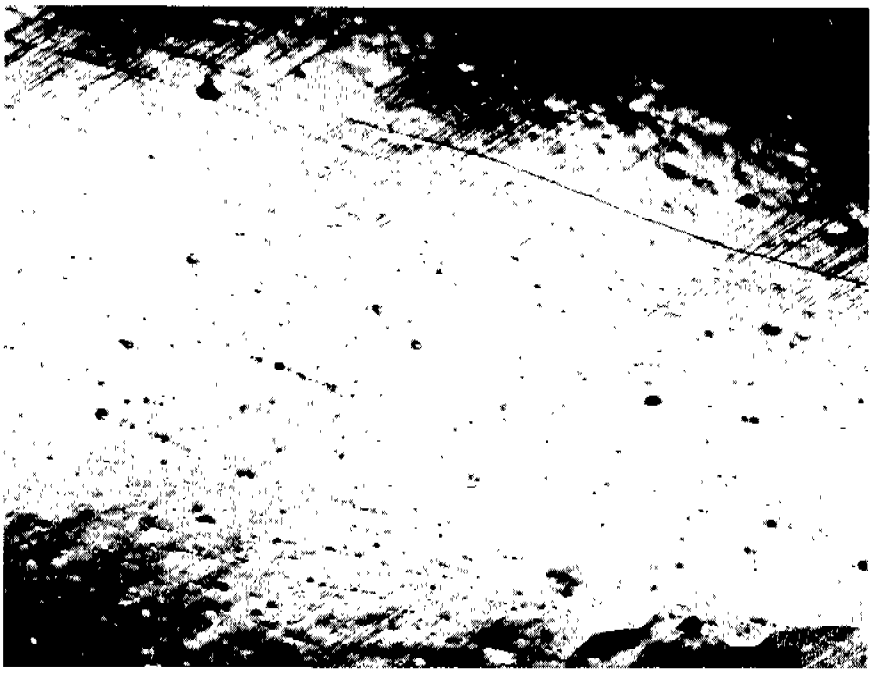

Fig. 61. Clustering of slip lines along the gauge length of a crystal (X150).

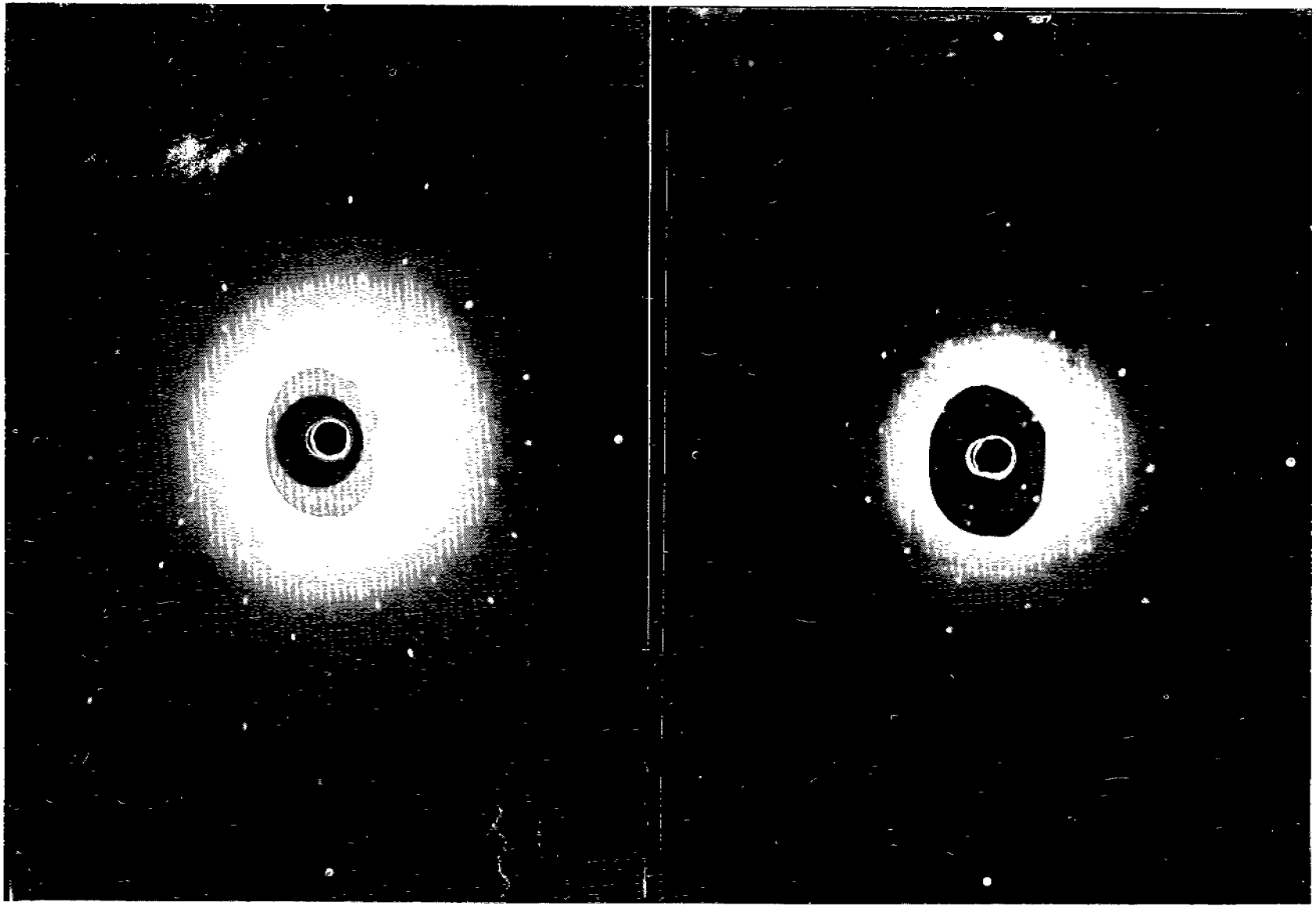

Fig. 62. Laue photogram of specimen A-1 taken prior to testing.

Fig. 63. Laue photogram of specimen A-1 taken after 5 percent elongation. Note splitting of spots and rotation of crystal axis.

and clear indicating an undeformed surface. Fig. 63 illustrates the rotation of the crystal during extension by slip. The amount of rotation depends upon the orientation of the specimen with respect to easy slip systems. Most crystals were extended about .08 inches or approximately 4 percent before being X-rayed. The asterism was always quite small, in fact so slight that no measurements could be made as to the planes responsible for it. A wider, more diffuse X-ray beam would give more arc length, but it would appear that the measurement would be a function of the X-ray rather than of the specimen——a very undesirable property.

Fig. 63 does have other interesting points. The individual spots appear to be split into three or four smaller spots. This is indicative of fragmentation of the crystal into smaller ones of slightly different orientation. No annealing treatments were used to determine whether this was akin to polygonization phenomena. Such behavior has not been previously reported for iron.

Twinning

The orientations of the specimens studied for twinning behavior are given in Fig. 64. Again a complete series of orientations was not investigated, but a fairly representative sample from various parts of the unit triangle was examined. Three of the samples, A-6, A-9 and A-11, were originally examined and measured for slip behavior and then, later, twin data were obtained from these crystals.

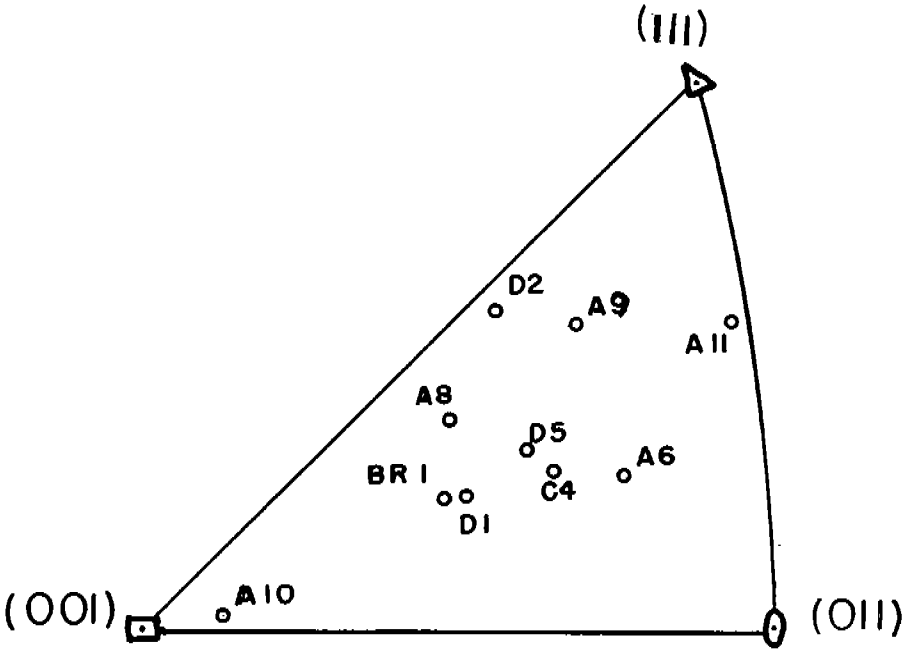

FIG. 64

Orientation of twinning specimens.

In every case the stress at which the first sharp "bang" and simultaneous drop in load occurred was chosen as the twinning stress and was resolved onto the plane or planes upon which twinning was found to have occurred. The stresses were resolved in the following directions on the stated planes: $(\bar{1}\bar{1}2)$, $[111]$; $(\bar{2}11)$, $[111]$; $(1\bar{2}1)$, $[111]$; (112), $[\bar{1}\bar{1}1]$; $(1\bar{1}2)$, $[\bar{1}11]$; $(\bar{1}12)$, $[1\bar{1}1]$. The values of resolved shear stress for twinning are plotted as dark circles in Fig. 55 and listed below in Table VII.

Table VII

Spec.	T°C	Twin Planes	Resolved Shear Stresses
A-8	-196	$(\bar{1}\bar{1}2)$ Fractured	18,200
A-10	-196	(112), $(1\bar{1}2)$	13,300; 15,300
BR-1	-196	$(\bar{1}\bar{1}2)$, $(1\bar{2}1)$ Fractured	20,600; negative
C-4	-196	$(\bar{1}\bar{1}2)$, (112)	14,500; 8,600
A-6	-196	$(\bar{1}\bar{1}2)$	11,500
A-9	-196	$(\bar{1}\bar{1}2)$	14,700
A-11	-196	$(\bar{1}\bar{1}2)$, $(1\bar{2}1)$, (121)	15,700; neg.; neg.
D-2	-196	$(\bar{1}\bar{1}2)$, Fractured	21,640 (Prestrained RT)
D-1	-196	$(\bar{1}\bar{1}2)$, $(1\bar{1}2)$, (112) Fractured	21,930; 21,830; 8796 (Prestrained RT)
D-5	-170	$(\bar{1}\bar{1}2)$, $(1\bar{1}2)$, (112)	11,600, 10,800, 8,000

The values of stress are found to vary about plus or minus 30 percent about the mean value for all specimens tested

at -196°C. The measurements of twinning in the specimens pulled to fracture are not as accurate as those stopped after 3 or 5 percent elongation. If these fracture specimens are discarded from the list then the variation is much less. In fact, the variation is now only about 14 percent. This scatter is quite large. If a critical resolved shear stress criterion were responsible for the onset of twinning, the scatter should be much smaller. However, for slip at any temperature, the scatter is of the same order. The most favorable evidence for a critical resolved shear stress being the criterion for twinning is the selection of the twinning plane. For most orientations of the unit triangle the plane (211) is subject to the greatest resolved shear stress, yet this plane was never found to be the twinning plane. However, it can be shown that this plane can twin only with a resulting shortening of the specimen; i.e., if it is being deformed in compression. Therefore, it should never be found to twin in a tensile test. In every case the twin plane or planes were those of highest resolved shear stress that could twin by extension of the crystal. Although the scatter is somewhat greater than would be desired for a stringent confirmation of the critical shear stress hypothesis, it is certainly comparable to the data obtained by this author and others for slipping stress where the critical shear hypothesis is generally firmly accepted. Because of the discontinuous nature of the twinning process, one would deduce that irregularities

in the crystal or slight maladjustments in the mechanics of the test (temperature, axiality, etc.) would have a more pronounced effect on the measured twinning stress than on the stress for slip. Then too, it has been found that slip can inhibit or prevent mechanical twinning in alpha iron. With this in mind, one might propose that any small amount of slip could severely alter the stress necessary to initiate and propagate the first mechanical twins.

To investigate the possibility of an effect of normal stresses on the selection of the twinning plane, the normal stresses were calculated for most of the possible twin planes and are listed, along with the corresponding shear stresses, in Table VIII. The constancy is much worse than for a shear-stress criterion. Various combinations of normal and shear stresses were proposed but none of these proved any more applicable than the straight shear stress theory. The symbol ⊗ denotes the planes upon which twins were found. The planes where twinning occurred with very low or perhaps negative shear stresses are accommodation twins resulting from the relief of localized stress concentrations. This has been reported recently by Paxton (27). That shear plays at least an important part is evidenced by Specimen D-5 tested at -170°C. The critical shear stress for this specimen was 10,970, somewhat lower than the mean value at -196°C. It is known from the slip investigation, that the resistance to shear of this material increases

TABLE VIII

SPECIMEN	YIELD STRESS	RESOLVED NORMAL STRESS ON						RESOLVED SHEAR STRESS ON					
		$(\bar{2}11)$	$(\bar{1}\bar{1}2)$	$(\bar{1}21)$	(112)	$(\bar{1}\bar{1}2)$	MISC.	$(\bar{2}11)$	$(\bar{1}\bar{1}2)$	$(\bar{1}21)$	(112)	$(\bar{1}\bar{1}2)$	MISC.
A-8	46,875	25,000	⊗ 19,400		29,100	9,000		20,600	⊗ 18,200		15,600	18,800	
A-10	31,250	7,550	18,400	2,100	⊗ 22,500	⊗ 17,300		11,800	13,100	6,100	⊗ 13,300	⊗ 15,300	
BR-1	50,940	22,800	⊗ 19,300	⊗	34,200	12,000		22,400	⊗ 20,600	⊗	15,700	21,200	
C-4	38,750	18,700	⊗ 12,100		⊗ 25,400	6,400		18,000	⊗ 14,500		⊗ 8,600	13,900	
A-6	37,140	17,200	⊗ 6,650		26,200	3,460		18,500	⊗ 11,500		4,320	9,950	
A-9	48,260	32,400	⊗ 14,300		24,200	3,220	(121)	22,100	⊗ 14,700		17,100	11,900	(121)
A-11	55,700	38,400	⊗ 9,220	⊗	30,800	1,700	⊗ 40,000 (112)	32,200	⊗ 15,700	⊗	7,200	9,200	⊗ (112)
D-1	55,630	26,900	⊗ 23,000		41,660	⊗ 1,700	⊗ 41,600	20,000	⊗ 21,930		14,900	⊗ 21,830	⊗ 8790
D-2	70,230	50,500	⊗ 30,300		29,000	6,800		28,000	⊗ 21,640		19,800	20,700	
D-5 -170°	30,730	17,000	⊗ 10,800		⊗ 19,600	⊗ 4,700		14,700	⊗ 11,600		⊗ 8,000	⊗ 10,800	

rapidly with decreasing temperature in the range -70 to -196°C.

The four specimens pulled to fracture show shear stress values about 25 percent higher than the mean value. For the prestrained specimens, the twinning stresses are calculated from the stress at fracture resolved onto the twinning planes. It was pointed out that pre-strain at room temperature stops or inhibits twinning before fracture. Twins do form in these specimens adjacent to fracture surfaces. The shock loads produced at fracture appear to favor twin formation. Fig. 65 shows profuse twinning adjacent to a fracture surface. Note the large displacement produced by one twin where it intersected an inclusion. The fracture is torn and interrupted where it is intersected by the twins.

Opposed to the wavy and indiscreet nature of the slip lines, the twins are easily distinguished by their straight line appearance and finite width. The large, wide twins propagate through the entire gauge section while the smaller, secondary, tertiary and higher order twins only propagate as far as needed to relieve the local stresses. That internal stresses remain after the first twinning has occurred is evident from the load time curve for several specimens. An example is shown in Fig. 66. After some twins have formed and the load has dropped, new twins are formed before the load reaches its previous value. These drops in load are not as pronounced as those accompanying the initial twins.

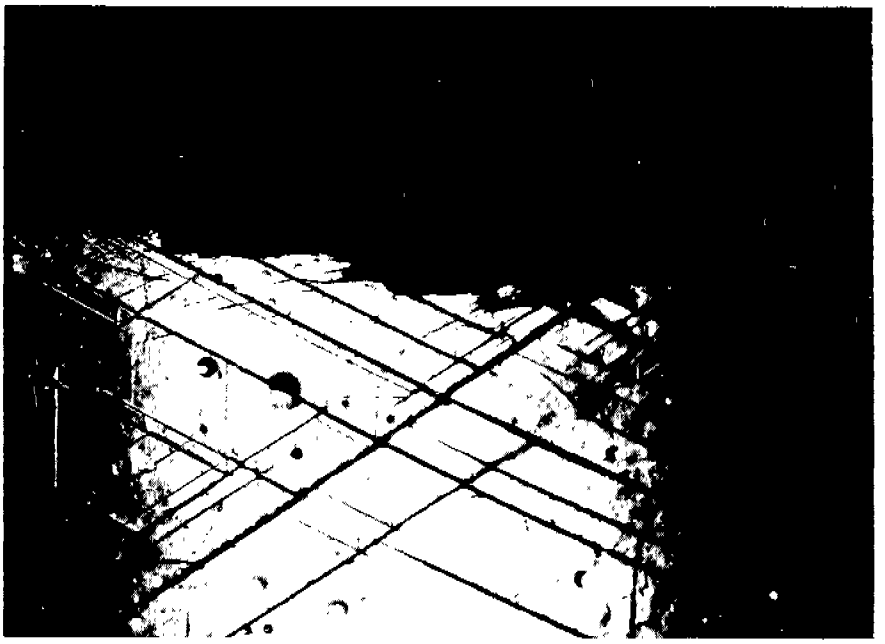

Fig. 65. Twins near a brittle Fracture surface. Note the shear along the twin which intersects the pit. Note also the hackly nature of the fracture.

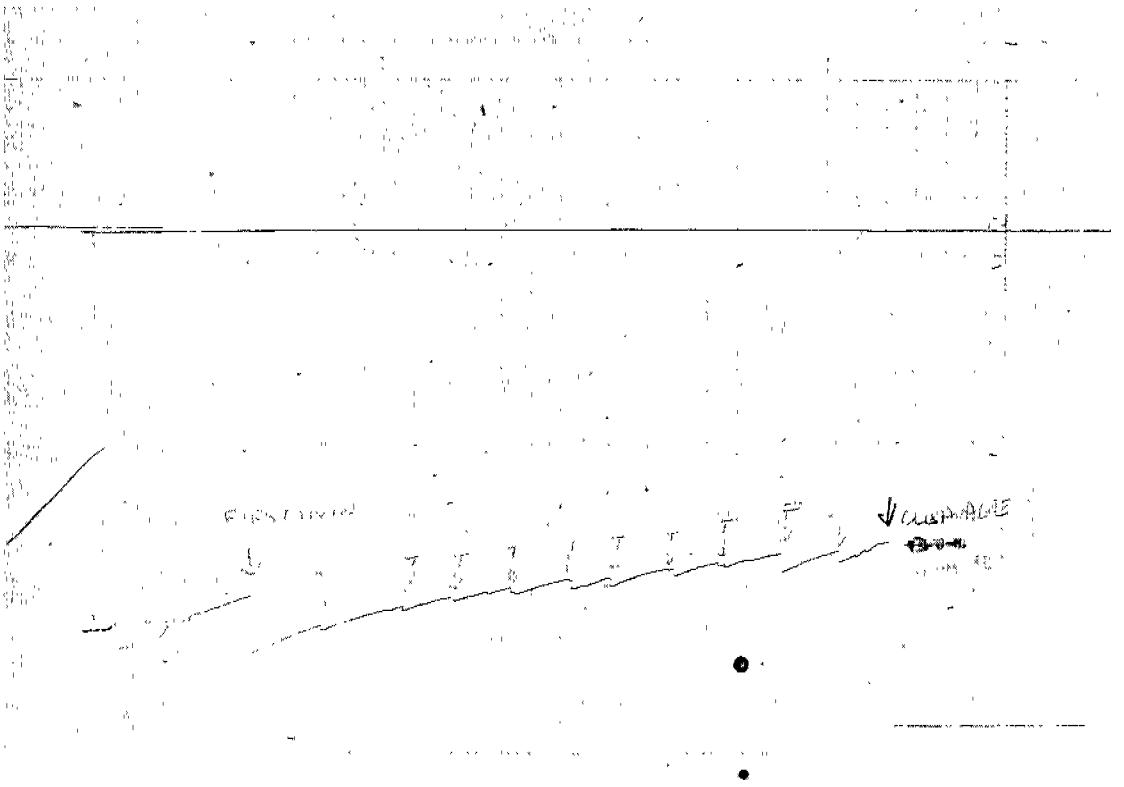

Fig. 66. Load (vertical) versus time (horizontal) curve for specimen E-2 tested at -196°C. Note where second and third twins (T) have occurred at lower stresses than the first twin.

At low magnifications the twins often appear to have one feathery edge. An example is shown in Fig. 67. At high magnifications, these separations are resolved into notches representative of cube corners. (See Fig. 68.) No angular measurements of the dihedrals of these notches were made. Perhaps they are {112} type traces, perhaps not.

Fracture

Introduction

The results of this final portion of the research are contained in the section called "Fracture." Originally, the term cleavage was intended, but the experimental observations have proved this to be entirely too specific a word. The orientations of all the fracture specimens are given in Figures 69, 70 and 71. Figures 69 and 70 are for the series of short gauge length specimens while Fig. 71 pertains to the large crystals such as those used for the slip and twinning studies. The term "brittle fracture," as used here, is defined as a fracture whose plane can be clearly indexed by optical trace methods in a specimen whose orientation can be uniquely determined by the interpretation of a relatively undistorted Laue back reflection photograph. Ductile fracture shall be defined as a chisel-edge fracture occurring at the neck after severe deformation.

Large Specimens

Eight large specimens which remained from the slip and

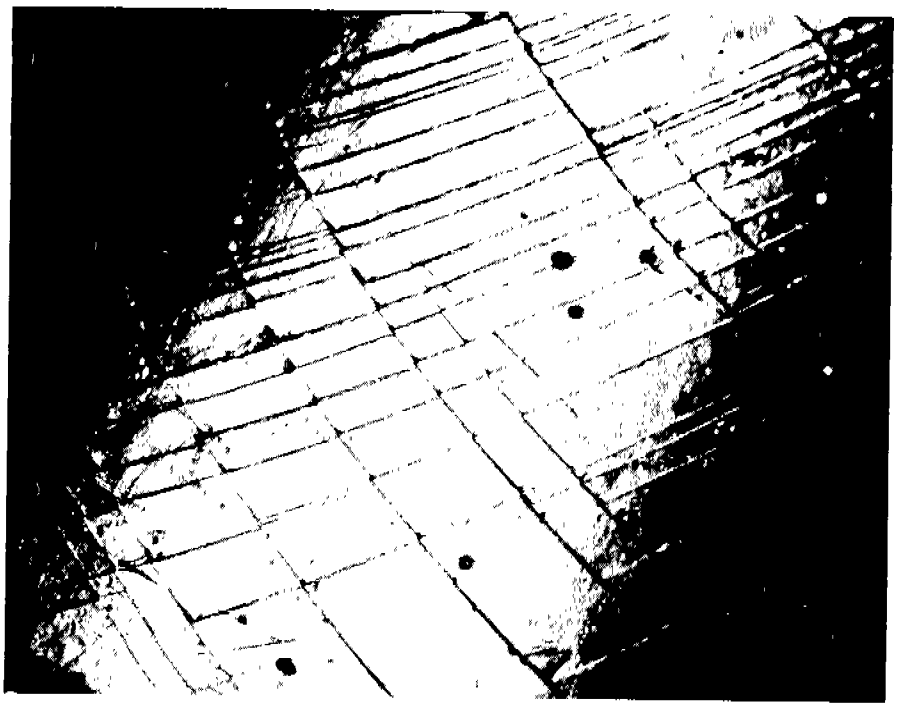

Fig. 67. Cooperative twinning on two sets of planes with different directions. Note feathery edges of twins (X75).

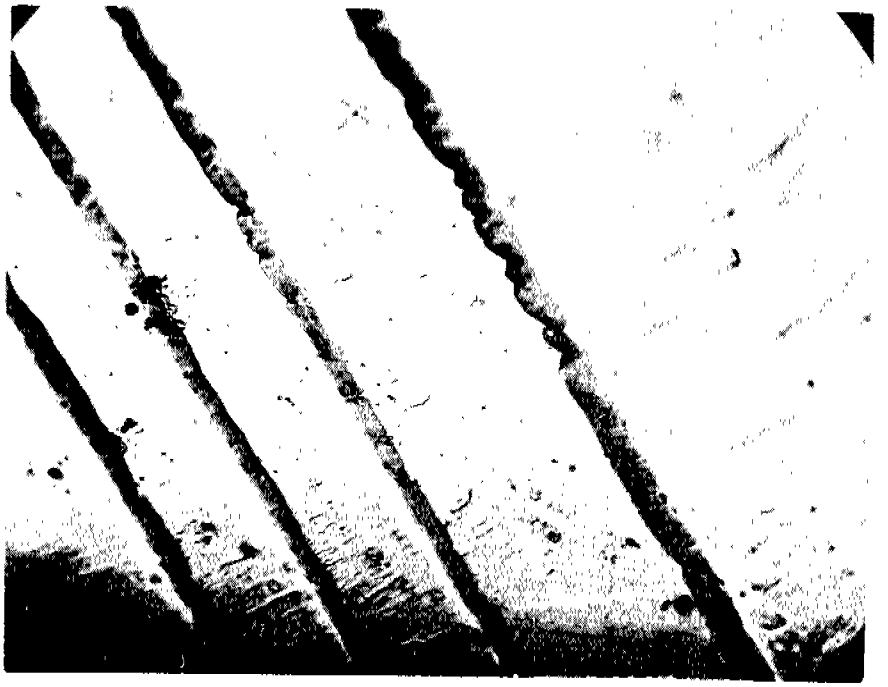

Fig. 68. Twin faces (dark bands) at high resolution showing the notching effect (X1000).

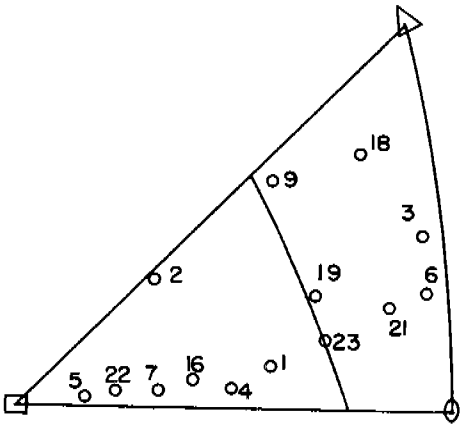

FIG. 69

FRACTURE ORIENTATIONS

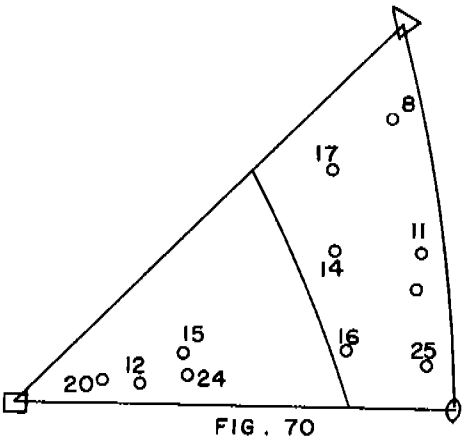

FIG. 70

FRACTURE ORIENTATIONS,
PRESTRAINED SPECIMENS

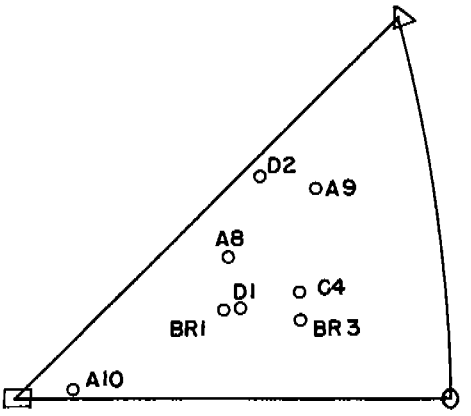

FIG. 71

FRACTURE ORIENTATIONS
LARGE SPECIMENS

twinning studies were pulled to fracture at -196°C. The results of these studies are given in Table IX.

The angle ϕ represents the angle between the specimen axis and the normal to the cleavage plane. The usual equation for the calculation of the resolved normal stress for cleavage (RNS) is

$$RNS = \frac{F}{A} \cos^2 \phi$$

where F is the load at fracture and A is the cross sectional area of the specimen. The diameters of the long specimens were measured at the minimum point, wherever it happened to occur along the gauge length. The cleavages, or fractures,

Table IX

Specimen	ϕ°	Load at Fracture	Area of Fracture	RNS
C-4	34	1700 pounds	.0358 in^2	39,400
A-8	30	1900 "	.0385 "	42,800
A-10	6	1850 "	.0353 "	52,100
BR-1	28	1700 "	.0378 "	39,800
Prestrained				
A-9	41	2800 "	.0433 "	49,000
BR-3	36	2500 "	.0426 "	47,500
D-1	28	1700 "	.0341 "	44,100
D-2	37	2500 "	.0391 "	50,500

occurred at random positions on the gauge lengths. It was believed that if any plastic flow had occurred--some always did--

it would be better to measure the area of the fracture surface and calculate the resolved normal stress from the equation

$$RNS = \frac{F}{A'} \cos \phi$$

where A' is the fracture area. All results were obtained in this manner, the areas being obtained from projections of the fracture surfaces on a ground glass. The areas of the ellipses were calculated from the formula

$$A = 0.7854\ D_1\ D_2$$

where D_1 and D_2 are the major and minor axes of the ellipse, respectively.

The cleavage planes were always (001), as expected. If the resolved normal stress law is to be verified, then plotting the resolved normal stress for fracture versus the angle ϕ should yield a horizontal straight line. The data for the large specimens are plotted in Fig. 72. The scatter is quite marked among the virgin specimens (not prestrained). The value for A-10 is 10,000 psi greater than the mean value for the virgin specimens. Considering the virgin specimens alone, the trend would be decreasing RNS with increasing angle. Since increasing angle means increased ratio of shear to normal stresses and hence increased tendency for slip, the RNS might be expected to increase if the fracture were propagating through a region strain-hardened by slip. The very inhomogeneous nature of slip along the gauge length, however, could provide that,

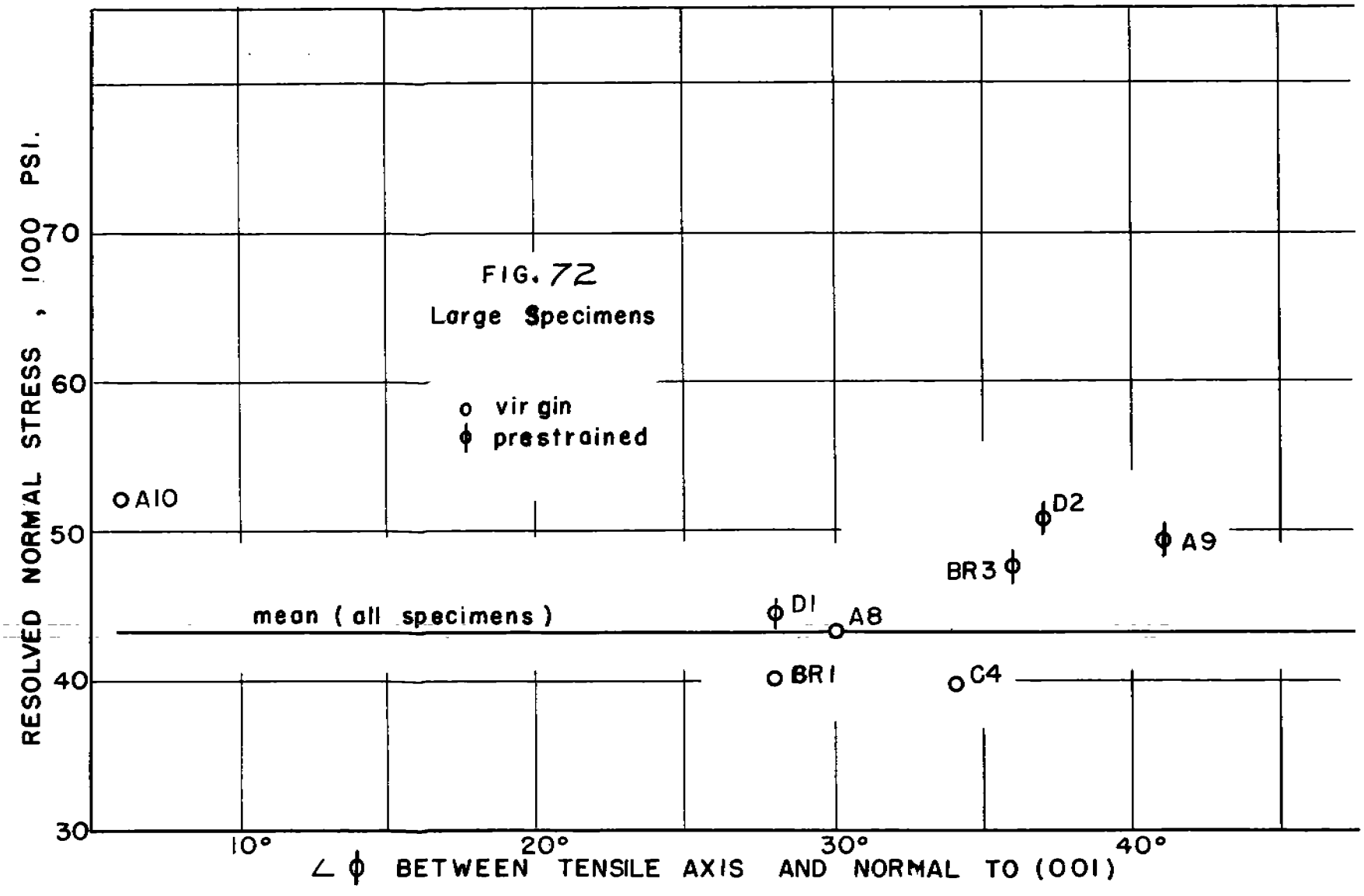

FIG. 72
Large Specimens

although large amounts of shear had occurred, the fracture could occur in a region where the slip was negligible.

The prestrained specimens again refute the argument that a downward trend of the curve should obtain. These prestrained specimens were pulled about 4% elongation at room temperature so that some slip should have occurred at all parts of the gauge length regardless of the degree of inhomogeneity of the deformation. When tested to fracture at -196°C, the RNS values lie approximately 5000 to 6000 psi above the virgin mean curve. Hence when the fracture is forced to occur in a region where slip induced by prestrain has occurred, the RNS at fracture is raised. The high RNS value of A-10 is then to be regarded as scatter due to material variables.

Small Specimens

The orientations of the small specimens are given in Figs. 69 and 70. Twenty-six specimens in this series were fractured at -196°C. The test methods for this group were modified by the results of the studies on the large specimens. First, all the specimens were plotted in one unit triangle for comparison. They were then separated into pairs of the same or similar orientation. One group (Fig. 70) was designated to be prestrained slightly past the yield point at room temperature and then fractured at liquid nitrogen temperature. The other group (Fig. 69) was to be tested directly at -196°C. The complete

series of results for these specimens is given in Table X. The symbols are defined as follows:

Where broke	N - at neck E - elsewhere
Type of Fracture	B - brittle D - ductile B & D - pronounced neck with cleavage plane

Brittle Fractures

Twelve specimens broke in what has been previously defined as a brittle fracture, or cleavage. The resolved normal stresses for these were calculated and are plotted in Fig. 73. Just as for the large specimens, the scatter is quite large. These small specimens were given a taper so that a reduced section existed at the center whose diameter was .003 to .005 inch less than the rest of the specimen. This was done so that slip resulting from prestrain or from "at-temperature" ductility would be forced to occur at a given point, and so that fracture would also occur at that same point. Thus the fracture would always be made to propagate through a region that had undergone slip if such slip had taken place. The severity of the taper was not sufficient to effect the predicted behavior as shown by the column of "where broke" in Table X. Again the brittle specimens tended to break randomly throughout the gauge length.

The resolved normal stress for fracture of specimen 12 was raised by prestrain, while two others, 15 and 24, was lowered. At first this seems incompatible. However, 12 broke at the neck

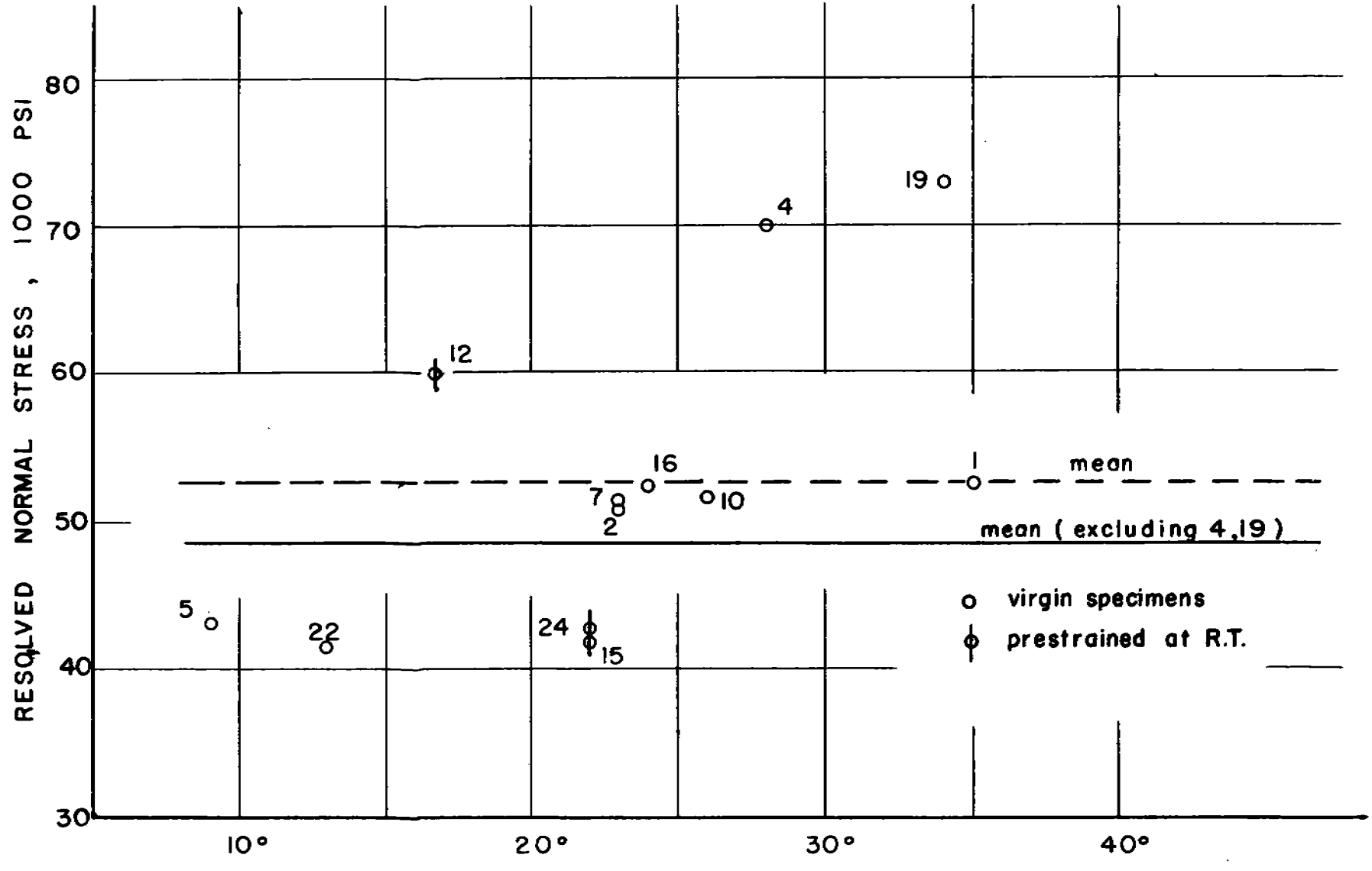

∠ ϕ = BETWEEN TENSILE AXIS AND NORMAL TO (001)

FIG 73 SMALL SPECIMENS

Table X

Spec.	ø	% RA at Fracture	Where Broke	Ductile Fracture Stress	Brittle RNS	Type of Fracture
7	23°	?	N	None	50,400	B
24P	22	?	E	None	42,500	B
16	24	?	N	None	52,400	B
15P	22	?	E	None	41,600	B
22	13	?	E	None	41,300	B
12P	17	?	N	None	59,900	B
5	9	?	E	None	42,800	B
20P	7	?	Broke in shoulder	None	--	B
19	34	?	N	None	73,000	B
14P	39	52.5	N	130,000	None	D&B
3	47	59.0	N	143,000	None	D
11P	43	56.9	N	124,000	None	D
18	47	47.7	N	140,000	None	D
8P	50	?	N	None	None	D&B
9	39	?	N	None	None	D&B
17P	45	55.5	N	128,000	None	D&B
21	43	56.0	N	146,000	None	D
25P	43	49.8	N	133,500	None	D
2	23	?	E	None	50,400	B
1	35	?	E	None	52,500	B
4	28	?	E	None	70,000	B
6	45	54.0	N	141,400	None	D
10	26	?	N	None	51,500	B
13	45	48.0	N	125,000	None	D&B
23	37	54.0	N	146,000	None	D
26		?	N	None	None	D&B

while 24 and 15 broke away from the neck. The fracture of 12 had to propagate through strain hardened material while in specimens 15 and 24 it did not necessarily, depending on the uniformity of the prestrain.

The mean level of resolved normal stress for the small specimens is about 5000 psi higher than for the large, thus indicating a size effect in this material. Two specimens, 4 and 19, are seen to be several thousand psi above the others. Rough measurements of ductility at the fracture show that these two specimens have reductions in area at the fracture in the range 10 to 13 percent while the others are roughly 0 to 4 percent. Accurate values of reduction in area at the fracture would be desirable since Steijn (14) found increasing cleavage stress for increased ductility at the fracture. Reductions in area at the neck were calculated, but they are of little or no meaning and showed no correlation with the resolved normal stress for fracture. Reductions in area at the fracture were impossible to measure since the original area of the specimens at the fracture point was not known.

Ductile Fractures

It is seen from Table X that for specimens where $\phi > 35°$ ductile fractures were obtained. The great circle through Figures 69 and 70 is the 35 degree boundary region. Although prestraining inhibited twinning prior to fracture in these

specimens, it did not prove to benefit the cause of brittle fracture in a specimen for $\phi > 35°$. In some cases, however, prestraining did cause fracture to occur on a more or less planar surface even though the ductility at the neck was on the order of 35 to 50 percent R.A. No optical or X-ray measurements could be obtained for these specimens. Their fractures were classed as D and B (ductile and brittle).

X-ray photograms of the ductile specimens yielded complete diffraction rings indicating that the severe distortion at the neck had caused the specimens to fragment so severely that they approached polycrystalline properties. The curve of fracture stress versus reduction of area at the fracture for the ductile specimens bears this out. (See Fig. 74.) This plot is similar to those obtained for polycrystalline metals. Conflicting data are reported on the effect of prestrain on the fracture stress of ductile materials. Some report prestraining increases the fracture stress; others report a decrease. No explanations are given. The downward trend of the curve for prestrained specimens has no obvious significance. There is a possible explanation for the lower values of the prestrained specimens. Since the shear given a specimen at room temperature can be applied at a low stress level if the criterion for ductile fracture is a given amount of shear, then less shear is needed to complete the fracture requirement at low temperatures.

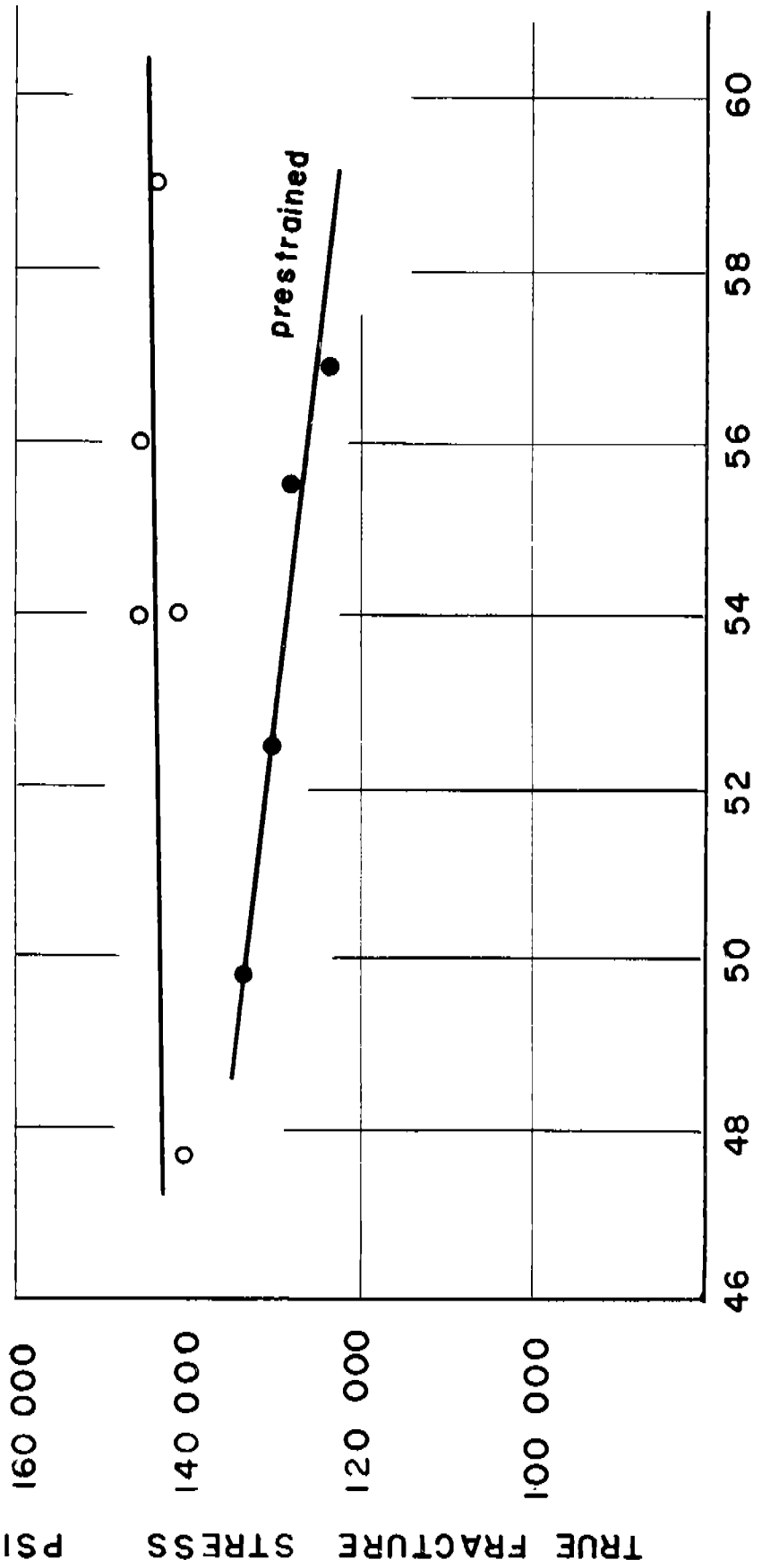
TRUE FRACTURE STRESS PSI
160 000
140 000
120 000
100 000
Prestrained
46
48
50
52
54
56
58
60
% REDUCTION IN AREA AT FRACTURE (NECK)

FIG 74

For purposes of comparison, the complete series of small specimens after fracture is shown in Figs. 75 through 79. No explanation, except inhomogeneity, is given for the fact that a specimen will neck severely and then fracture above the neck on a more or less planar surface, since the reduced section of the crystal had already undergone a given value of stress earlier in the history of the specimen. For prestrained specimens, the fracture could propagate through metal that was strain hardened less than the material at the neck, but for virgin specimens this is not true.

The Nature of the Fracture Surface

The process of brittle fracture in iron single crystals is undoubtedly quite complex as evidenced by scatter and necking behavior of the various specimens. That the atomic processes involved in fracture are even more complex is evident from studies of the fracture surfaces. Fig. 80 shows a portion of the fracture surface of specimen BR-1. This is indeed not an atomically smooth plane. Notice the two dimensional grid work or cell structure. Zapffe (39) reports these to be traces of other cleavage planes ($\{001\}$). This is a possibility although it is more likely that twins could be responsible for this behavior. The traces of (211) twins on a (100) surface could intersect angles of 18°26', 36°52', 71°34' and 90°. The traces of Figure 80 are seen to be

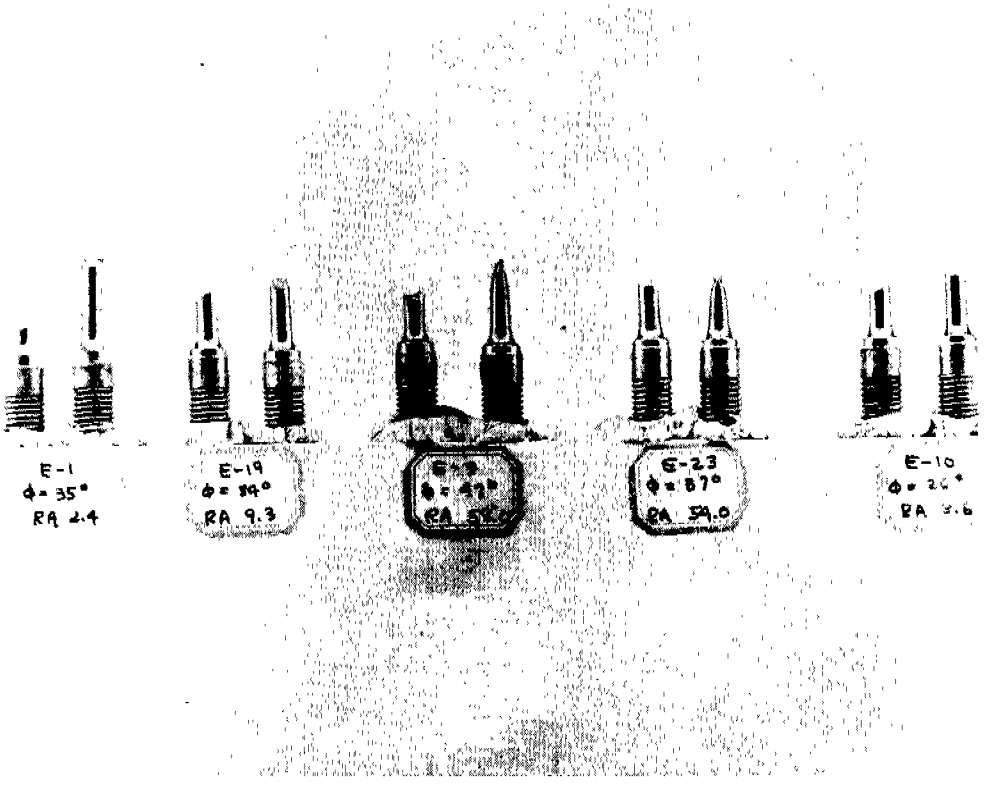

Fig. 75. Fracture specimens (virgin).

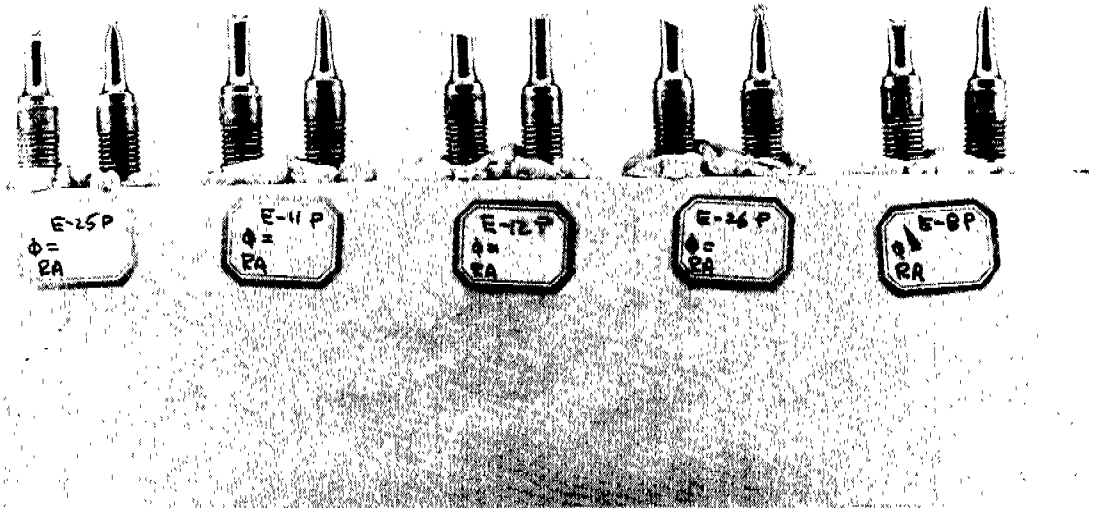

Fig. 76. Fracture specimens (virgin).

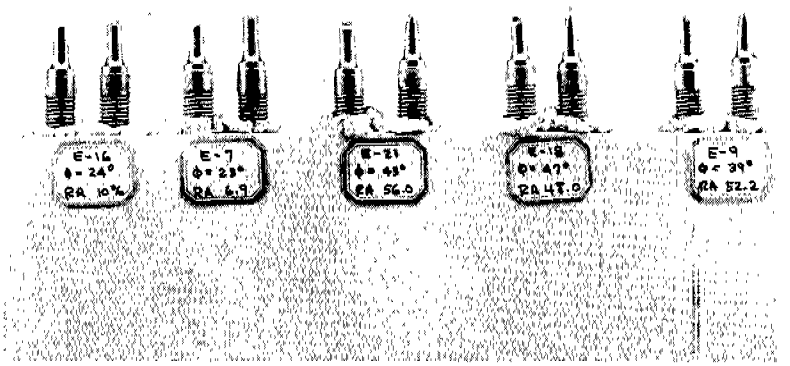

Fig. 77. Fracture specimens (virgin).

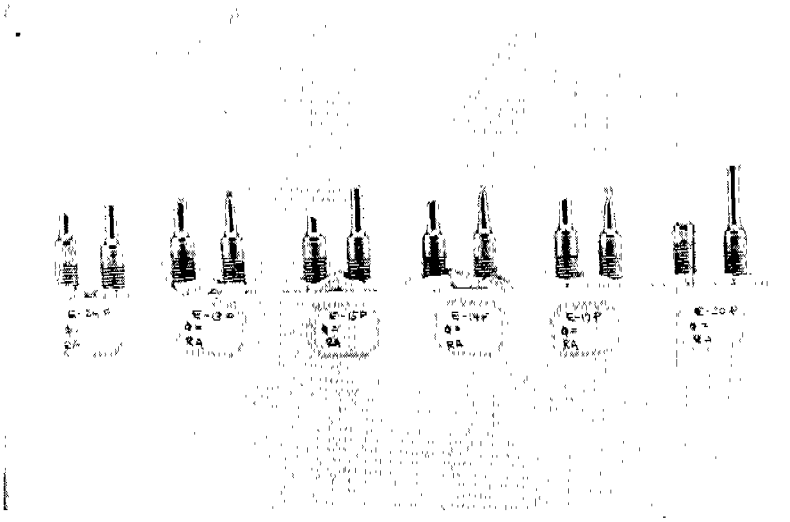

Fig. 78. Fracture specimens (prestrained).

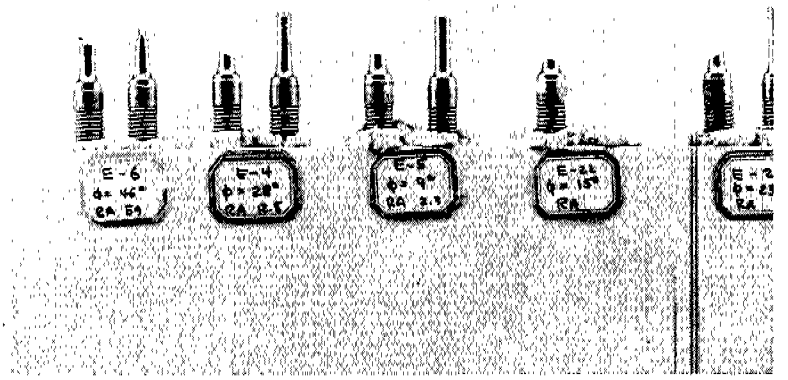

Fig. 79. Fracture specimens (prestrained).

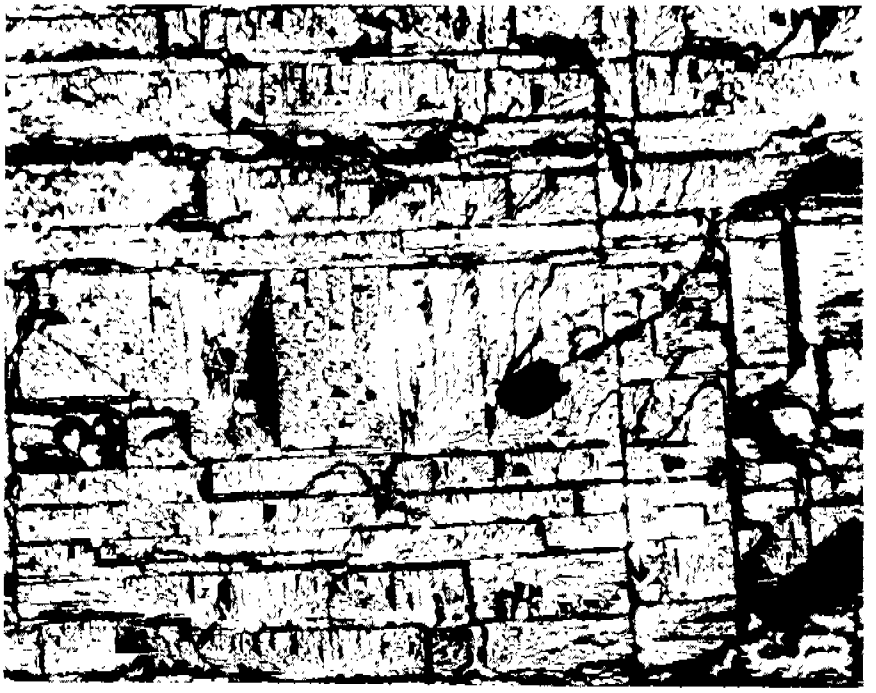

Fig. 80. Fracture surface of Br-1 (X75).

Fig. 81. Fracture surface of Br-3 (X100).

orthogonal while those of Figure 81 are at 71° to each other, thus confirming the twin hypothesis.

Within the cell structures of Fig. 80, two other substructures are evident. The first is a series of "corner structures" which are orthogonal to the large cells. These are probably small cleavage facets of the type $\{001\}$. The second sub-structure is a series of wavy lines similar to the contour lines of a topographical map. These are shown at higher resolution in Fig. 81 and at very high magnification in Fig. 82. It is believed that these lines are found where fracture has occurred by shear. They are indeed similar if not identical to the slip lines observed on the surface of these iron crystals and are found much more frequently in prestrained specimens.

Fig. 83 shows the second major type of fracture structure. This is a one-dimensional grating composed of the same type of lines or bands that form the cell structure. This type of fracture is always found in conjunction with the cell structure and usually occupies a part of the fracture surface near one edge. It may vary from 10 percent to 90 percent of the fracture surface. The direction of these lines nearly always coincides with the long axis of the ellipse formed by fracture surface, which means that they occur in the direction of maximum shearing stress. The "corner" sub-structure is never found with the line structure: only the shear lines are present between the bands. The complex nature of the fracture surfaces

Fig. 82. Fracture surface of Br-3, showing shear lines and "corner structure" (upper left).

Fig. 83. Fracture surface of A-10 along one edge of the fracture. Note one dimensional array of band structure.

confirms the observation that the mechanism of brittle fracture in iron is not due to a single stress criterion and hence the scatter in the RNS data is to be somewhat expected. The ductility of this material appears to be very high at -196°C; however, it should be remembered that this is a very slow strain rate, 0.01 inch per minute. Increasing the strain rate by a factor of seven such as done by Steijn (14) could considerably lessen the effect of a shear stress, thereby reducing the scatter in the resolved normal stress law and perhaps changing the appearance of the fracture surfaces. Had the very ductile nature of this material at this strain rate and low temperature been anticipated, one or the other would certainly have been changed. It would be most desirable to lower the temperature but easier to raise the strain rate.

One would expect increased strain rates to increase the tendency for brittle fracture, perhaps so much that every orientation in the unit triangle would fracture brittlely with even zero ductility at the fracture. Lower strain rates should decrease the brittleness but reduce the scatter. It appears that the combination of material, strain rate and temperature was unfortunate in that it caused the behavior to fall in a transition region where scatter is known to be very high. Increased or decreased strain rate would have yielded more precise information on either the brittle or ductile behavior of these crystals yet it would not have yielded

so many interesting and intriguing results.

CONCLUSIONS

1. The integrated glide ellipse can occupy any position in the ⟨111⟩ zone. Deviations from the three low index planes, {110}, {112}, and {123} are real and cannot be accounted for by experimental error.

2. The selection of the glide ellipse is determined by the relative shearing strengths along the ⟨111⟩ zone and the position of the maximum shear stress plane containing the slip direction. The distribution of shearing strengths along the ⟨111⟩ is markedly affected by temperature; lower temperatures increasing the shearing strengths near {112} more than those near {110}, thus low temperatures favor {110} slip regardless of the distribution of the applied stress.

3. The critical resolved shear stress law is a valid criterion for slip in iron on a experimental basis. The measurements are too coarse to detect the effect of a normal stress. This critical shear stress is found to vary only slightly with temperature in the range 0 to 200 degrees Centigrade but to increase rapidly from 0° to liquid nitrogen temperatures.

4. Mechanical deformation of the single crystal surface increases the visibility of the slip lines although it may also increase the stress required for slip. Fragmentation of the lattice can occur at any of the temperatures studied, the degree being dependent on the extent of deformation.

5. A nearly constant resolved shear stress is found to be a criterion for mechanical twinning on $\{112\}$ planes and in $\langle 111 \rangle$ directions.

6. The initial twinning plane is always the one predicted by the critical shear stress theory, in that the direction of twinning must be considered. Accommodation twins are found to occur to provide for the relief of internal stresses.

7. Slip induced by room temperature prestraining prevents or at least severely inhibits twinning prior to fracture at -196 degrees Centigrade. Twinning accompanying the fracture process occurs adjacent to the fracture surfaces in both virgin and prestrained specimens.

8. The resolved normal stress law appears to explain brittle fracture in this material better than any other criterion, although the scatter is significantly high. Higher strain rates should increase the brittleness and decrease the scatter.

9. For angles between the tensile axis and an {001} plane greater than 65° the crystals are found to fracture in a ductile fashion by shear.

10. Room temperature prestraining increases the brittle fracture stress if the fracture propagates through a strain hardened region and decreases it if the fractures occur in regions of little or no slip. Prestraining lowers the fracture stress of ductile specimens according to the predictions of a theory of additive shears to failure.

11. Fractographic studies indicate the mode of fracture of the brittle specimens to be one of combined shear and cleavage; the proportion of the shear part being increased by large angles of ϕ and by prestrain.

ACKNOWLEDGMENT

The author wishes to express his sincere thanks to his advisors, Dr. R. F. Mehl and Dr. G. T. Horne, paedagogi; for their invaluable technical assistance and moral support.

To Mrs. C. S. Yang and Mr. Y. T. Chou for their command performance of the X-Ray and metallographic work and for their willingness to comply with the authors every whimsy--deepest gratitude.

To Admiral J. W. Ludewig for his guidance in matters of administration and protocol, and to the several members of the Metals Research Laboratory whose cooperative efforts contributed to the completion of this endeavor--many thanks.

Finally, to Drs. O. T. Marzke, J. R. Low, W. Hibbard and Finn Jonassen, members of the project advisory committee, for their help, patience and understanding the author wishes to express his appreciation.

This research was made possible by contract NObs-50230 SR-108 Bureau of Ships, Department of the Navy.

BIBLIOGRAPHY

1. Barrett, C. S.: The Structure of Metals, 2nd. Edition, McGraw-Hill, New York (1953).

2. Taylor, G. I. and Elam, C. F.: Proceedings of the Royal Society of London A112 (1928) p. 337.

3. Taylor, G. I.: Proceedings of the Royal Society of London A118 (1928) p 1.

4. Fahrenhorst, N. and Schmid E. : Zeitschrift für Physik 78 (1932) p 383.

5. Barrett, C. S., Ansel, G., and Mehl, R. F.: Transactions of the American society for Metals 25 (1937) p 702.

6. Chen, N. K. and Maddin R.: Transactions AIME 191 (1951) p 937.

7. Opinsky, A. and Smoluchowski, R.: Plastic Deformation of Crystalline Solids, Mellon Institute Symposium (1950).

8. Opinsky, A. and Smoluchowski, R.: Journal of Applied Physics 22 (1951) p 1488.

9. Vogel, F. L. and Brick, R. M.: Technical Report #2 (NCRRL) Flight Research Laboratory, W-P Air Force Base, Contract AF33(038)-15889.

10. Seitz, F. and Read, T. A.: Journal of Applied Physics XII (1941) p 538.

11. Taylor, G. I.: Proceedings of the Royal Society of London CXLV (1934) p 362.

12. Cottrell, A. H.: Progress In Metal Physics, Vol. I Interscience Publishers, New York (1949).

13. Chalmers, B. and Martius, U. M.: Proceedings of the Royal Society of London A213 (1952) p 176.

14. Steijn, R. and Brick, R. M.,: Technical Report #2 (NCRRL) Flight Research Laboratory, W-P Air Force Base, Contract AF33(038)-15889.

15. Evans, J. N.: Proceedings of the Royal Society of Edinburgh 32 (1912) p 416.

16. Preston, G. D.: Nature, London, 119 (1927) p 176.

17. Mathewson, C. H. and Edmunds, G. H.: Transactions AIME (1928).

18. Clark, R. and Craig, G. B.: Twinning, Progress in Metal Physics, Interscience, London (1952).

19. Barrett, C. S.: Cold Working of Metals Symposium, ASM (1948).

20. Schmid, E. and Boas, R.: Plasticity of Crystals, London (translation from the German) (1950).

21. Gough, H. J. and Cox, H. L.: Proceedings of the Royal Society of London A123 (1929).

22. Gough, H. J. and Cox, H. L.: Proceedings of the Royal Society of London A127 (1930).

23. Yakovleva and Yakutovitch: Experimental and Theoretical Physics, USSR 10 (1930).

24. King, R.: Nature, London 169 (1952) p 543.

25. Chalmers, B: Proceedings of the Royal Society of London 47 (1935) p 733.

26. Low, Jr., J. R.: Acta Metallurgica 1 (1953).

27. Paxton, H.: Acta Metallurgica 1 (1953) p 141.

28. Ludwik, P.: Elemente der Technologischen Mechanik, Springer, Berlin (1909).

29. Holloman, J. H.: Fracture of Metals Symposium, American Welding Society, New York (1946).

30. Holloman, J. H. and Jaffe, L. D.: Ferrous Metallurgical Design, J. Wiley & Sons, New York (1947).

31. Zener, C.: Revue of Modern Physics 17 (1945).

32. Sachs, G.: Effect of Strain on Fracture, Fracture of Metals Symposium, ASM (1947).

33. Zener, C.: The Micromechanism of Fracture, Fracture of Metals Symposium, ASM (1947).

34. Low, Jr., J. R.: Private Communication.

35. Jacquet,: Voluminous References to Electropolishing, Comptes Rendus.

36. Greninger, A. B.,: Transactions AIME 117 (1935) p 61.

37. Opinsky, A. J.,: Doctorate Thesis, Carnegie Institute of Technology (1950).

38. Paxton, H.: Private Communication.

39. Zapffe, C. A.,: Voluminous References on Fractography of Metals.